Diagenetic and Paleoceanographic variations in sedimentary Mn, Ba, and CaCO$_3$, with emphasis on the eastern Mediterranean sapropel S1

Anja Reitz

GEOLOGICA ULTRAIECTINA

Mededeling van de
Faculteit Geowetenschappen
Universiteit Utrecht

No. 251

Diagenetic and Paleoceanographic variations in sedimentary Mn, Ba, and CaCO$_3$, with emphasis on the eastern Mediterranean sapropel S1

Anja Reitz

Diagenetic and Paleoceanographic variations in sedimentary Mn, Ba, and CaCO$_3$, with emphasis on the eastern Mediterranean sapropel S1

Diagenetische en paleoceanografische variaties in sedimentair Mn, Ba, en CaCO$_3$, met nadruk op sapropel S1 in de oostelijke Middellandse Zee

(met een samenvatting in het Nederlands)

Diagenetische und paläo-ozeanographische Variationen von sedimentärem Mn, Ba, und CaCO$_3$, unter besonderer Berücksichtigung des Sapropel S1 im östlichen Mittelmeer

(mit einer Zusammenfassung in deutscher Sprache)

PROEFSCHRIFT

ter verkrijging van de graad van doctor aan de Universiteit Utrecht
op gezag van de Rector Magnificus Prof. dr. W.H. Gispen
ingevolge het besluit van het College voor Promoties
in het openbaar te verdedigen op
10 juni 2005 des morgens te 10.30 uur

door

Anja Reitz

Promotor: **Prof Dr Gert J. de Lange**
Department of Earth Sciences – Geochemistry
Faculty of Geosciences
Utrecht University
Utrecht, The Netherlands

Aan een verwarrende hoeveelheid
mogelijkheden ligt zo vaak een eenvoudige
onderliggende structuur ten grondslag.

Maarten't Hart

Und allen Plänen gegenüber begleitet mich die Frage:
„Was soll der Unsinn?“; eine Frage, die überhaupt
ganz und gar von mir Besitz zu nehmen droht.

Theodor Fontane

für meine Oma Anna

Table of contents

Chapter 1

Introduction and summary

Early diagenetic processes, largely driven by the supply of organic matter and its degradation, determine in part the geochemical composition of marine sediments. Changes in organic matter production, i.e. sea surface primary production (from hereon 'productivity') have a significant influence on these diagenetic processes, and thereby on the sedimentary composition. Productivity changes can be induced by climatic changes of the Earth that vary over a broad range of time-scales caused by variations with a distinct periodicity (e.g. Milankovitch cycles) or irregular variations (e.g. caused by tectonic changes).

Recent diagenetic processes can be investigated using pore water profiles, whereas paleo-diagenetic changes can be deduced by comparison to these recent processes. Since diagenesis is not only responsible for the degradation of C_{org} but also for the redistribution of trace-metals as authigenic precipitates in marine sediments, studying diagenetic processes might be a suitable tool to reconstruct paleoceanographic changes.

This thesis reports on recent and paleo-diagenetic processes in selected marine C_{org}-rich sediments, mainly those at eastern Mediterranean sapropel S1. This chapter gives a general introduction to the background of the major processes discussed in chapters 2-6.

1.1 Marine productivity
Marine Carbonates

The marine budget of calcium is mainly regulated by the formation and dissolution of skeletal carbonates and their incorporation into deep-sea sediments. Foraminifera (calcite), coccolithophorids (calcite) and pteropods (aragonite) are the most important carbonate-secreting organisms in the oceans. The production of these organisms and thus the occurrence of their shells is dependent on the fertility of the ocean. Generally, high fertility regimes are dominated by diatoms (e.g. in coastal upwelling areas) and low fertility regimes by coccoliths (e.g. in the Mediterranean).

In response to physicochemical parameters, carbonate shells are subject to dissolution after they sink through the water column, resulting in the formation of the calcite and aragonite compensation depth (CCD and ACD) below which no calcite and aragonite, respectively will be accumulated. The oceanic deepwater is usually undersaturated with respect to aragonite and high-Mg calcite (Berner and Honjo, 1981) wherefore these carbonate polymorphs are predominantly found in shallow water depth or at high latitudes (Wilkenson and Given, 1986).

However, $CaCO_3$ may also be potentially affected by diagenetic organic matter degradation which might cause dissolution (e.g. Jahnke et al., 1994) as well as authigenic precipitation. This authigenic carbonate precipitation has been shown to occur as dolomite and aragonite/calcite e.g. in lagoonal systems or by advection of methane saturated fluids at cold seeps (e.g. Middelburg et al., 1990; Aloisi et al., 2004a) and as high Mg-calcite it is believed to occur e.g. in the eastern Mediterranean C_{org}-poor marls (e.g. Milliman and Müller, 1973).

Organic matter and biogenic barium

A complex combination of chemical (e.g. availability of nutrients), physical (e.g. temperature, light), and biological (e.g. growth rate) variables is controlling the primary production in the ocean; from which the nutrient availability is probably the limiting factor in most marine systems (Neinhuis, 1981). In terms of productivity the marine environment can be classified in eutrophic and oligotrophic regions; the latter one is particularly pronounced in the eastern Mediterranean.

The total organic matter (TOC) in the marine system consists of two principle fractions, the dissolved phase (<0.45 μm; ~95% of TOC)) and the particulate phase (>0.45 μm). The latter detrital fraction consists mainly of organic aggregates of various types: faecal material, dead organisms, and complex organic particles. The photosynthetic fixation of CO_2 during primary production, generating $~40*10^{15}$ gCyr^{-1} (Antoine et al., 1996), is the most important input of organic carbon to the ocean. However, only 1 to 0.01% of this primary production is accumulated in the marine sediments (Berger et al., 1989) because most of it is recycled in the upper water column. At depth CO_2 and nutrients are restored back into the water column due to remineralization and oxidative destruction of dead organisms.

Overall the preservation of organic matter in marine sediments is complex and still an issue under debate. Hedges and Keil (1995) postulated that key factors controlling the preservation of C_{org} are (i) productivity in surface waters, (ii) sediment accumulation rate, (iii) bottom water oxicity, and (iv) organic matter source. Even though enhanced amounts of organic matter can be degraded it can be traced back by tracers like biogenic barium (barite). In contrast to the direct productivity indicators such as C_{org}, calcium carbonate (e.g. Brummer and Van Eijden, 1992), and opal (e.g. De Master et al., 1992), barite is a more refractory chemical species under oxic conditions that is strongly linked to export production (e.g. Goldberg and Arrhenius, 1958; Dehairs et al., 1980; Dymond et al., 1992; Van Santvoort et al., 1996). The reported average 30% preservation (Dymond et al., 1992) of it makes it a suitable proxy for paleoproductivity. Yet, the exact formation mechanisms of biogenic barium within the water column are still poorly understood, however, it is generally assumed that biogenic barium either precipitates in so called micro-environments of decaying organic compounds due to the accompanied sulfate release (Dehairs et al., 1980; Bishop, 1988) or due to the dissolution of celestite (from acantharia) and the resulting sulfate and barium release (Bernstein et al., 1992).

1.2 Early Diagenesis/organic matter remineralization

The diagenetic remineralization of organic matter is catalyzed by different types of microorganisms, which utilize in order of decreasing energy supply first oxygen followed by nitrate and/or Mn-oxides, Fe-oxides and sulfate as secondary oxidants (e.g. Froelich et al., 1979; Berner, 1980).

Berner (1981) established the following vertical diagenetic zone sequence: (i) the oxic environment, where pore waters contain measurable dissolved oxygen; little C_{org} is preserved; (ii) the anoxic environment, where the pore water contains no measurable oxygen; diagenesis proceeds via secondary oxidants. The anoxic environment again can be subdivided in (a) the non sulphidic suboxic environment, where pore waters contain no measurable dissolved sulphides, the supply of metabolizable organic matter is relatively large, but limiting; the used oxidants are nitrate, MnO_2, and Fe_2O_3; (b) the sulphidic environment, where H_2S and HS$^-$ are produced due to bacterial reduction of dissolved sulphate; a sufficient supply of organic matter is available; (c) the non-sulphidic methanic

environment, where pore waters contain dissolved methane; large amount of metabolizable Corg are present and sulphate is sequentially utilized (Fig. 1).

The use of secondary oxidants creates a change in redox conditions that is usually characterized by a color change form reddish-brown (oxic) to grayish-green (anoxic) indicating the redox boundary between oxic (positive redox potential) and anoxic (negative redox potential) conditions within the sediment column. This distinct color change is produced by suboxic Mn and Fe oxide dissolution and its precipitation where their dissolved ions encounter oxygen at the oxic/suboxic redox boundary.

Manganese is the most mobile element with respect to early diagenetic redox changes. The diagenesis of manganese may leave distinct spikes in the solid phase. However, its diagenetic mobility is reflected by the solid phase as well as by the pore water. Burdige and Gieskes (1983) described a diagenetic model of manganese by subdividing four different diagenetic zones. (1) The oxidized zone, where the dissolved Mn^{2+} concentration in pore water is zero, (2) the Mn oxidation zone, where the dissolved Mn^{2+} concentration profile increases with depth due to diffusion of Mn^{2+} from below across the redox boundary resulting in the oxidation of hydrous manganese oxides, (3) the Mn reduction zone, where Mn^{2+} is released into the pore water because solid manganese oxides are buried below the redox boundary and subsequently undergo reduction, and (4) the equilibrium zone, where dissolved Mn^{2+} reaches its maximum.
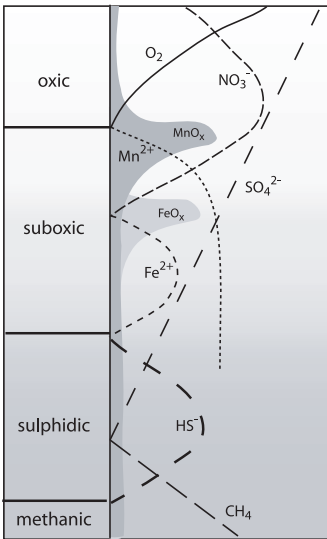

Fig. 1 Diagenetic zonation according to Berner (1981; left panel), including schematic pore water profiles of the involved oxidants and schematic authigenic Mn and Fe oxides are indicated by the shaded profiles (right panel).

Diagenetic overprinting eliminates primary sedimentary signals but contemporaneously secondary diagenetic signals provide information about the the driving processes and its magnitude (e.g. Wilson et al., 1985). These driving processes are often abrupt changes in sedimentation rate, oxygen level in the bottom water, and/or organic matter input. Post-depositional changes that often generate transient conditions of early diagenetic processes are particularly pronounced in (i) C_{org}-rich turbidites (e.g. Wilson et al., 1985; Thomson et al., 1993), (ii) sapropels of the eastern Mediterranean (e.g. Thomson et al., 1995, 1999; Van Santvoort et al., 1996), and (iii) glacial/interglacial transitions (e.g Thomson et al., 1996). Regarding (i) and (ii) post-depositional oxidation lead to oxidation of the upper sediment part, which relocated the redox-boundary into deeper sediment parts producing pronounced solid phase Mn double peaks. In fact, the concepts applied to the eastern Mediterranean sapropels were initially developed from the investigations on C_{org}-rich turbidites (e.g. Wilson et al., 1985) For the most recent sapropel S1 it was shown that bottom water was re-ventilated at the end of sapropel formation producing a Mn enrichment in the upper sediment part (e.g. Thomson et al., 1995, 1999). While sediment accumulation continued, oxygen penetrated further into the sediment producing a second Mn enrichment just above the Mn redox-boundary leading to the present day double Mn-peak feature (Fig. 2). The Mn double peaks that are found in glacial/interglacial transition sediments are produced by non-steady state diagenesis possibly starting as a downward prograding redox front
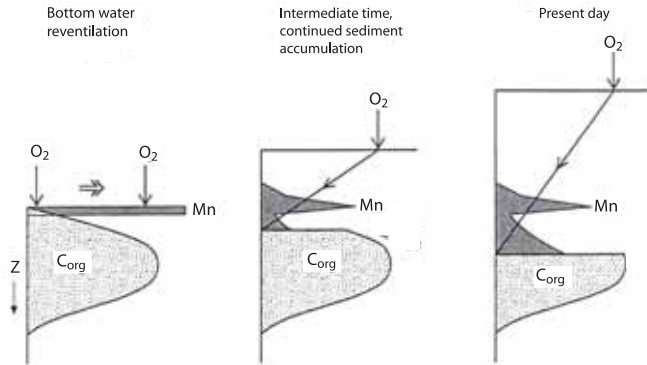
Fig. 2 Post-depositional oxidation of sapropel S1; left panel: bottom water re-ventilation leading to MnO_x enrichment in the upper sediment layer; mid panel: continued sediment accumulation and oxygen penetration; right panel: present day situation, further oxygen penetration and decomposition of C_{org} generated the typical Mn double peak feature (modified after Thomson et al., 1999).

(Colley et al., 1984) that over time and with distance to the surface decelerates and finally stops (Wilson et al., 1985) or even slowly moves upwards if e.g. the sedimentation rate or the C_{org} input increases (Fig. 3). Thus both cases are related to the same diagenetic processes but with slight differences in the more recent relative organic matter fluxes.
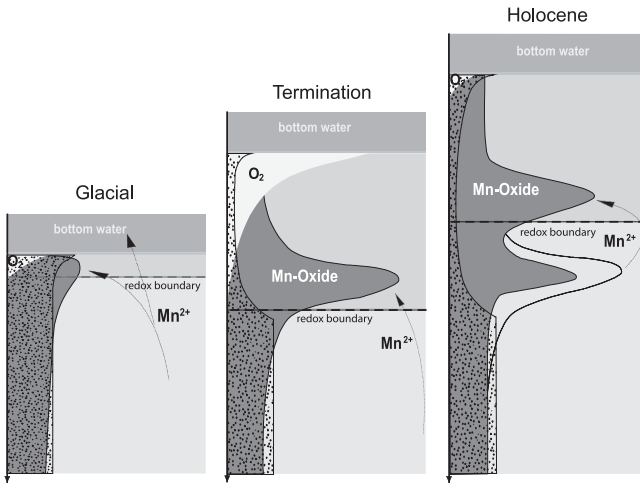
Fig. 3 Post-depositional relocation of the Mn redox-boundary in glacial/interglacial transition sediments; the development of the redox-boundary movement from the glacial (left panel) to the Holocene (right panel) is shown, including estimated O_2 pore water penetration, supposed Mn^{2+} fluxes, and simplified solid phase C_{org} (stippled) and Mn (dark grey) profiles (modified after Reitz et al., 2004a).

1.3 The Mediterranean and sapropel formation

The geodynamic evolution of the Mediterranean has been mainly regulated by the collision of the African plate with Eurasia and its subduction under the European margin. The formation of volcanic arcs, faults, and fractures on land as well as below the seafloor are the result of this ongoing process.

The Mediterranean Sea is a semi-enclosed basin; at present Atlantic Surface Water enters the western Mediterranean via the shallow strait of Gibraltar (284 m) and flows into the eastern Mediterranean via the Strait of Sicily (330 m) where it is transformed into Levantine Intermediate Water. Deep water formation occurs in the Northern Mediterranean areas such as the Gulf of Lions, the Adriatic (Pinardi and Masetti, 2000; Schlitzer et al., 1991) and the Aegean Sea (Roether et al., 1996; Josey, 2003). The anti-estuarine circulation makes it an oligotrophic sea, which is particularly

pronounced in the eastern basin.

The entire Holocene sediment record is characterized by generally light-brown C_{org}-poor sediments (0.1-0.2 wt.% e.g. Van Santvoort et al., 1996, 2002) as a result of the low productivity that are intercalated by C_{org}-rich sapropels. These sapropels are discrete olive-green to blackish layers containing between 2 and 30 wt.% of C_{org}, ranging in thickness between a few centimeters to decimeters (Kidd et al., 1978) that have been formed when the general circulation situation frequently changed.

During sapropel S1 formation the thermohaline circulation was weakened due to strong northern hemisphere insolation (i.e. during minimum precession) that resulted in elevated temperatures and consequently a pressure difference between land and ocean, leading to an intensified monsoonal flow (Rossignol-Strick et al., 1982; Rossignol-Strick, 1985). These conditions caused increased precipitation/runoff and so elevated input of freshwater and possibly nutrients. The enhanced freshwater supply reduced the surface water density leading to suppression or even elimination of deep water formation. Within a period of 23 kyr, these insolation variations are mainly controlled by the precession of the Earth's orbit (e.g. Hilgen, 1991; Lourens et al., 1992).

The exact mechanisms inducing sapropel formation are still under debate. In general two different scenarios or the combination of the two have been proposed to explain sapropel formation: (1) *anoxic preservation*: in this hypothesis primary production remains unchanged but anoxic bottom waters, possibly induced by stagnation of circulation and stratification of the water column, resulted in a better preservation of organic matter (e.g. Olausson et al., 1961; Tang and Scott, 1993); (2) *enhanced productivity*: this hypothesis assumes that enhanced primary production in the photic zone is the cause of increased organic matter accumulation and preservation within the sapropel horizons (e.g. Calvert, 1983; Pedersen and Calvert, 1990; Calvert and Pedersen, 1992).

1.4 Synopsis

The original geochemical signal in C_{org}-rich or formerly C_{org}-rich sediments is usually highly overprinted by a sequence of diagenetic processes depending on the amount of metabolizable organic carbon and the environmental conditions determining the redox potential. As mentioned above, biogenic barium can be used as a tracer for the original interval of C_{org}-rich sediment accumulation even when the latter has been largely removed during subsequent early diagenesis. To evaluate the reliability of the commonly used indirect (normative) approach to obtain the biogenic barium a comparison of the direct (by sequential extraction) and indirect (normative calculation) determination of biogenic barium and the detrital Ba/Al ratio has been carried out in **chapter 2**. The investigation of a range of different deep-sea sedimentary environments has shown that the detrital Ba/Al ratio is the crucial factor in the normative approach. The investigation and reliability of biogenic Ba as an indicator of paleoproductivity is essential as a basis for further research on sapropels and other C_{org}-rich sediments. For the studies of the following chapters it was important only to determine the boundaries of enhanced C_{org} accumulation, which could be determined from the Ba/Al ratio without further processing.

Diagenetic processes not only result in the oxidation of organic matter but also in the remobilization of mineral phases as Mn and Fe oxides. In **chapter 3** the interrelation of a redox-horizon due to non-steady state diagenetic conditions between the last glacial and the Holocene has been reconstructed by the combination of high resolution geochemical and rock-magnetic analyses.

The movement of the redox horizon led to the formation of conspicuous solid phase double peaks for Mn (compare Fig. 3) and Fe but also to definite rock-magnetic anomalies in the vicinity of the redox horizon referring to dissolution of magnetic mineral phases owing to suboxic diagenesis. The progress of the oxidation front could be reconstructed from the total Fe concentration and its relation to the ferromagnetic susceptibility. Furthermore, it was possible to reconstruct the small-scale advance of the redox-boundary by combining the ratio of ferromagnetic to total susceptibility with that of V/Al which displays the step-wise upwards movement of the redox front.

Such a Mn double peak feature as observed in chapter 3 is also known form eastern Mediterranean sapropel S1 sediments, where the double peaks developed due to post-depositional oxygen penetration and C_{org} burn-down. In this case the Mn redox boundary and consequently the actively forming Mn peak is the lower one that is located directly on top of the residual sapropel, whereas the upper passive one indicates the beginning of re-ventilation and consequently the end of sapropel formation. However, the magnitudes of the upper Mn peaks are much higher (>3 wt.%) within sediments from the eastern Mediterranean intermediate water depth interval (1000 to 2000 m). As indicated in **chapter 4** the change in redox conditions within the water column is responsible for this Mn-enrichment. The intermediate water depth interval preferentially gained Mn^{2+} that encounters oxygen and precipitates as MnO_x where anoxic and oxic waters meet, whereas the Mn^{2+} got diagenetically lost from the deeper sediments into the anoxic bottom waters. This hydrogenetic mechanism leading to the large diagenetic surficial peaks is supported by the incorporation of molybdenum and lithium at a fixed ratio to Mn in a similar manner as it was observed in other Mn-enriched oxic sediments.

However, the eastern Mediterranean manganese profile shapes can be diagenetically altered in areas that experienced substantial tephra or turbidite depositions such as those initiated by the Santorini explosive eruption in ~1630 B.C. This perturbation can be identified from the increased Sr/Ca and some element/Al ratio profiles. In **chapter 5**, the additional formation of Mn peaks i.e. near-surface caused by the loss of oxygen tension due to the surface blanketing and the consequent alteration of the characteristic double peak feature induced by MnO_x reduction at depth due to these perturbations is described.

The Sr/Ca ratio, however, is not only increased in the Santorini eruption related turbidites above sapropel S1 but also in the sapropel sediments itself. This enhanced Sr/Ca ratio is associated with the enhanced Sr-rich aragonite content in the sapropel that reaches levels of up to 40 wt.% at the Sirte continental slope (northern Africa). The observed high aragonite contents can not be attributed to pteropods that have low Sr contents but, could be explained by a near-costal source delivering Sr-rich aragonite skeletons or fragments thereof or by secondary diagenetic formation processes that are known to produce Sr-rich aragonite. In **Chapter 6** the relationship of decreasing aragonite values with distance to the African coast and water depth is emphasized. This relationship together with the SEM observation for the Sirte transect S1 sediments as well as the lack of variation in porosity, all point to a detrital/biogenic near-coastal source for the Sr-rich aragonite needles rather than a diagenetic one. However, a diagenetic contribution can not be excluded.

C h a p t e r   2

Biogenic barium and the detrital Ba/Al ratio: A comparison of their direct and indirect determination

Abstract

Biogenic barium concentrations obtained from a direct determination by a three-step sequential extraction procedure are compared to those obtained from the widely used indirect normative calculation based on total digestion. A comparison of the biogenic barium from the direct/sequential extraction and the indirect/normative calculation clearly shows that the detrital Ba/Al ratio is the critical factor in the normative approach, and that erroneous assumptions based on this ratio may introduce significant errors to the calculated biogenic barium. Overall, the crustal average Ba/Al ratio of 0.005 to 0.01 is much higher than our directly determined global average of 0.0037. This would result in an underestimation of the biogenic barium and thus of the primary productivity calculated using the Ba-flux obtained from the normatively calculated Ba record. Using our $(Ba/Al)_{det}$ ratio of ~0.0037 leads to normatively calculated biogenic barium results that are in reasonable agreement with the biogenic barium from sequential extraction for samples of the Atlantic, Pacific and Indian Ocean. Our directly determined 'regional' $(Ba/Al)_{det}$ ratios deviate from those calculated or assumed from hinterland ratios and our global average $(Ba/Al)_{det}$ is lower than the commonly reported. Therefore, in sediments with a significant terrigenous fraction, the sequential extraction technique is always required.

1. Introduction

Changes in productivity in the world's oceans strongly influence the biogeochemical cycle of carbon which in turn may affect atmospheric CO_2 concentrations and global climate. To trace back productivity in time, sedimentary archives of past productivity need to be studied and proxies representing fluxes of organic carbon, carbonate and opal are needed. They should reflect productivity in a linear fashion yet should show a better preservation than these primary indicators of biological processes. Several authors (e.g. Goldberg and Arrhenius, 1958; Chow and Goldberg, 1960; Church, 1970; Bishop, 1988) have recognized sedimentary biogenic barite ($BaSO_4$) as a potential proxy to reconstruct past variations of surface ocean biological productivity. As one of the more refractory chemical species under oxic conditions, biogenic barite is strongly linked to export

productivity and exhibits more predictable preservation patterns than direct productivity indicators (Dymond et al., 1992, Van Santvoort et al., 1996).

The formation mechanism of barite in undersaturated seawater is still poorly understood. However, it is generally assumed that barite is primarily precipitated in micro-environments due to sulphate release from decaying organic components (Dehairs et al., 1980; Bishop, 1988) or due to sulphate and barium release by dissolution of celestite derived from acantharia (Bernstein et al., 1992). Moreover, Tendal (1972) reported active intracellular formation of barite in benthic xenophyophores, yet how this influences estimates of biogenic barite formation is still unknown. As these barite forming processes take place well below the photic zone a relation between water depth and barium concentration in the sediment is obvious and has been shown by several investigations (e.g. von Breymann et al., 1992) on continental margin sediments. Dymond et al. (1992) developed an algorithm based on sediment trap data to link biogenic barium accumulation rates in sediments to export production from the water column. This algorithm was applied by several other authors and was subsequently modified by François et al. (1995), Nürnberg (1995), Dehairs et al. (2000) and Pfeifer et al. (2001).

Biogenic barite is largely preserved in deep-sea sediments, which is its essential advantage as a proxy for (paleo)productivity. Dymond et al. (1992) assumed an average preservation factor of 30% for Atlantic and Pacific Ocean sediments, Paytan and Kastner (1996) archived the same factor for Pacific Ocean sediments and Schenau et al. (2001) stated a low factor (0-10%) for Arabian Sea sediments; these factors are much higher than those for the preservation of organic carbon (<0.1%; Berger et al., 1989; Martin et al., 1991) or carbonate (about 10%; Archer, 1996; Milliman et al., 1999). However, since the preservation of biogenic barium is a function of sediment mass accumulation rate there will be regional differences (Dymond et al., 1992). Dissolution of biogenic barium is believed to end after burial in oxic and suboxic sediments owing to the supersaturation of interstitial waters with respect to barite (e.g. Gingele and Dahmke, 1994). Yet, accumulation of authigenic barite in consequence of diagenesis has been established in some continental margin settings of intensive high productivity (Torres et al., 1996, Kasten et al., 2001).

The biogenic barium contents are commonly calculated normatively as the difference between the bulk Ba concentration and the estimated detrital contribution of the Ba associated with alumosilicates (Dehairs et al., 1980; Dymond, 1981; Dymond et al., 1984). However, this approach might introduce major errors for sedimentary environments that receive large quantities of detrital material (Dehairs et al., 1980; Dymond et al., 1992; Fagel et al., 1999; Gingele et al., 1999), such as the Chilean continental slope (>80%; Hebbeln et al., 2000). To avoid this problem, Klump et al. (2000) analyzed riverbed samples from coastal Chile sediments to determine regional detrital Ba/Al ($(Ba/Al)_{det}$) ratios. An alternative direct detection of biogenic barium and of the $(Ba/Al)_{det}$ ratio by sequential extraction (Schenau et al., 2001; Rutten and De Lange, 2002) avoids such source of error.

In this study we apply this direct method (sequential extraction) to samples representing two detrital Ba end-member examples. The directly obtained biogenic barium values and the $(Ba/Al)_{det}$ ratios will be compared to those obtained from the indirect method (normative calculation) of biogenic barium and current literature values for the $(Ba/Al)_{det}$ ratios (see methods section).

2. Materials and methods

The surface sediment samples (0-1 cm) were retrieved in the Atlantic Ocean during RV Meteor cruises M6/6 to M34/6 (GeoB 1041 to GeoB 3724) and in the Pacific Ocean during RV Sonne cruise SO-102 (GeoB 3301 to GeoB 3377) by multicorer (Fig. 1).

To each of the 22 samples a total digestion and a sequential extraction were applied (for GeoB 1119, only sequential extraction). For both procedures five sample duplicates, two international standards (SO1 and SO3) and one in-house standard were processed for monitoring precision (by duplicates) and accuracy (by standards) of total digestion, sequential extraction and subsequent analyses. Bulk concentrations of Ba and Al were determined after total digestion of 125 mg freeze-dried and homogenized sediment in a 2.5 ml 3:2 mixture of $HClO_4$ (60%) and HNO_3 (65%), and 2.5 ml HF (40%) at 90°C. After evaporation of the solution close to dryness at 190°C, the residue was dissolved in 25 ml HCl (4.5%) and homogenized for two hours at 90°C. Analysis of elements within the resulting solution was carried out by inductively coupled plasma atomic emission spectrometry (ICP-AES Optima 3000, Perkin Elmer).

The different particulate Ba phases were determined by a sequential extraction technique (after Schenau et al., 2001; Rutten and de Lange, 2002). This sequential extraction technique differs decisively from that of Cardinal et al. (1999) and Paytan et al. (1993) as it commences with the extraction of barite instead leading off with an acid-decalcification step risking pre-dissolution of
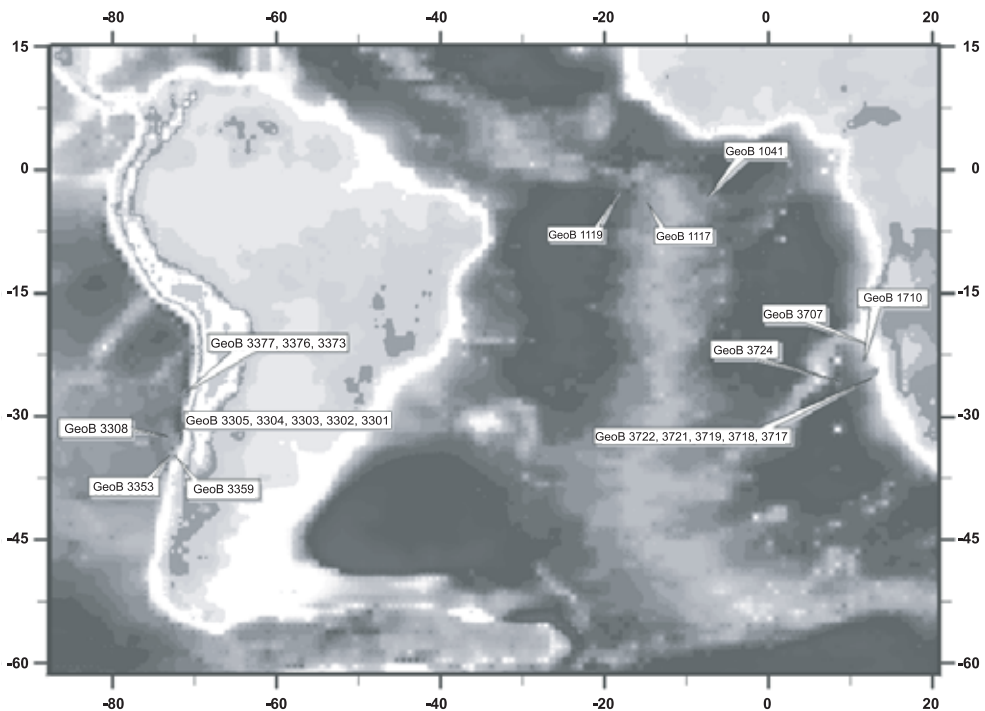

Fig. 1. Multicorer sampling locations in the Atlantic and Pacific Ocean used in this study.

biogenic barium. It has been shown by Cardinal et al. (1999) that barite dissolves already in diluted acids. Rutten and de Lange (2002) showed that the extraction method we used is a truly separation of barite from other Ba-phases (99.4 % recovery of barite) in the sediment.

For the sequential extraction, 125 mg of freeze-dried and homogenized sediment was successively leached with several different solvents (Table 1). In the first step with 2 M NH_4Cl (pH 7) the barite

Table 1. 3-step sequential extraction procedure after Schenau et al, (2001) and Rutten (2001) who also give futher details of the procedure.

Step	Ba phase extracted	Extractant
1	Barite (Ba_{bar})	8 x 25 ml 2 M NH_4Cl (pH 7)
2	Ba associated with Mn/Fe oxides (Ba_{ox})	25 ml solution of 0.15 M Na-citrate & 0.5 M $NaHCO_3$ (pH 7.6) plus 1.125 g Na-dithionite
3	Ba associated with alumosilicates (Ba_{det})	2.5 ml of a 3:2 mixture of $HClO_4$ and HNO_3, and 2.5 ml HF

(Ba_{bar}) – mainly biogenic barium – is extracted from the sediment. This first step was repeated eight times, but analysis of the individual extraction solutions shows that for all samples no more extractable barium is in the solvent after the fourth time. The second step leaches all Ba associated with iron or manganese oxides (Ba_{ox}), and the third step dissolves the remaining Ba associated with all other compounds of the sediment. The extractants were analyzed by ICP-AES. The overall precision of the measurements was better than 3% and the accuracy for the samples of total digestion was always in the permitted range of the standards used. Only the results from the first step (Ba_{bar}) for which the relative error is <2% and the third step (Ba_{det}) for which the relative error is <5% will be reported, since the second step has not extracted measurable Ba concentrations. Barium associated with carbonates, potentially extracted in the first step, will be neglected since concentrations in carbonates are very low (~30 ppm; Lea and Boyle, 1989). For the Pacific surface samples the procedure was carried out two times, first on decarbonated samples (with the exception of GeoB 3359 & 3353) and secondly on original samples. The Ba_{bio} (CFB) of the original samples is on average 5% higher than the Ba_{bio} of the acid-decarbonated samples. This refers to a loss of biogenic barium due to the treatment with a weak acid as it has been stated by Cardinal et al. (1999).

The biogenic/excess Ba concentration (Ba_{excess}/Ba_{bio}) was calculated by the following equation (normative method):

$$Ba_{bio} = Ba_{excess} = Ba_{tot} - (Al * (Ba/Al)_{det}) \qquad (1)$$

where Ba_{excess} is the biogenic barium (mainly barite), Ba_{tot} and Al are the bulk concentrations, respectively, and $(Ba/Al)_{det}$ signifies the reference Ba/Al ratio used for detrital correction. The detrital ratio is usually derived from the average crustal composition varying between 0.005 and 0.01 (e.g. Turekian and Wedepohl, 1961; Rösler and Lange, 1972).

We are aware of the ongoing discussion whether Al or rather Ti should be used as a terrigenous denominator (e.g. Murray and Leinen, 1996). However, this study is a comparison of two methods, one of which using Al is commonly applied. To permit comparison to published data, we, therefore apply Al as a terrigenous reference. The bulk Al to Ti ratio of all analyzed Atlantic and Pacific surface sediments result in a correlation coefficient of $r^2 = 0.981$, and for the detrital fraction (third sequential

extraction step) $r^2 = 0.975$, thus no major difference in conclusion would be obtained if Ti instead of Al were used as a denominator.

3. Results

The barium carrier phases of the analyzed Atlantic and Pacific surface sediments are mainly barite and alumosilicates (Table 2). Barium associated with iron and manganese oxides was below detection limit (<10 μg/kg) and is not listed in the table.

3.1 The low detrital Ba end-member (Atlantic Ocean surface sediments)

Sequential extraction results for biogenic barium range from 240 mg/kg in the equatorial region to 1298 mg/kg in the Cape Basin depending on export production, water depth, and the position of the lysocline reflecting differences in the sedimentation rate and calcite dissolution. The bulk barium concentration obtained by total digestion ranges from 209 mg/kg in the equatorial region to 1358 mg/kg in the Cape Basin and the detrital barium obtained by the third step of the sequential extraction ranges from below the detection limit (10 μg/kg) to 218 mg/kg. The Al concentration obtained by the third step of the sequential extraction ranges from 1.7 to 53.1 g/kg (Table 2; the Al concentrations from the third sequential extraction step differ from the Al concentrations obtained by total digestion by about 25%). The main carrier phase for barium in these parts of the Atlantic Ocean is biogenic barium, which makes up about 95% of the total barium. Thus the bulk barium is almost equal to the biogenic/excess barium.

The investigated sediments have average $CaCO_3$ contents of approximately 60 weight % (Müller/Wagner, unpublished data) and biogenic barium is in consequence highly diluted by carbonate. Sedimentation rates (Holstein, 2002; Pfeifer, 1998) range from 5-20 cm/ka above the CCD and are below 0.5-1 cm/ka below the CCD. These differences in sedimentation rates obscure the expected biogenic barium to detrital barium relationship with increasing water depth (Fig. 2).
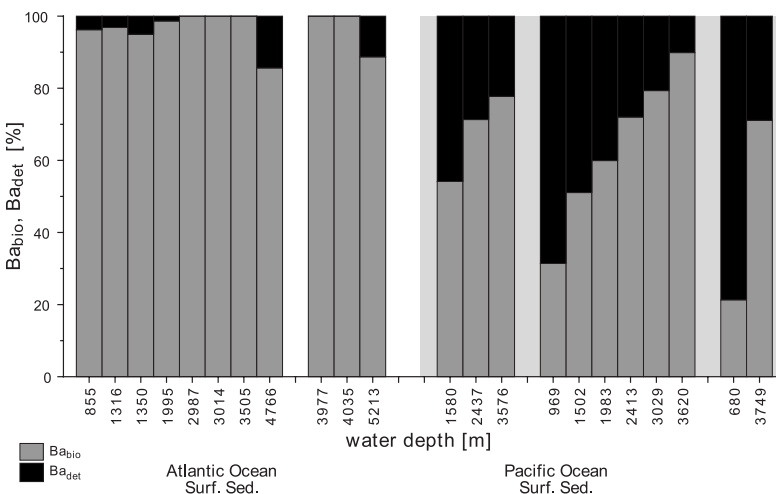

Fig. 2 Sequential extraction results from the analyzed Atlantic and Pacific Ocean surface sediments in % of total Ba concentration.

Table 2. Sample locations of the multicorer and analyzed data

Surface sediments	Location	Water depth [m]	Latitude	Longitude	Ba_bar [mg/kg]	Ba_bar [%]	Ba_tot [mg/kg]	Ba_det [mg/kg]	Al_det [g/kg]	(Ba/Al)_det [g/g]	'regionally averaged (Ba/Al)_det	Ba_excess[a] [mg/kg]
GeoB 3717		855	24°50.0'S	13°21.0'E	643	96	667	25	11.6	0.0022		552
GeoB 3718		1316	24°53.7'S	13°09.6'E	967	97	987	32	12.2	0.0026		1026
GeoB 3707		1350	21°38.0'S	12°11.6'E	1027	95	1080	54	17.2	0.0031		1081
GeoB 3719	Cape	1995	24°59.7'S	12°52.3'E	929	99	931	13	8.9	0.0014		783
GeoB 1710	Basin	2987	23°25.9'S	11°42.2'E	992	100	967	<d.l.	6.2	-		860
GeoB 3721		3014	25°09.1'S	12°24.0'E	979	100	950	<d.l.	6.3	-		843
GeoB 3722		3505	25°15.0'S	12°014'E	645	100	623	<d.l.	3.7	-		520
GeoB 3724		4766	26°08.3'S	08°55.7'E	1298	86	1294	218	53.1	0.0041		1063
GeoB 1117	Equat.	3977	03°48.5'S	14°43.2'W	240	100	218	<d.l	1.7	-		194
GeoB 1041	region	4035	03°28.2'S	07°35.8'W	268	100	241	<d.l	2.5	-		249
GeoB 1119		5213	02°59.9'S	18°22.7'W	938	89	996[b]	119	43	0.0028	0.0027[c]	77
GeoB 3373	Transect	1580	27°30.1'S	71°12.4'W	372	53	689	315	60.5	0.0052		200
GeoB 3376	27.5°	2437	27°28.0'S	71°21.7'W	703	74	999	283	56.4	0.0050		529
GeoB 3377		3576	27°28.0'S	71°31.5'W	1078	79	1447	309	60.6	0.0051	0.0051[c]	962
GeoB 3301		969	33°08.8'S	71°58.9'W	141	31	453	307	71.7	0.0043		239
GeoB 3302		1502	33°13.1'S	72°05.2'W	303	52	596	290	69.2	0.0042		330
GeoB 3303	Transect	1983	33°12.4'S	72°10.5'W	413	62	696	276	69.5	0.0040		543
GeoB 3304	33°	2413	32°53.4'S	72°11.5'W	680	73	959	264	66.4	0.0040		807
GeoB 3305		3029	32°51.1'S	72°25.4'W	969	80	1288	252	68.1	0.0037		1187
GeoB 3308		3620	33°07.9'S	73°44.9'W	1627	93	1887	183	51.2	0.0036	0.0039[c]	1818
GeoB 3359	Transect	680	35°13.0'S	72°48.5'W	69	25	340	236	75.1	0.0034		-
GeoB 3353	35°	3749	35°15.0'S	73°34.6'W	582	70	851	255	71.3	0.0033	0.0034[c]	358

Atlantic Ocean (rows GeoB 3717–GeoB 1119); Pacific Ocean (rows GeoB 3373–GeoB 3353).

Key: Ba_bar (biogenic barium; sequential extraction step 1), Ba_tot (bulk; total digestion), Ba_det (detrital barium; sequential extraction step 3), Al_det (detrital aluminum fraction; sequential extraction step 3), (Ba/Al)_det (detrital Ba/Al ratio derived from Ba_det divided by Al_det), Ba_excess (excess barium; Klump et al., 2000; Pfeifer et al., 2001). <d.l. (below the detection limit of 10 µg/kg): [a] results from Klump et al., 2000 and Pfeifer et al., 2001; [b] data from Pfeifer et al., 2001; [c] average of results from column (Ba/Al)_det.

3.2 The high detrital Ba end-member (Pacific ocean surface sediments)

Biogenic barium results obtained by sequential extraction range from 69 mg/kg to 1627 mg/kg. The bulk barium results obtained by total digestion range from 340 mg/kg to 1887 mg/kg and the detrital barium obtained by the third step of the sequential extraction ranges from 183 mg/kg to 315 mg/kg. The Al also obtained by the third step of the sequential extraction ranges from 51.2 g/kg to 75.1 g/kg the average difference to Al concentrations by total digestion is 7% (Table 2). The ratio of the biogenic to detrital carrier phase of barium is generally about 60:40 for all analyzed samples. However, considering the three transects as described by Klump et al. (2000), the regional ratios of biogenic to detrital barium a significantly different. The noticeable dissimilarity between the three transects, that all lie within the Chile Costal Current (CCC) and that of the Gunther Undercurrent (GUC), reflects the spatial variation of the biogenic and detrital barium phase, which is clearly expressed in the distinct decrease of the $(Ba/Al)_{det}$ ratio from 27°S to 35°S. The sediments are dominated by terrigenous material and have low $CaCO_3$ concentrations of about 11% (Hebbeln et al., 2000). In consequence, the general trend of biogenic barium increase with water depth and detrital barium decrease with increasing distance from land is well displayed (Fig. 2).

4. Discussion

4.1 Sequential extraction vs. normative calculation

For the low detrital Ba end-member (Atlantic) sediments the relative proportions of biogenic barium are similar for direct determination by sequential extraction and for the indirect method by normative calculation using a detrital Ba/Al factor of 0.004 (Pfeifer et al., 2001; Fig. 3a). The $(Ba/Al)_{det}$ ratio of 0.004, which is lower than the average crustal value, has been introduced by Gingele and Dahmke (1994) for Atlantic sediments north of 30°S. Nevertheless, the biogenic barium data obtained by normative calculation are systematically about 15% lower (except of GeoB 3718 and GeoB 3707) than those obtained by sequential extraction indicating an overestimation of the $(Ba/Al)_{det}$ ratio. If calculating the biogenic barium with the $(Ba/Al)_{det}$ ratio determined from sequential extraction the accordance is better (calculated values are about 6% lower, except GeoB 3718 and GeoB 3707; Fig. 3a).

Considering the high detrital Ba end-member (Pacific) biogenic barium results, the directly and the indirectly determined concentrations differ distinctively from each other (Fig. 3b). In the 33°S transect the calculated concentrations (Klump et al., 2000) are on average 27% higher than the directly obtained concentrations indicating an underestimation of the detrital Ba fraction. For all other samples the calculated concentrations (Klump et al., 2000) are on average 44% lower than those of sequential extraction indicating an overestimation of the detrital Ba fraction.

Calculating the biogenic barium normatively, using the regional $(Ba/Al)_{det}$ ratios determined from the sequential extraction, yields results that are in good accordance with the directly determined biogenic barium from sequential extraction (Fig. 3a & b).

4.2 The detrital (Ba/Al) ratio of deep ocean sediments

The $(Ba/Al)_{det}$ ratio is a crucial factor in the normative approach as the regional $(Ba/Al)_{det}$ ratios may vary widely and usually are not available. Until recently it was difficult to confidently determine the $(Ba/Al)_{det}$ ratio directly and an 'average' crustal Ba/Al ratio ranging from 0.005 to 0.01 was
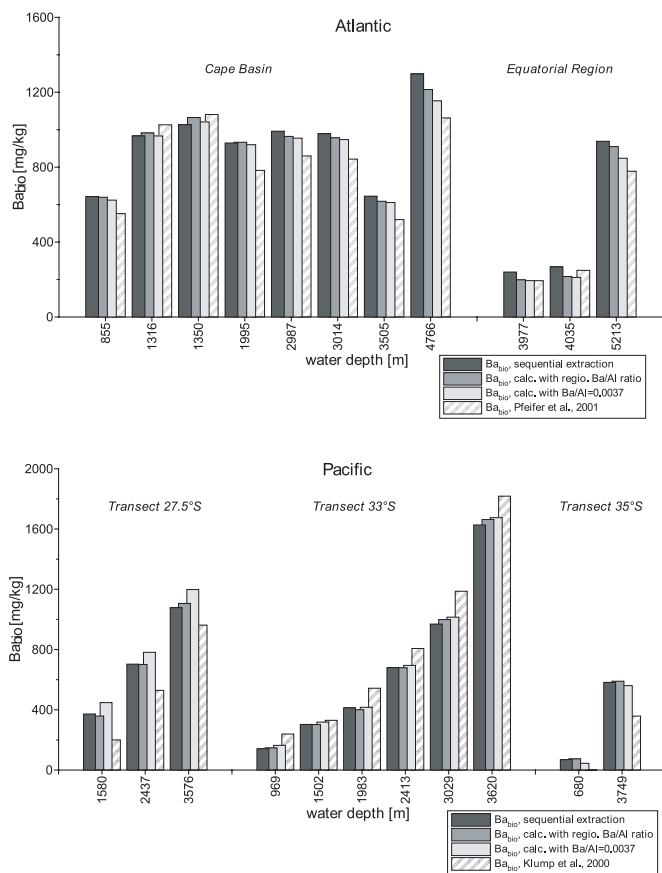
Fig. 3a & b. Comparison of sequentially extracted biogenic barium (Ba$_{bio}$) and normatively calculated (using different (Ba/Al)$_{det}$ ratios and data from Klump et al., 2000 and Pfeifer et al., 2001) concentrations in surface sediments of different regions and water depths.

commonly used (Table 3). Regional estimates for the (Ba/Al)$_{det}$ ratios in marine sediments are reported in several studies (e.g. Emeis, 1993; Gingele and Dahmke, 1994; Rutsch et al., 1995; Dean et al., 1997; Nürnberg et al., 1997; Klump et al., 2000; Pfeifer et al., 2001; and Rutten, 2001; see also Table 4). Using an estimated (Ba/Al)$_{det}$ ratio in the normative calculation potentially introduces large errors into the determination of Ba$_{excess}$. According to Dymond et al. (1992), the uncertainty in the (Ba/Al)$_{det}$ ratio could produce an error of ±15% in samples with 30% detrital barium, an error of ±50% in samples with 50% detrital barium and almost a factor of 10 uncertainty with 75% detrital barium in the sample.

Klump et al. (2000) determined the detrital Ba/Al ratio for the normative calculation by analyzing Chilean river samples. The (Ba/Al)$_{det}$ ratios they used are for three transects: 27.5°S 0.0073 (this study: 0.0051), transect 33°S 0.0033 (this study: 0.0039), and transect 35°S 0.0028 (this study: 0.0034; Table 4). Our results clearly show that the detrital component of the continental slope sediments has a regionally different composition depending on more than just the source material and weathering processes in the hinterland. Lamy et al. (1998) obtained a distinct decrease in grain-size of the surface sediments from the northernmost transect (coarse silt) to the southernmost transect (medium to fine grained silt) indicating notable decrease in aeolian sediment supply from North to South of this area. This can most likely be explained by the CCC influence. Variability in this current system may be too complex to permit such a straightforward explanation. For example, predominant and possibly variable current systems resulting in alternate source material and the mixing thereof, as

well as bathymetry may influence particularly the relationship between the biogenic and detrital barium fraction. Mixing of material from different sources may readily explain the differences observed in $(Ba/Al)_{det}$ for hinterland and continental slope within each transect (Fig 3b). The deviation between extrapolated and directly determined $(Ba/Al)_{det}$ results demonstrates that the normative approach has to be applied with care to determine the biogenic barium for calculating (paleo)productivity using average $(Ba/Al)_{det}$. In sedimentary environments where the detrital phase makes up 40% or more, as that is the case in the Chilean sites, the sequential extraction should be used to obtain valid biogenic barium concentrations.

Table 3. Average crustal/shale Ba/Al ratio estimates.

Area/material	Detrital Ba/Al ratio	Reference
Ba/Al ratios abundance of alumosilicate detritus	0.005 – 0.01	Taylor and McLennan, 1985; Taylor, 1964; Rösler and Lange, 1972
shale	0.0073	Turekian and Wedepohl, 1961
shale	0.006	Krauskopf, 1967
average post-Archean shale	0.0065	Taylor and McLennan, 1985
crust	0.0052	Taylor, 1964
upper continental crust	0.0068	Taylor and Mc Lennan, 1985; Wedepohl, 1995
upper continental crust	0.0086	Wedepohl, 1995
continental crust	0.0073	Dymond et al., 1992
global	0.0075	Wedepohl, 1991
	0.0065	Bowen, 1979
	0.0061	

Using the sequential extraction method it is now feasible to directly determine the barite fraction (Ba_{bar}) and the detrital barium fraction (Ba_{det}). The results of the third step of the sequential extraction thus allow the calculation of the ratio of barium to Al $(Ba/Al)_{det}$ in the sediment. Although the sequential extraction cannot distinguish biogenic barite from that of hydrothermal origin (Schenau et al., 2001), it is unlikely that significant levels of hydrothermal barite would occur in the samples analyzed in this study. In fact, it is usually anticipated that hydrothermal barite accumulation is closely restricted to areas of hydrothermal activity alone (Dymond et al., 1992).

In the case of Indian Ocean sediments an average $(Ba/Al)_{det}$ ratio of 0.0039 was obtained for Arabian Sea sediments with the same sequential barium extraction (Schenau et al., 2001). At the sites close to the continents, particularly at the steep slope area off Oman, $(Ba/Al)_{det}$ values were higher (~0.0043) than in the deep-sea areas (~0.0033). Their results emphasizes our observation that at continental margins the geological setting and oceanographic situation is more complex and thus require a much more attentive investigation with respect to the determination of biogenic barium.

The newly obtained average $(Ba/Al)_{det}$ ratio for "the Pacific" is 0.0041, for "the Atlantic" it is 0.0031 (excluding data below detection limit; including data from Pfeifer et al., submitted) and for "the Indian" it is 0.0039 (Arabian Sea surface sediments; after Schenau et al., 2001). To obtain a new global average $(Ba/Al)_{det}$ ratio, based on sequential extraction results available hitherto, we calculated the average of the regional $(Ba/Al)_{det}$ ratios of the two detrital Ba end-member examples of this study, the average $(Ba/Al)_{det}$ of Arabian Sea surface sediments, and that of South Atlantic Ocean surface

Table 4. Regional estimated and calculated average detrital Ba/Al ratios

Region	Detrital Ba/Al ratio (estimated)	Detrital Ba/Al ratio (analyzed*)	Reference
Atlantic			
northern Argentine Basin	0.0048		Pfeifer et al., 2001
Southern Argentine Basin	0.006		Pfeifer et al., 2001
Atlantic ocean north of 30°S	0.004[1]	0.0027[a]	[1]Gingele and Dahmke, 1994; [a]this study
Southern Ocean Atlantic sector	0.0067		Nürnberg et al. 1997
Atlantic Ocean off West Africa (Congo Fan)	0.0045		Rutsch et al., 1995
Eastern Mediterranean Sea: oxic sediment	0.003		Rutten, 2001
organic rich sediment	0.0032		
Pacific			
Northern California shelf	0.007		Dean et al., 1997
Chilean continental slope:			
27.5°S	0.0073[2]	0.0051[a]	[2]Klump et al., 2000 ;
33°S	0.0033[2]	0.0040[a]	[a] this study
35°S	0.0028[2]	0.0034[a]	
Indian			
Arabian Sea	0.0035[3]	0.0039[b]	[3]Emeis, 1993; [b] after Schenau et al., 2001

*analyzed using the extraction method as described in this study.

sediments of the Argentine Basin and the Angola Basin (0.0035; Pfeifer et al., submitted). This leads to a global average of 0.0037.

The results of biogenic barium calculated with the global average are in good accordance with the sequential extraction results (91%). In comparison, the results calculated with the regional ratios for $(Ba/Al)_{det}$ of this study show the best agreement with that from sequential extraction (96%). The biogenic barium of Klump et al. (2000) and Pfeifer et al. (2001) are only 76% of that obtained with the sequential extraction (Fig. 3a&b). Thus, using the archived "global" average of this study leads to 15% better results. If rapid results are to be obtained using the normative approach, then for the investigated sedimentary environments a $(Ba/Al)_{det}$ ratio of 0.0037 gives the most convincing results.

4. Conclusions

Barium in marine sediments occurs mainly as biogenic barite or is associated with alumosilicates. Applying the commonly used normative calculation to determine biogenic barium, the $(Ba/Al)_{det}$ ratio is the crucial factor of the equation. In our comparison of samples from a range of deep-sea sedimentary environments the following aspects and implications can be summarized:

1. With the direct sequential extraction method it is now possible to obtain biogenic barite results without the common uncertainties, associated to the commonly used indirect normative approach.

2. The $(Ba/Al)_{det}$ ratio determined 'directly' from the sequential extraction deviates significantly from the average crustal ratio of 0.005-0.01 but also differs from that of the direct hinterland in case of the analyzed Pacific surface sediments.

3. An average factor of 0.0037 might be applicable on a global scale if fast results are needed. However, application of even such improved average $(Ba/Al)_{det}$ factor may introduce large errors in the normative attempt in particular in sediments with high detrital background with unknown and potentially variable $(Ba/Al)_{det}$. In this case a sequential extraction is indispensable.

A future evaluation of the $(Ba/Al)_{det}$ ratio and the biogenic barium via sequential extraction is required to assess its full potential and limitations for palaeoceanographic studies.

Acknowledgements

A combined geochemical and rock-magnetic investigation of a redox horizon at the last glacial/interglacial transition

Abstract

A high-resolution study of an active Fe^{2+}/Fe^{3+} redox horizon has been carried out on sediments of the central equatorial Atlantic. The multidisciplinary approach combining geochemical and rock-magnetic parameters gives evidence of the interrelation of the redox horizon with the last change from glacial to interglacial conditions (T1). Distinct enrichments of redox-sensitive elements (Mn, Fe, V, and U) reveal a characteristic depth-sequence, indicating non-steady-state diagenetic conditions caused by a decrease in productivity and an increase in oxygen content in the bottom water during T1 and a reversal during the Holocene. Thus, the redox boundaries first moved down into the sediment and subsequently upwards. The movement of the redox boundaries led to the development of conspicuous double peaks for Fe and Mn. The reconstruction based on geochemical data is supported by susceptibility and magnetization measurements of the sediments displaying well-defined anomalies in the vicinity of active and paleo-redox boundaries. The combination of geochemical and rock-magnetic parameters, like the ferrimagnetic susceptibility, and total Fe concentration (χ_{tot}/Fe) are suitable for characterizing distinct zones of dissolution and precipitation of ferromagnetic mineral phases (e.g. magnetite). Moreover, the small scale movement of the Fe^{2+}/Fe^{3+} redox-boundary, could be traced in detail by overlaying the peak-shape pattern of V/Al and of χ_f/χ_{tot}.

1. Introduction

During the Quaternary the interaction of atmospheric and oceanic circulation patterns, which controls the productivity and preservation of organic matter, changed repeatedly in response to orbitally forced glacial/interglacial cycles (Wagner, 1999; Berger et al., 1994; Imbrie and Palmer Imbrie, 1998). Deep-ocean sediments are archives for such climate variations, which can be revealed by the analysis of various properties determined by geochemical, geophysical or sedimentological methods (cf. Fischer & Wefer, 1999). In particular, geochemical and rock-magnetic investigations of marine sediments can give useful information on long-term variation of a number of climate-driven processes (e.g. accumulation of organic carbon, oxygen content in bottom water etc.).

Abrupt changes of organic matter input and/or the oxygen level in the bottom water are shown

to generate transient conditions of early diagenetic processes (Wilson et al., 1985). Diagenetic processes may not only overprint primary sedimentary signals, but can also generate secondary diagenetic signals contributing valuable information about the magnitude and type of the driving processes (e.g. Wilson et al., 1985). Evidence for changes in the sedimentary and depositional environment are particularly pronounced in the following sediment sequences: (1) turbidites (e.g. Prahl et al., 1989; Thomson et al., 1993), (2) sapropels of the Mediterranean Sea (e.g. De Lange et al., 1989; Thomson et al., 1995; Van Santvoort et al., 1996), and (3) glacial/interglacial transitions (e.g. Thomson et al., 1996).

Environmental changes like increases in productivity and sedimentation rate and/or a reduction in deep-water circulation may result in oxygen deficiency in the bottom water, thus enhancing the burial and preservation of non-oxidized organic matter in deep-sea sediments (Arthur et al., 1984; Emerson and Hedges, 1988; Tyson and Pearson, 1991). Primary productivity and the preservation of organic matter in sediments of the modern equatorial Atlantic is influenced by changes in oceanic and atmospheric circulation patterns. In sediments of the tropical and equatorial Atlantic cyclic formations of organic-rich layers were formed from Pleistocene to recent during glaciations by enhanced primary productivity and better preservation of organic matter due to the reduction of bottom water exchange (see summary by Funk et al., 2003a, and references therein).

The diagenetic remineralization of the buried organic matter occurs via a sequence of pathways catalyzed by different types of microorganism, which use dissolved oxygen followed by a sequence of secondary oxidants. In order of decreasing energy supply these are nitrate and/or Mn-oxides, Fe-oxides and sulfate (Froelich et al., 1979; Curtis, 1983), and their use creates a change in redox conditions. This change in redox conditions is usually accompanied by a change in sediment color from brown to grey. In the following, we present a brief overview of the characteristic geochemical and rock-magnetic patterns that result from this diagenetic sequence.

1.1 Geochemical and rock-magnetic characteristics as proxies for diagenetic overprinting

In marine sediments Lyle (1983), König et al. (1997, 1999), and Robinson et al. (2000) attribute the color change from reddish/brownish in the oxic part to grayish/greenish in the anoxic part to a redox change of iron, which is bound to clay minerals. The enrichment and distribution of redox-sensitive elements around the color transition is controlled by the type and course of the diagenetic processes. Consequently, the element enrichments in the vicinity of a color change represent secondary authigenic formations. The behavior of redox-sensitive elements is thought to be indicative for the oxygen content of the bottom water during the formation of the facies (Calvert and Pedersen, 1993).

The penetration depth of oxygen into the sediment is controlled by the accumulation rate and reactivity of organic carbon and the oxygen content of the bottom water. A change in any of these parameters will result in a change of redox conditions in the sediment. Under oxic conditions manganese and iron form insoluble oxides, whereas vanadium and uranium are present as soluble anions. Under anoxic conditions the latter two are reduced to insoluble species of lower charge (Mangini et al., 2001), but the former two are mobilized.

Variations in the rock-magnetic characteristics of marine sediments are mostly climate-driven (Bloemendal et al., 1988; Frederichs et al., 1999). Changes in concentration and composition of magnetic materials are mainly a result of a change in the source area and transport mechanism but are

also affected by secondary processes like reductive diagenesis and production of biogenic magnetite (Bloemendal et al., 1989, 1992; Van Hoof et al., 1993; Tarduno and Wilkison, 1996; Passier et al., 1998). Since the amount of magnetic minerals in marine sediments is very low, they have a high potential to display even the slightest changes in the geochemical environment.

In this study we compare the depth of the color transition and the glacial/interglacial transition in a core from the central equatorial Atlantic. We use a high resolution multidisciplinary approach, combining geochemical and rock-magnetic results. This has enabled us to determine the fixation of the Fe-redox transition at the last glacial/interglacial transition. In addition, we have reconstructed the development and the movement of the Fe^{2+}/Fe^{3+}-redox boundary in response to climate change. By the aforementioned reconstruction we developed a better knowledge of the climate-induced environmental changes effective to sediments located on the border of an upwelling area.

2. Materials and methods

2.1 Core location and stratigraphy

Gravity core GeoB 2908-7 with a total length of 10.94 m was recovered during Meteor cruise M29/3 in the central equatorial Atlantic (00°06.4'N, 23°19.6'W) in the area of the Central Equatorial Fracture Zone from 3809 m water depth (Fig. 1). The Central Equatorial Fracture Zone System is known as the current pathway for the Antarctic Bottom Water (AABW) from the western to the eastern Atlantic Ocean (Mercier et al., 1994). The core station is located in the Equatorial Divergence zone, a region of intensified productivity due to northeast trade wind controlled surface currents. Additionally, this area receives a strong eolian input from the Saharan dust plume, raining out within the ITCZ (Inter Tropical Convergence Zone; Fig. 1). According to Sarnthein et al. (1981)
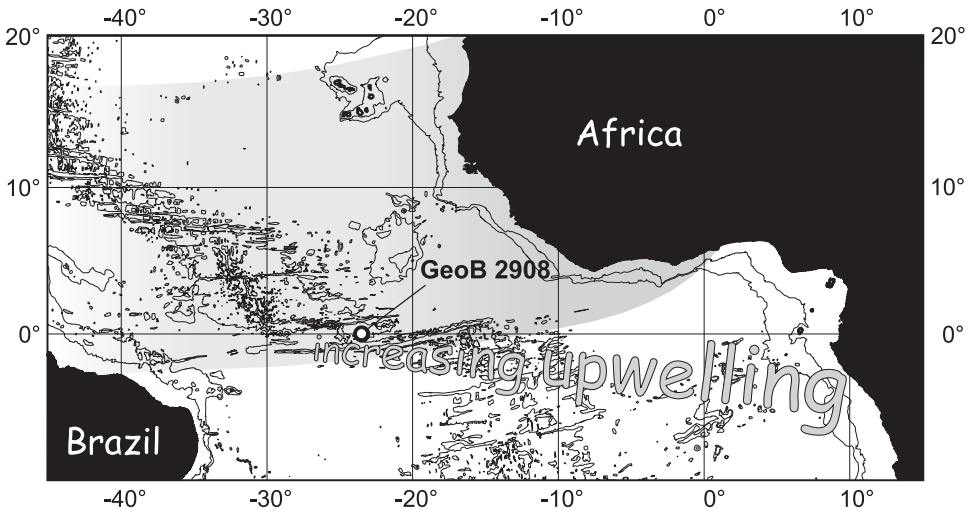

Fig. 1. Map of the equatorial Atlantic Ocean showing the location of gravity core GeoB 2908-7. Upwelling related to the Equatorial Divergence intensifies eastward, increasing productivity and organic matter accumulation. The shaded area indicates the region of Saharan dust fall for the boreal winter situation (after Funk et al., 2003b).

and Bloemendal et al. (1992) the Saharan dust plume is the predominant source of magnetic minerals and detrital iron in the Equatorial Atlantic.

The sediment core consists mainly of undisturbed pelagic sediments (Baumann et al., 1995) principally foraminiferal/nannofossil oozes (Wagner and Klemd, 1995). The first 95 cm of the sediment core represent the last 26.19 ky (age model after Funk et al., 2003a). The color change from light olive (anoxic) to light brown (oxic) is located at 46 cm (Fig. 2). Below 46 cm the sediment is grey to olive-green. The distinct color change is located at about 10 cm below the midpoint of T1 (13.5 kyr, Raymo, 1997; ablation phase at the oxygen isotope boundary 2/1).

2.2 Geochemical analysis

Bulk element analyses of the sediment sequence 0-95 cm were performed by Inductively Coupled Plasma-Atomic Emission Spectrometry (Perkin-Elmer optima 3300 RL ICP-AES) and Inductively Coupled Plasma-Mass Spectrometry (Finnigan Sola ICP-MS) in 1 cm resolution after a 3-step total digestion in a microwave device (Ethos 1600 and Mega 2, MLS). (1) Digestion of 50 mg of freeze-dried sediment in a mixture of 3 mL HNO_3 (65% s.p.), 2 mL HF (48% s.p.) and 2 mL HCl (30% s.p.) at 200°C; (2) evaporation of the solution close to dryness; (3) dissolution and homogenization of the residual in a solution of 0.5 mL HNO_3 (65% s.p.) and 4.5 mL MilliQ-water, finally the solution was filled up to 50 mL with MilliQ-water. To each batch of 10 samples, one blank and a reference standard (MAG-1, USGS; Gladney and Roelandts, 1988) have been added and treated in the same way as the sediments. Each sample solution was analyzed in 3 replicates, and a deviation of less than 3% was accepted for ICP-AES and less than 10% for ICP-MS.

Dissolution effects (e.g. calcium carbonate) should be minimized by normalizing the measured elements to aluminum (Al). It is assumed that Al is exclusively bound to the alumosilicate phase (Calvert and Petersen, 1993) and behaves as a conservative element with respect to diagenetic overprinting (Thomson et al., 1998). Hence this technique emphasizes the effects of diagenetic element mobilization (Brown et al., 2000).

2.3 Rock-magnetic analysis

Hysteresis measurements were carried out at a 1 cm resolution with a PMC M2900 alternating gradient force magnetometer (AGM). For the measurements <50 mg miniature samples as described by von Dobeneck (1996) have been prepared. The 3 step hysteresis analysis started with the determination of the minor loop applying a maximum field strength of 300 mT and a field increment of 2 mT. In the second step the backfield curve was determined by first magnetizing the sample and subsequently magnetizing it in the opposite direction. Finally, the major loop was determined applying a maximum field strength of 1000 mT and a field increment of 5 mT in the third step. The hysteresis measurements were processed with the program HYSTEAR (von Dobeneck, 1996) to acquire the basic hysteresis parameters, which are (1) the saturation magnetization M_s, (2) the remanent saturation magnetization M_{rs}, (3) the coercivity B_c, and (4) the remanent coercivity B_{cr}. Accordingly, the magnetization (i.e. magnetogranulometric M_{rs}/M_s ratio by Day et al., 1977), and magnetic stability of a sample can be derived. The hysteresis based total susceptibility χ_{tot} (per mass unit) integrates all induced magnetization signals; the non-ferromagnetic susceptibility χ_{nf} represents exclusively the paramagnetic (iron-bearing silicates and clays) and the diamagnetic (biogenic carbonate and opal) sediment matrix. The difference between them is given by the ferromagnetic

susceptibility χ_f, which is a quantitative measure of the abundance of ferromagnetic and antiferromagnetic minerals.

3. Results

3.1 Geochemical characteristics

Down-core variations of element/Al-ratios are plotted in Figure 2. A conspicuous depth sequence of redox-sensitive element enrichments around the color transition is distinctively visible. The sequence starts with a broad Mn/Al double-peak above the color change that is followed downward by an Fe/Al double-peak of which the upper one is located directly at the color change. Just below the upper Fe/Al peak, increasing values of V/Al occur, followed in turn by increasing values of U/Al.

The productivity-related Ba/Al ratio shows increasing values below the glacial to interglacial transition (T1). These increased values form a broad peak extending over at least 30 cm; in addition, there is a slight but distinct increase from about 5 to 15 cm depth. The Sr/Al plot displays higher values from about 0 to 15 cm depth followed by a distinct broad depletion between 15 and about 40 cm. Below that depth mean values prevail.
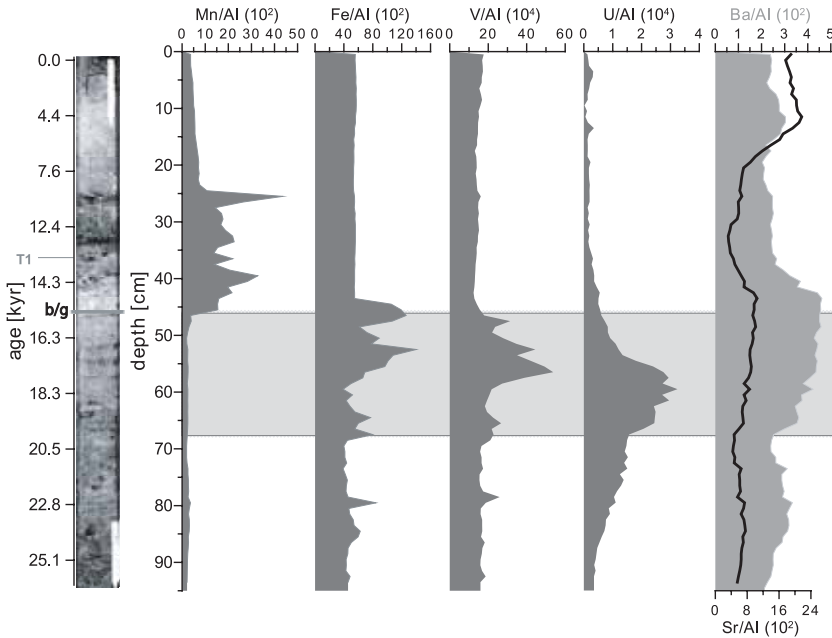
Fig. 2 Results of geochemical, solid phase analyses within the first meter segment of gravity core GeoB 2908-7. The sediment age on the left hand side of the core picture is given after Funk et al., 2003a. The midpoint of the termination is represented by the horizontal light grey line labeled as T1. The color change from brownish/reddish (0-46 cm) to greenish/grayish (47-95 cm) is marked by the horizontal grey line labeled b/g (brown/grey). From left to right the enrichment sequence of redox-sensitive element to aluminum ratios are depicted. The last plot to the right displays the productivity-related Ba/Al ratio and the CaCO$_3$ accumulation-related Sr/Al ratio. The horizon of diagenetic mineral dissolution is shown as a light grey background rectangle.

3.2 Rock-magnetic and combined rock-magnetic/geochemical characteristics

Concentration-dependent parameters

The ratio of ferrimagnetic susceptibility to total susceptibility (χ_f/χ_{tot}; Fig. 3) shows a pronounced drop at about 47 cm followed by a gradual recovery to its original level at about 66 cm. This reduction in χ_f/χ_{tot} correlates with the visible color change from brown to gray. Other rock-magnetic anomalies also occur in this part of the core. These are reductions in the total susceptibility to iron-ratio (χ_{tot}/Fe), and in the remanent magnetism to aluminum-ratio (M_{rs}/Al). The non-ferrimagnetic susceptibility (χ_{nf}) shows three main peaks. One pronounced peak is located above T1 and two smaller ones are found within the marked redox horizon.

Grain size sensitive parameters

The profile of B_c, which is indicative of the presence of stable magnetite, shows a distinct maximum just above the zone of the color change (Fig. 3). This is followed by an interval with lower values down to a depth of about 65 cm. The quotients of the magnetogranulometric M_{rs}/M_s (saturation remanence to saturation magnetization) and B_{cr}/B_c (remanent coercivity to coercivity) enable the characterization of the magnetite grain-size spectrum (Day et al., 1977; modified by Dunlop, 2002a,b; Fig. 4). The designated fields of the diagram represent (a) stable single-domain particles (SD), (b) pseudo-single-domain particles (PSD), and (c) magnetically less stable multi-domain particles (MD). The samples of this study show a distinct dominance of PSD particles (0.1–10 μm).
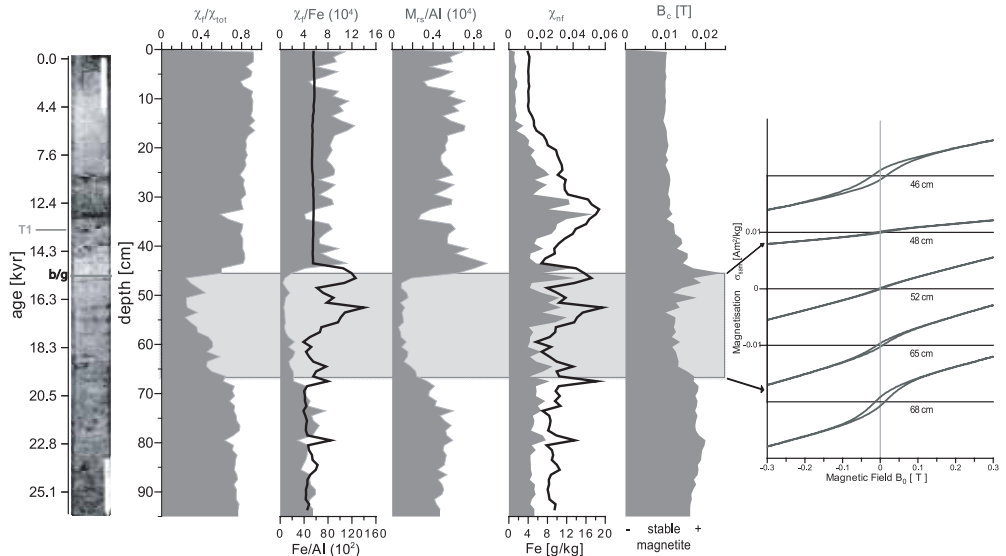
Fig. 3. Rock-magnetic and combined rock-magnetic/geochemical results of the first meter segment of gravity core GeoB 2908-7. The first three plots (χ_f/χ_{tot}, χ_f/Fe, and M_{rs}/Al) indicate diagenetic magnetic mineral dissolution. The Fe/Al ratio as an indicator for secondary iron mineral precipitation is superimposed. The χ_{nf} displays the non-ferrimagnetic susceptibility and is correlated with the concentration of total Fe. The B_c is supposed to be an indicator for the occurrence of stable magnetite. On the right hand side hysteresis loops are shown from the vicinity of the horizon of diagenetic mineral dissolution.
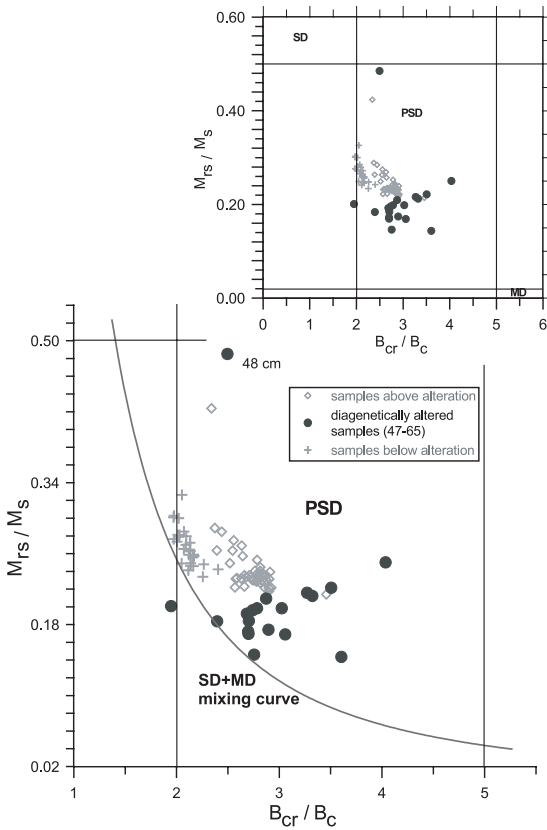
Fig. 4. Day plot representation of the quotients of M_{rs}/M_s and B_{cr}/B_c to characterize the magnetite grain size spectrum including the theoretical SD+MD mixing curve (after Dunlop, 2002b). Upper right corner: Day plot including grain size spectra of SD (single domain), PSD (pseudo-single domain), and MD (multi domain). The enlarged PSD section shows more clearly that the two groups of sample points above and below the interval of diagenetically-induced magnetite dissolution are paralleling the SD+MD mixing curve. Samples from the altered interval indicate coarser grain sizes and do not follow the mixing curve.

4. Discussion

4.1 Development of the redox-horizon from the last glacial to Holocene times.

Productivity changes over time

The Ba/Al ratio (Fig. 2), which is considered to be an indicator for paleo-productivity (e.g. Dymond et al., 1992; Gingele and Dahmke, 1994; François et al., 1995), displays relative changes in productivity over the last 26 kyr. During the glacial (from about 50 cm downward), which had its midpoint at about 21 kyr (Rühlemann et al., 1999a), productivity was relatively high. In upwelling areas like the region of the core site, productivity is about 10 times higher than in oligotrophic areas (Reading and Levell, 1996). Accordingly, the oxygen content of the bottom water was relatively low, and thus the preservation of organic matter was increased (Verardo and McIntyre, 1994). Hence, the upper part of the broad Ba/Al ratio enrichment interfaces into the early stage of T1 starting between 19 and 16 cal. kyr. BP (Rühlemann et al., 1999a). The current asymmetry of the tropical Atlantic Ocean, with high productivity in eastern upwelling regions and oligotrophy in the westerly region, has been predominant over the last 300 kyr (Rühlemann et al., 1999b).

The depletion of Ba/Al is most obvious at the mid-point of T1 (13.5 kyr BP) and clearly indicates that the major shift to more oligotrophic conditions had already occurred by that time. According to

Lototskaya (1999), T1 lasted for about 7 kyr. A re-establishment of higher productivity conditions starts at about 7 kyr BP (Fig. 2). This was most likely driven by the movement of the intertropical convergence zone (ITCZ) into its recent position, which encompasses the core site at its southern flank. These observations are supported by the downcore variations of the Sr/Al ratio, indicating simultaneous variations in the $CaCO_3$ content. The obvious change in productivity (from glacial to T1) are also reflected in the distinct increase in sedimentation rate (4.3 and 2.3 cm/kyr for glacial and interglacial, respectively; Funk et al., 2003a).

Such a strong shift in the environmental conditions as observed at the transition from glacial to T1 – probably associated with an increase of the oxygen level of the bottom water – is likely to have caused variations in the diagenetic sequence and the redox conditions in paleo-surface sediments (Wallace et al., 1988; Thomson et al., 1984, 1996). A typical observation for such an environment is a downward prograding redox front (Colley et al., 1984) developing conspicuous solid phase enrichments. Over time, the downward progression usually decelerates and finally stops as the O_2 supply becomes limited due to the increasing distance from the sediment surface (Wilson et al., 1985). In the following, the observed metal enrichments are discussed in the context of the proposed redox boundary relocation.

Mn and Fe enrichments

The maximum depth of the formerly progressing oxidation front is presumably marked by the top of the lower Fe peak (at 54 cm; Fig. 2). Most likely the oxidation front remained for a prolonged time at this position due to stable diagenetic conditions (i.e. a balance between the upward flux of reducing and downward flux of oxidizing constituents). A supplementary indicator for the depth limit of the oxidation front is the uranium enrichment, since it only forms under permanently and strongly reducing conditions (Shaw et al., 1990). The main process that leads to an uranium enrichment is the diffusion of $[UO_2(CO_3)_3]^{4-}$ from the bottom water into the sediment, followed by a reduction and precipitation as uraninite (UO_2) below the Fe-remobilization depth (Klinkhammer and Palmer, 1991; Crusius et al., 1996). Accordingly, the maximal penetration depth of the Fe^{2+}/Fe^{3+} redox boundary is indicated by the plateau-like top of the U-enrichment (Fig. 2). The upward U-tailing conversely developed during the upward trend of the oxidation front and the element-redox-boundaries, respectively. The recent position of the redox-front can be recognized by the distinct color change (at 45 cm) as described by Lyle (1983).

The zone of the upper Fe-peak (color transition) coincides with the lower limit of elevated Mn-concentrations (25-46 cm). Even though pore water data are not available at this depth, the recent to sub-recent formation of the Fe-peak can be explained by the oxidation of Fe^{2+} by MnO_2 following Eq. 1 (e.g. Burdige, 1993):

$$2Fe^{2+}aq. + MnO_2 + 2H_2O \rightarrow 2FeOOH + Mn^{2+}_{aq.} + 2H^+ \tag{1}$$
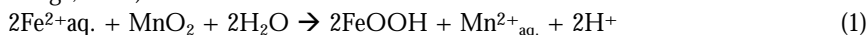
This hypothesis of Fe-oxidation by Mn-reduction is further supported by magnetite formation at this depth as it will be shown below. A transitory Fe^{3+} phase ($Fe(OH)_3$) is thought to form due to the reaction of Fe^{2+} with Mn-oxides (e.g. Tarduno and Wilkison, 1996). The required Fe^{2+} is most likely released in association with the degradation of organic material from underlying sedimentary units involving the reduction of Fe-oxides, as described for Mediterranean sapropel S1 (Passier et al., 1996). Diffusing upward, this Fe^{2+} will react with MnO_2, thus releasing Mn^{2+} while being immobilized as $Fe(OH)_3$. Subsequently, this Mn^{2+} is diffusing upwards, where it is typically oxidized

above the oxygen penetration depth. This process has formed a Mn-enrichment zone between 25 and 46 cm. The distinct peak at 25 cm represents, however, the most dramatic change to higher productivity from T1 to the Holocene. As the oxygen penetration depth in that region is estimated to be <10 cm at present (Wenzhöfer et al., 2002), it is unlikely that the Mn-peak at 25 cm is still actively forming. Moreover, the shape of the upper 25 cm of the Mn/Al profile shows a distinct decrease towards the top (Fig. 2) indicating a continuing upward movement of the Mn-redox-boundary.

This statement can be substantiated by a simple model calculation supposing that the Fe of the lower Fe-peak is the source of Fe^{2+} that has been generated via C_{org} degradation (Fig. 2 and 5). Assuming that the major part of the upwardly diffusing Mn^{2+} has originally been oxidized at the upper Mn-peak, the amount of Fe in the upper Fe peak should be equal to twice the amount of Mn in the upper Mn peak (Eq. 1). The calculation is based on the average amount of Mn respective to Fe in the peak surface area minus the corresponding background concentration, assuming a porosity of 0.7 and a grain density of 2.65 g/cm^3. Based on an area of 1 cm^2, the total amount of Mn in the upper peak is 0.01 g (188 mol) and that of Fe in the upper peak is 0.021 g (376 mol) corresponding to the assumption made. According to Fick's first law a build-up of the upper Mn-peak would last for about 6 kyr assuming a diffusion coefficient of 118.26 dm^2/yr, a δ Mn concentration of 50 µmol/dm^3 and a δ distance of 19 cm (Fig. 5).

However, it is most likely that the upper Fe peak still forms in the described way whereas the Mn-oxidation level moved upwards during the last 4 to 5 kyr due to the relocation of the oxygen penetration depth in the sediment. Since pore water data are lacking to unambiguously identify active reaction horizons, further evidence is required to substantiate the proposed development of the redox fronts. In the following we demonstrate that careful evaluation of rock-magnetic data can help to overcome this problem to a certain degree.
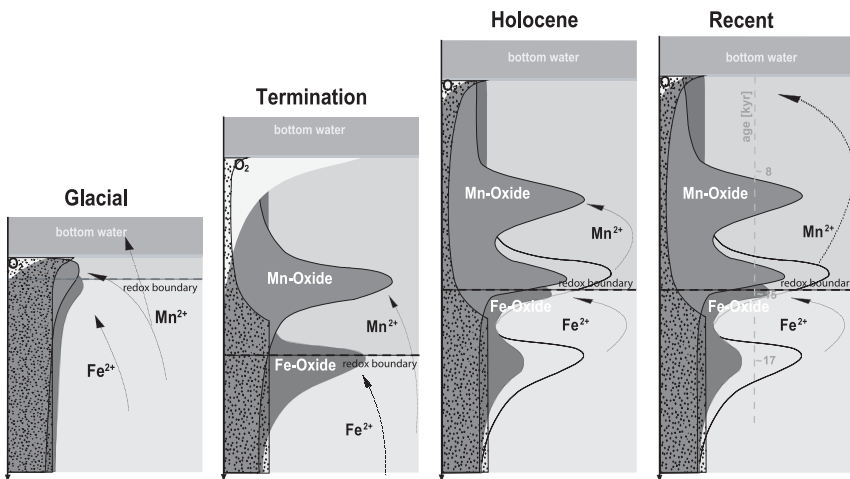

Fig. 5. Model sketch for the development of the Fe^{2+}/Fe^{3+} redox boundary movement from the glacial to the recent situation, including simplified solid phase Mn, Fe and C$_{org}$ profiles, estimated O$_2$ pore water penetration, and supposed Fe^{2+} and Mn^{2+} fluxes.

4.2 Characterization of diagenetic dissolution of magnetic minerals

The χ_{rf}/χ_{tot} ratio (Fig. 3) is thought to represent the proportion of mainly ferro- (magnetite) to antiferro- (haematite/goethite) magnetic minerals. Since magnetite is the main carrier of the magnetization, the χ_{tot}/Fe_{tot} ratio (ferrimagnetic susceptibility to total Fe) indicates potential changes in the magnetite abundance that are related to variations in the Fe-content of the sediment. The comparison of this ratio to the Fe/Al ratio provides a good way of identifying diagenetic dissolution and precipitation processes of Fe-oxides. The diagenetic destruction of the terrigenous magnetic fraction is displayed by the M_{rs}/Al (remanent saturation magnetization to aluminum; Fig. 3) ratio. The zone where major dissolution of magnetic minerals has occurred and partly still occurs extends from 47 to 66 cm indicated by the plots of χ_{rf}/χ_{tot}, χ_{tot}/Fe_{tot}, and M_{rs}/Al (Fig. 3). This depth interval appears also in the hysteresis loops (Fig. 3) as the diagenetically overprinted interval. The limbs of the hysteresis curve within the diagenetically overprinted interval are almost linear, which points to the absence of single domain grains. Conversely, the hysteresis loops above and below that interval affected by dissolution, are typical of single-domain magnetite (Frederichs et al., 1999).

Reductive dissolution of ferrimagnetic minerals is considered to be a grain-size selective process (Karlin et al., 1987; Robinson et al., 2000). The ultra-fine (<0.1 μm) particles have a larger specific surface area and are thus the first to be dissolved. Accordingly, there will be a shift to coarser residual grain sizes. The fine-grained material is characterized by SD and MD particles (Day et al., 1977). Dunlop (2002a,b) modified the Day plot in order to estimate grain-size trends and distinguish MD from SP (super paramagnetic) mixtures. From the PSD grain-size spectrum it is obvious that the samples from the diagenetically overprinted interval (black circles; Fig. 4) reveal coarser grain-sizes than those above and below. The latter two can be subdivided into two groups, namely (1) below the horizon of alteration with a slightly smaller PSD grain size (grey crosses) and (2) above with a mid-PDS grain size (open grey rhombs). These two groups represent a narrow size distribution of smaller grains and a parallelism with the SD+MD mixing curve introduced by Dunlop (2002b) due to magnetite associated with magnetosomes from magnetotactic bacteria. Dunlop (2002b) concluded that the Day plot is sufficient to locate the exact position of the redox boundary in the sediment column. In the present study such a precise distinction is not possible because the interval of dissolution of magnetic minerals - leaving behind magnetite with coarser grain sizes extends over about 20 cm. Consequently, it is not clear from the Day plot if the redox boundary is located at the upper or lower limit of this latter group.

In the upper zone of dissolution an enrichment of fine stable magnetite is indicated by its B_c-distribution (Fig. 3). Karlin et al. (1987) discussed the authigenesis of fine-grained magnetite crystals in close proximity to a color-boundary and the redox-transition from Fe^{2+} to Fe^{3+} in marine sediments, similar to that observed in gravity core GeoB 2908-7 at about 46 cm. This observation can be explained by the metabolic activity of Fe^{2+} oxidizing magnetotactic bacteria, which are known as nitrate reducers (Karlin et al., 1987; Rhoads et al., 1991; Robinson et al., 2000), but which might also be able to use MnO_2 as an electron acceptor. This appears to be a likely process since the geochemical data from the same depth interval show that Fe^{2+} is oxidized by MnO_2 to Fe-hydroxides. According to Tarduno and Wilkison (1996) the ephemeral ferric iron phase that is formed due to the reaction with MnO_2 can further be used in bacterial reduction producing magnetite. This also explains the existence of sample "48 cm" in the Day-diagram (Fig. 4), which in contrast to all other samples of the dissolution interval is located in the finer PSD sector and is most

likely secondary magnetite.

In agreement with the geochemical evidence, these observations support the hypothesis that the restricted horizon is rather a secondary signal of early diagenesis than a primary signal of climatic change which has also been shown for the sapropel setting (e.g. Passier et al., 1998). In consideration of the anomalies of particularly χ_f/χ_{tot}, χ_{tot}/Fe, and M_{rs}/Al it can be stated that these parameters reflect in the first instance the dissolution processes of the magnetic mineral phase which are primarily the magnetic iron-titanium-oxides supplied to the sediment by terrigenous input (Funk et al., 2003b) . The correlation of χ_{nf} and Fe (total) illustrates the subordinate part of the magnetic iron particles with respect to the total iron concentration. The fluctuations, particularly in the plots of χ_{tot}/Fe and χ_f/χ_{tot}, near the redox-horizon correspond to "non-steady state" diagenetic conditions.

4.3 Relationship between the shape of the peaks and the movement of the redox-front

The shapes of selected geochemical and rock-magnetic concentration profiles (i.e., χ_f/χ_{tot} and V/Al) can give additional information concerning the course of the proposed movement of the redox boundary. From the results so far it is obvious that the Fe^{2+}/Fe^{3+} redox front reached its relatively deepest penetration during T1 and is moving upwards at present. However, due to the significant enrichment of MnO_2 between 25-46 cm which acts as an effective long-term sink for Fe^{2+}, the upward movement of the Fe^{2+}/Fe^{3+} front is probably very slow. The abundance of MnO_2 in this horizon will thus guarantee ongoing formation of Fe-oxide enrichments which means a more permanent situation of non steady-state.

Since the upward movement of the redox front more or less overprinted the signatures of the downward movement, the latter signal is now partly obscured. However, the V/Al and χ_f/χ_{tot} ratios are suitable to partly identify some details of the upward movement of the redox boundary related to the change from T1 to Holocene. At least three abrupt steps of the upwards movement are visible.

The V/Al ratio (Fig. 6) shows a distinct enrichment below the upper Fe-peak in the suboxic to anoxic zone. According to Shaw et al. (1990) and Hastings et al. (1996) vanadium can be enriched by in-situ reactions and under nearly anoxic conditions of the bottom water due to penetrations from the overlying water. They postulate the extraction of vanadium out of the pore water and enrichment into the sediment just below the reduction zone of Fe-oxyhydroxides. Hence, anoxic events can be identified by a distinct increase of V-accumulation. The shape of the V-peak displays the gradual upwards migration of the oxidation-front and consequently the vanadium redox boundary.
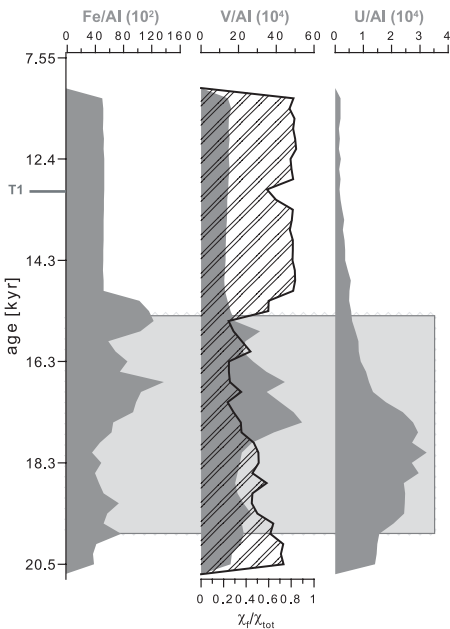

Fig. 6. Detailed geochemical and rock-magnetic solid phase profiles in the vicinity of the color change (redox boundary). Particularly V/Al and χ_f/χ_{tot} clearly trace the stepwise upward movement of the iron-redox boundary from T1 to Holocene.

In the case of the subordinate enrichment the front may have remained for a prolonged time at that location forming a distinct vanadium peak, before moving upwards until conditions again became favorable for a V enrichment. The tailing upwards form of the curve can be viewed as an indicator for its predisposition for slightly reducing conditions. Accordingly, it was a discontinuous upward movement, which reflects the sensitivity of redox conditions during the climatic transition from T1 to the Holocene. By plotting the χ_f/χ_{tot} over the V/Al (Fig. 6) the aforementioned process becomes more obvious. The χ_f/χ_{tot} shows small peaks in between the V/Al peaks. Hence, there are still peaks of elevated magnetic susceptibility even in the zone of magnetite dissolution.

Presumably, the redox front moved down relatively rapidly. On its discontinuous, stepwise upward movement the magnetic signal was dissolved almost entirely in those horizons where the redox front remained for a prolonged time and formed a zone of V/Al enrichment. During periods of more rapid upward movement only a small part of the magnetic susceptibility was lost, as indicated by the two small peaks within the zone of dissolution.

4. Conclusions

The combination of high resolution geochemical and rock-magnetic results displays unambiguously the horizon of diagenetic overprinting in terms of the occurrence of magnetic mineral dissolution and secondary redox-sequential element enrichments (Mn, Fe, V and U). The changes in the redox-environment that lead to non-steady state diagenesis, have been the result of changing environmental conditions between the last glacial and the Holocene. A direct comparison of the shape of selected geochemical and rock-magnetic parameter-depth plots in the vicinity of the redox horizon, especially for χ_f/χ_{tot} and V/Al, has enabled us to trace the later redox-boundary relocation (from T1 to Holocene) in detail.

This study has shown that a multidisciplinary high resolution analysis of diagenetically overprinted sediments is required to record the exact shape of characteristic geochemical and rock-magnetic enrichments and dissolution, respectively. By means of these records it is possible to trace the relocation of element redox boundaries. Moreover, the combination of geochemical and rock-magnetic methods appears to be a promising tool to identify and trace the processes of early diagenesis, which are particularly effective to sediments located on the boundary of high productivity areas that have been subject to climate-induced geochemical changes. On the other hand our results show, that the use of rock-magnetic parameters as a climatic indicator in sediments with strong diagenetic overprinting might be limited.

Acknowledgements

Source and development of large manganese enrichments above eastern Mediterranean sapropel S1

Abstract

The residual dark unit of the most recent eastern Mediterranean sapropel (S1) is usually overlain by sediments with enhanced concentrations of Mn in two separated peaks. Consideration of the variability and magnitude of the upper Mn peaks in S1 units taken at different locations and water depths in the basin leads to the conclusion that Mn must have been added preferentially but variably to sediments at intermediate (1-2 km) water depths, implying a Mn supply by loss from sediments elsewhere, inferred here to be the sediments in deep (>2 km) waters. A decreasing mean level of oxygenation with increasing water depth during sapropel formation, supported by other geochemical and micropalaeontological evidence, is invoked to propose a two stage mechanism involving loss of reduced Mn^{2+} from the deepest sediments into anoxic waters, and a variable gain of MnO_x precipitated in oxygenated waters by sediments on higher topography in the basin. In those S1 units from intermediate water depths that receive these extra hydrogenetic MnO_x inputs, large (>3 wt.%) upper Mn peaks are maintained continuously at the top of the forming S1 unit because pore waters are anoxic at shallow sediment depth while bottom waters are oxic to some degree. The development of the upper Mn peak is thus best considered as diagenetic even though the additional Mn may result from multiple hydrogenous input events. The MnO_x that forms these diagenetic localizations adsorbs Mo and Li from seawater in a similar manner to other Mn-enriched oxic sediments, nodules and crusts, with a Mn:Mo ratio of ~600:1, a Mn:Li ratio of ~750:1, and a $\delta^{98/95}Mo_{MOMO}$ of -2.5‰.

1. Introduction

Eastern Mediterranean sediments are generally C_{org}-poor, but discrete C_{org}- and sulfide-rich units known as sapropels have formed repetitively in the sediment sequence over the past 3 Ma at least (Rohling, 1994). A close relationship between sapropel formation and orbital precession-driven solar insolation variations has been interpreted to imply that an enhanced flux of monsoonal fresh water to the surface ocean must control sapropel formation in this semi-isolated basin (Rossignol-Strick, 1985; Hilgen, 1991; Lourens et al., 1996; Tuenter et al., 2003). At present C_{org}–poor sediments form (Van Santvoort et al., 2002) because the basin's deep waters are ventilated regularly so that high O_2

contents are maintained throughout the water column (Béthoux, 1993; Roether and Well, 2001). The scenario proposed for sapropel formation envisages that increased runoff leads to water column stabilization and probably to enhanced production (Rohling, 1994). Deep-water dysoxia or anoxia then develops in the poorly-ventilated deep waters allowing formation of sapropel with enhanced C_{org} preservation and diagenetic sulfide production in the sediments.

Among the major elements, Mn is the most mobile in sediments because of the ready interconversion of its different chemical species in response to the early diagenetic redox changes that occur in sediment pore waters. The remineralization of reactive organic matter in sediments induces the reduction of manganese oxyhydroxide, $Mn(III,IV)O_x$ to soluble Mn(II) when sediment pore waters become anoxic at depth. The Mn^{2+} thus formed diffuses in pore water solution until O_2 is re-encountered when MnO_x is again precipitated, either in the sediments or in the overlying seawater. This behavior means that Mn is best suited to studies of changes in water column oxidation status during formation of the most recent sapropel (S1) between 9.8 and 5.7 ^{14}C kyr ago (De Lange et al., submitted for publication). Two distinctly separated Mn peaks are generally found in the sediments immediately above the visual expression of sapropel S1. These peaks have been related to changes in water column oxygenation that occurred at the end of this most recent sapropel episode, and have been important in quantifying the post-depositional oxidation that most S1 units have experienced since their formation (De Lange et al., 1989; Higgs et al., 1994; Thomson et al., 1995, 1999; Van Santvoort et al., 1996). Pore water investigations have revealed that it is generally the *lower* of the two Mn peaks that is forming actively, and that the maximum of this lower Mn peak marks the present limit of oxic conditions in the sediments (Van Santvoort et al., 1996).

The genesis of the *upper* MnO_x peak that often contains higher Mn contents than the lower peak (but usually still <1 wt.% Mn) is less certain (Pruysers et al., 1993; Thomson et al., 1995, 1999; Van Santvoort et al., 1996). This peak usually appears to coincide with the end of sapropel formation, and the geochemical proposition is that it is related in some manner to the resumption of ventilation and the return of high O_2 levels in bottom waters at the end of S1 sapropel times (Thomson et al., 1995, 1999; De Lange et al., 1999). Upper Mn peaks therefore formed before, and are older than, the corresponding lower Mn peaks that are located a few cm deeper in the sediments. Cita and co-workers (Cita et al., 1989; Camerlenghi et al., 1992; De Capitani and Cita, 1996; Hieke et al., 1996) have also reported a prominent dark layer with variable Mn contents up to 22.8 wt.% Mn above S1 in the sediments of a diapiric crestal area on the Mediterranean Ridge. This layer has been termed the "Marker Bed", and its formation ascribed to an expulsion of hydrothermal fluid. There is danger in considering any Mn feature as a marker bed in the sense of a chronostratigraphic horizon that can be traced over a wide area, because of the early diagenetic mobility of Mn described above. Thomson et al. (1999) noted that the Marker Bed is similar to upper Mn peaks in published photographs, both in appearance and in position relative to the S1 sapropel, and have proposed that the Marker Bed and upper Mn peaks are equivalent. The unusually large Mn contents measured in some Marker Bed locality cores do however require further explanation.

Regarding source and formation mechanism, large Mn enrichments might be:

(i) *diagenetic*, i.e. formed within the sediments by early diagenesis. Van Santvoort et al. (1996) have demonstrated that the lower Mn peaks above the residual S1 unit are forming actively by this mechanism as outlined above. Very high Mn contents can be produced by this mechanism in surficial sediments in cases where the surficial oxic zone is a few cm or less deep as Mn is continuously refined

into this thin oxic layer or zone (e.g. Lynn and Bonatti, 1965; Shimmield and Price, 1986; Kadko et al., 1987). In order to have produced the upper Mn peaks in eastern Mediterranean sediments, this mechanism would imply that finite bottom water O_2 contents were present during sapropel deposition in order to maintain an oxic surficial layer in the sediments so as to prevent the escape of Mn^{2+} from the sediments to bottom waters.

(ii) *hydrogenetic*, i.e. precipitated from the water column (e.g. Force and Cannon, 1988; Frakes and Bolton, 1992; Calvert and Pedersen, 1996). If bottom water oxygen levels fall to sufficiently low but not necessarily zero levels, then Mn^{2+} from pore waters will diffuse out of the sediments and escape to bottom waters (Balzer, 1982; Kristensen et al., 2003). This process develops high Mn^{2+} concentrations in sub-oxic or anoxic water columns, as in the isolated basins of the Black Sea, the Cariaco Trench, silled fjordic basins (Calvert and Pedersen, 1996), within the oxygen minimum zone of the northern Indian Ocean (Schenau et al., 2002), and deep anoxic eastern Mediterranean brine basins (De Lange et al., 1990). A sharp solubility gradient of Mn exists along the oxic-/anoxic interfaces in such water columns. Dissolved manganese contents in anoxic waters might be ~1000 times greater than in oxic surface waters where Mn concentrations are typically <10 ppb Mn because Mn^{2+} in solution is favored by the low Eh values of anoxic waters (Force and Cannon, 1988). If the stability of such an anoxic water column breaks down, then increased dissolved O_2 levels introduced with ventilation will precipitate dissolved Mn^{2+} as MnO_x that rains back down through the water column to the underlying sediments. Such a process occurs regularly in winter in the deep basins of the Baltic Sea (Huckriede and Meischner, 1996; Sternbeck and Sohlenius, 1997). In order to produce the upper Mn peaks in eastern Mediterranean sediments, this mechanism would imply first that low bottom water O_2 contents must have developed during sapropel deposition in order to allow Mn^{2+} to escape from sediments into the bottom waters, and second that an increase in ventilation at the end of sapropel times introduced sufficient O_2 to re-precipitate this Mn^{2+}. If sapropel formation ended with a single ventilation event, then this latter mechanism might be expected to form the largest upper Mn peaks at sites in deepest water depths. This is not the case as will be seen below.

(iii) *hydrothermal*, i.e. produced through an emission of hydrothermal fluid. Manganese can be enriched in a range of forms in the vicinity of hydrothermal vents (Roy, 1992; Mills and Elderfield, 1995). Investigations undertaken over active vents on the mid-ocean ridge system have shown that, although the Fe^{2+} component of the emitted metal-rich reduced fluids tends to be precipitated from black smoker plumes in the proximity of vents, the emitted Mn^{2+} precipitates in a variety of near- and far-field occurrences. Manganese is sufficiently fractionated from Fe^{2+} that it can still be traced in plumes thousands of kilometers distant from the source vents (Klinkhammer and Hudson, 1986). It therefore seems likely that the authigenic flux of Mn precipitated in the deep ocean contains a hydrothermal component (Roy, 1992). To produce the upper Mn peak, this mechanism would imply a sufficiently high water column O_2 content to precipitate emitted Mn, but any relationship in time to sapropel deposition is fortuitous.

Manganese enrichments formed by diagenetic, hydrogenous and hydrothermal mechanisms are all expected to form initially as some MnO_x species. Once buried, and as anoxic conditions develop over time, all types may contribute to surficial diagenetic MnO_x enrichments by the reduction mechanism outlined above.

This work investigates the Mn peaks observed above S1 sapropel units in a suite of 11 cores collected at different locations and water depths (650-3400 m) in the eastern Mediterranean basin

(Figure 1). Particular emphasis is placed on cores with large upper peak Mn concentrations in order to explore the source and mechanism of their formation.

2. Material and methods

Data obtained at the Utrecht and SOC laboratories at different times and by different analytical methods were assembled from cores selected to give a geographical and bathymetric coverage of the eastern Mediterranean basin (Fig. 1 and Table 1). Those from box cores BP10, BP15, BP18, SL125, ABC26, SL9, and SL114 were performed by Inductively Coupled Plasma-Atomic Emission Spectrometry (ICP-AES) in 0.5 cm resolution after a 3-step digestion to ensure total dissolution: (1) digestion of 125 mg of freeze-dried sediment in a mixture of 2.5 ml 3:2 concentrated $HClO_4$ and HNO_3 with 2.5 ml conc. HF at 90°C; (2) evaporation of the solution to near dryness at 160°C; (3) dissolution of the residual in 25 ml 1 M HCl at 90°C. Ten samples from 9.5-14.5 cm in core BP18 were not completely digested in this manner; for these samples the procedure was applied to ~60 mg of sediment with an extra digestion step that involved evaporating the sample to near dryness with 5 ml conc. HCl after step (2). Analyses of samples at 1 cm resolution from box core MC562 were performed by Inductively Coupled Plasma Mass Spectrometry (ICP-MS) after a 3-step total digestion described by Reitz et al. (2004a). Samples from box core T87-29B and hydraulic piston core 971C from ODP Leg 160 were analyzed by ICP-AES after a 1:5 fusion with $LiBO_2$ (Totland et al., 1992) in 0.5 and 1 cm resolution, respectively. Further analyses of Mo and Li in selected samples from these
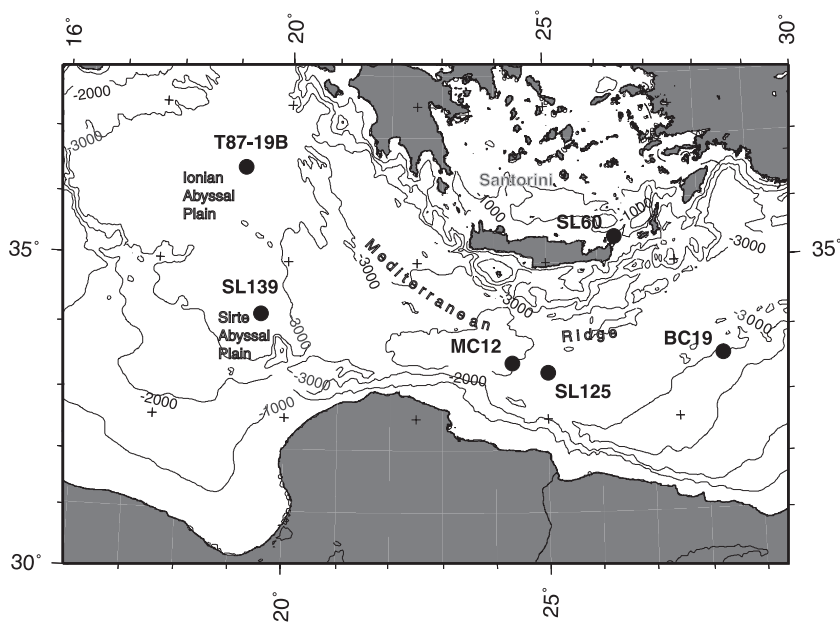

Fig. 1 Map of the eastern Mediterranean Sea with locations of the cores investigated.

two cores were later made in the manner described above for core BP18. For the different procedures sample duplicates, international standards and in-house standards were processed to monitor the precision (by duplicates) and accuracy (by standards) of the analyses.

Organic carbon content was determined according to the method described by van Santvoort et al. (1996). International and in-house standards and duplicates were processed to monitor precision and accuracy.

A sequential extraction with different solutions (Table 2) was applied to five 125 mg samples of box core BP18; one background sample from the sediment above the upper Mn peak (5.5-6cm),

Table 1: Positions, water depths and other details of the cores investigated.

Core	Latitude [°N]	Longitude [°E]	Corer type	Ship / year	Water depth [m]	Maximum Mn content in upper Mn peak [wt.%]
BP15	32°77.8′	19°87.6′	Box	Pelagia / 2001 (Biopass)	665	0.13
MD90-917	41°18′	17°37′	Piston	M. Dufresne / 1990	1010	3.3
MC562	32°46.3′	19°11.5′	Multi	Meteor / 2001 (M51-3)	1391	9.4
T87-29B	34°32.7′	16°34.0′	Box	Tyro / 1987	1530	4.7
BP18	33°10.0′	19°73.3′	Box	Pelagia / 2001 (Biopass)	1850	24.6
SL125	33°39.4′	24°33.0′	Box	Prof. Logachev /1999 (Smilable)	1946	2.9
BP10	33°22.2′	19°76.7′	Box	Pelagia / 2001 (Biopass)	2108	0.88
ABC26	33°21.3′	24°55.7′	Box	Tyro / 1987	2150	1.2
ODP971C	33°42.8′	24°42.1′	Piston	JOIDES Resolution / 1996 (ODP Leg 160)	2152	13.6
SL9	34°17.2′	31°31.4′	Box	Prof. Logachev /1999 (Smilable)	2302	2.4
SL114	35°17.2′	21°24.5′	Box	Prof. Logachev /1999 (Smilable)	3390	0.74

three from the upper Mn peak (10.5-11cm, 12-12.5cm, and 13-13.5cm), and one from the lower Mn peak (17-17.5cm). All samples and two standards (international standard MAG-1 and an in-house manganese nodule standard) were processed in duplicate to monitor the precision of the sequential extraction. Recovery with respect to the standard total element concentrations of Mn, Ba, Fe, and Li was 99%, 94%, 99%, and 107%, respectively.

Pore water analyses of BP10 were done by Inductively Coupled Plasma Mass Spectrometry (ICP-MS) after onboard sampling of the box core at in situ temperature (~13°C) in a nitrogen-filled glove box and centrifugation to separate pore waters. Sample duplicates were analyzed to monitor over all precision and analyses were done in triplicate; reproducibility was better than 10% for Mn concentrations <1.5 µmol l^{-1} and better than 5% for concentrations >1.5 µmol l^{-1}.

Determination of molybdenum isotope fractionation was performed at the University of Bern by double-spike inductively coupled plasma-multicollector mass spectrometry by methods described by Siebert et al. (2001).

Bulk element data (e.g. Fe, Mn and Ba) are normalized to Al to take account of fluctuations in aluminosilicate content, on the assumptions that the element/Al ratio in detrital material should be relatively constant, and that increases in these ratios above detrital levels indicate where diagenetic

enhancements of these redox-sensitive elements occur (e.g. Van Os et al., 1994; Van der Weijden, 2002). On the large upper Mn peaks, a major fraction of Ba appears to be associated with MnO_x rather than present as biogenic barite. As the latter is an important indicator for sapropel formation, a correction for this MnO_x-associated Ba is needed. The Ba associated to the maximum upper MnO_x (($Ba/Mn)_{mum}$ ~0.0031) was determined by sequential extraction; this ratio has been used to correct the Ba/Al ratio in cores with a major upper Mn peak (>3 wt.% Mn; section 3.2), using:

$$Ba/Al = (Ba_{tot} - Mn_{tot} * (Ba/Mn)_{mum})/Al_{tot} \qquad (1)$$

where Ba_{tot}, Mn_{tot} and Al_{tot} are the bulk element concentrations determined from total digestion. Although, Ba_{excess} values could have been calculated (Reitz et al., 2004b), the illustration of Ba/Al has been preferred over the Ba_{excess} since the cores are from a wide variety of locations showing detrital background Ba/Al values between 0.0021 (SL9) and 0.0059 (MC562 on the Libyan shelf).

Table 2: Sequential extraction procedure

Step	Repeats	Extractant	Shaking time	Phase extracted	Reference
1	x1	25 ml demineralized water	2 h	dried pore water salts	
2	x2	25 ml 1 M $MgCl_2$; pH8	4 h	absorbed ions	Ruttenberg, 1992
		25 ml demineralized water rinse			
3	x5	25 ml 2 M NH4Cl; pH7	min. 4 h	carbonates	De Lange (1992)
4	x2	25 ml 0.17 M Na-citrate / 0.6 M	16 h	amorphous	Kostka and Luther
		$NaHCO_3$ / 0.11 M ascorbic acid; pH 8		(hydr)oxides	(1994)
5	x1	25 ml 1 M Na-acetate; pH 5	16 h	residual carbonates	Rutten et al. (1999)
		(buffered with acetic acid)			
6	x2	25 ml 0.2 M Na-citrate / 0.35 M	5 h	crystalline	Kostka and Luther
		Na -acetate (pH 4.8)		(hydr)oxides	(1994)
		plus 1.25 g Na-dithionite			
	x2	25 ml demineralized water rinse			
7		Total digestion		residual minerals	Lord (1982)
				and pyrite	

3 Results and Discussion

3.1 General characteristics of Mn-enriched horizons above sapropel S1

The interpretation of C_{org}, Ba/Al, Fe/Al and Mn/Al profiles through S1 units has been reviewed by Thomson et al. (1999), and the data for the new cores discussed in this section have many similarities to the limited number of eastern Mediterranean cores containing S1 for which detailed inorganic data have been reported previously. A full set of parameters is presented for core BP10 (Fig. 2) to illustrate the geochemical criteria that define the original and residual S1 boundaries. Abbreviated displays with only the Mn/Al and Fe/Al profiles are also shown for cores BP15, ABC26, SL9, and SL114, where the thickness of the visual S1 unit and the amount of oxidation experienced since deposition were evaluated in a similar manner to that applied to core BP10 (Fig. 2).

Unless they are from areas of unusually high sediment accumulation rate (Mercone et al., 2000,

2001), S1 units are generally thinner than the unit originally laid down because of post-depositional oxidation. This oxidation greatly diminishes or destroys the original C_{org} and sulfide contents in the upper part of the sapropel and thus lightens the characteristic dark color that accompanies high C_{org}
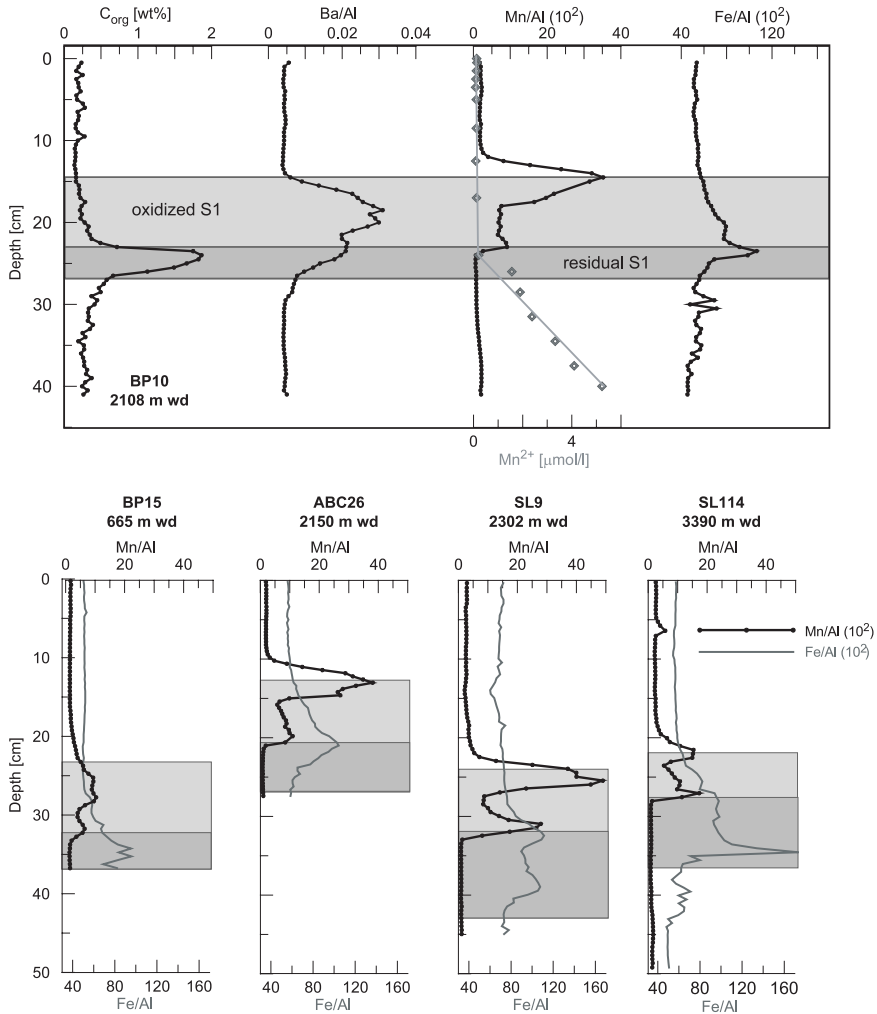
Fig. 2 Upper panel: Element concentrations (C_{org}) and ratios (Ba/Al, Mn/Al and Fe/Al) in the sediment and pore water Mn^{2+} concentration versus depth in core BP10. These profiles illustrate how geochemical data are used to define the original S1 thickness and divide it into oxidized and residual sections according to criteria described in the text (section 3.1). The residual S1 and the oxidized S1 zones are illustrated by the dark and light grey shadings, respectively. Original element concentrations are µg/g unless otherwise indicated; 10^2 indicates that the ratio was multiplied by 100. Lower panel: Mn/Al and the Fe/Al ratio profiles versus depth for four cores from different eastern Mediterranean locations and water depths. Shadings as above indicate residual and oxidized S1 zones in each core.

and S contents in sapropels (De Lange et al., 1989, 1994; Higgs et al., 1994; Thomson et al., 1995, 1999; Van Santvoort et al., 1996). Fortunately biogenic Ba (as barite) that accompanies settling C_{org} appears to be preserved in sapropels even after C_{org} has been oxidized extensively (Thomson et al., 1995). Thus, the positions and shapes of the Ba/Al and Mn/Al profiles allow deduction of the original thickness of S1 as follows (Thomson et al., 1995, 1999; Van Santvoort et al., 1996; Mercone et al., 2000; Rutten and De Lange, 2002; Fig. 2). For all cores of figure 2 except core BP15 from the shallowest water depth, the upper Mn/Al peak occurs exactly at the top of the zone of high Ba/Al values that marks the original S1 unit, as seen in the detailed profiles of core BP10, while the lower Mn/Al peak is situated immediately above the zone of high C_{org}. This is evidence of the post-depositional oxidation of sapropel S1 that has occurred between the two Mn peaks over the last 6 kyr. At the same time the pore water Mn^{2+} profile (Fig. 2) is evidence for the continuing suboxic/anoxic reduction of MnO_x in underlying sediments to fuel formation of the lower Mn peak.

There is little or no evidence of any Fe enrichment accompanying the upper Mn peak in these cores. By contrast a clear enrichment of Fe occurs along with the lower (diagenetic) Mn peak in all cores, which indicates the formation of Mn and Fe oxyhydroxides by precipitation of Mn^{2+} and Fe^{2+} diffusing upwards from below by bottom water O_2 (De Lange et al., 1989; Van Santvoort et al., 1996; Passier et al., 2001; Rutten and De Lange, 2003). The lower Mn peak with associated Fe formed after S1 formation, as explained above, by the oxidation front that began to penetrate into the sediment after S1 formation, and this process continues to the present in most cases. The behavior of Fe in sapropels differs further from Mn in that Fe and S form pyrite in sapropels, and the high Fe/Al values in the visual sapropel, where Mn values are low and C_{org} and S values are high, indicate the presence of pyrite (Passier et al., 1996). These authors also reported sulfide formation in excess of the available Fe for sapropel S1. This excess may not only have resulted in the downward sulfidization process and associated consumption of all available Fe^{2+} during S1 formation, but may also have resulted in a HS⁻ flux into the water column. The latter would maintain low Fe^{2+} concentrations in the water column.

3.2 Large upper Mn peaks in oxic conditions above sapropel S1

The previous section demonstrated that S1 units in different cores display some compositional variability and consistent evidence of the post-depositional oxidation experienced since their formation. Among the major elements, Mn is the element that shows the greatest concentration variations in S1 units. In this section five cores are examined that have much larger upper Mn peaks than the <1 wt% levels in all cores presented in Fig. 2. One of these, core BP18 from the Libyan slope, has the highest upper Mn peak concentration yet reported in the eastern Mediterranean at 24.6 wt%.

(i) Large upper Mn peaks above the S1 sapropel in oxic conditions: the Libyan continental slope

Core MC562 was recovered west of Cape Sirte in 1391 m water depth and has a maximum upper Mn peak value of 9.4 wt.% Mn, while core BP18 was recovered from north-west of Cape Sirte at 1850 m and has 24.6 wt.% Mn in the upper Mn peak. XRD analysis of the BP18 sample with the highest Mn concentration established birnessite as the main Mn phase and an absence of Mn-carbonate phases (rhodochrosite/kutnahorite; C. Vogt, pers. comm. 2004). This finding is supported by sequential extractions that reveal that nearly all the extra Mn content in the upper peak is extracted

in the amorphous oxyhydroxide fraction (Fig. 3).

The uncorrected Ba/Al profile of core BP18 displays a narrow peak that coincides exactly with the upper Mn peak (Fig. 3). For the samples discussed in this chapter that have Mn concentrations >0.5 wt.%, a correction for Ba absorbed to MnO_x has been made because sequential extraction confirms that some Ba is associated with amorphous oxides in the peak and is therefore unrelated to biogenic barite (see Material and Methods section). The Fe/Al profiles of both cores display small Fe enrichments at the upper Mn peak, but this is interpreted as a sorption of Fe^{2+} on MnO_x (Koschinsky and Halbach, 1995), because sequential extraction of core BP18 samples release a fraction of the total Fe at the upper Mn peak in the absorbed ion fraction, a feature that is not observed in samples from above or below the peak. It seems that a sorption of Fe^{2+} on to MnO_x
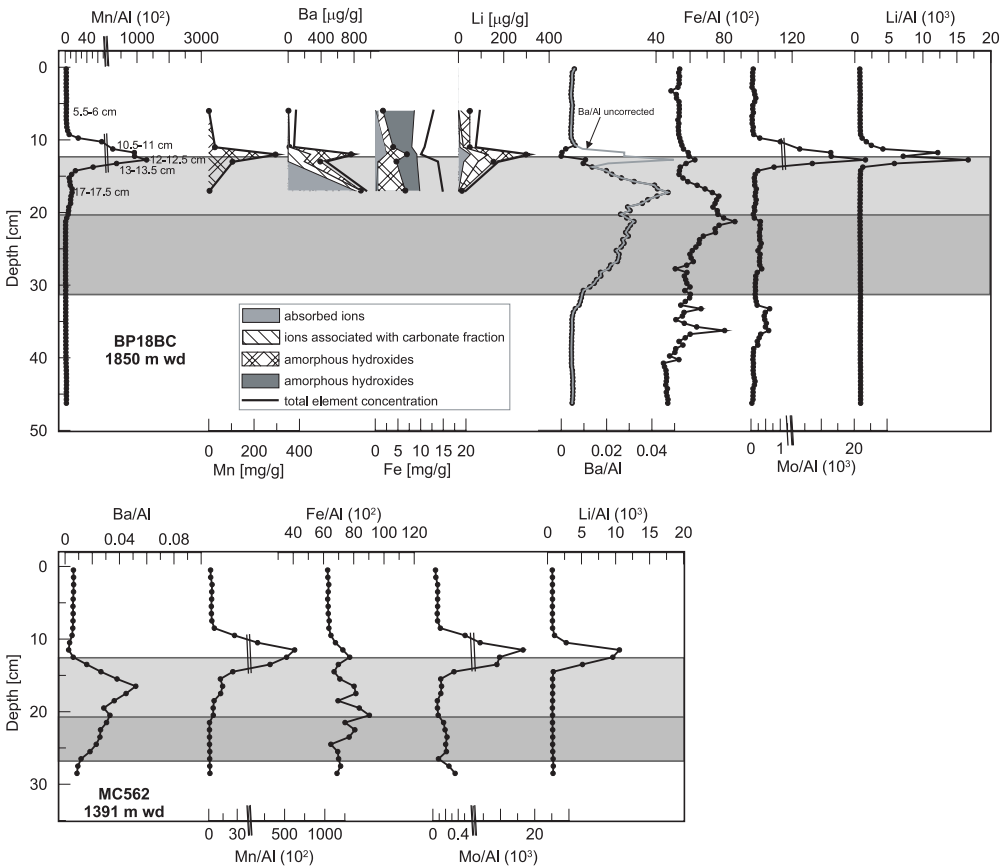
Fig. 3 Upper panel: Element ratios versus depth in core BP18 and elemental concentrations of Mn, Ba, Fe, Li (cumulative presentation) in 5 samples analyzed by sequential extraction. The amount of Ba sorbed on MnO_x is shown as a grey line on the Ba/Al plot. Lower panel: Element ratio profile versus depth for core MC562. Shadings as in Figure 2 indicate the residual and oxidized S1 zones. Note that Mn/Al and Mo/Al plots have an x-axis change of scale. All element concentrations are in μg/g, 10^2 and 10^3 indicates that the ratio was multiplied by 100 and 1000, respectively.

can be discerned when Mn concentrations exceed 5 wt.% (compare Fig. 3 and 5; MC562 with ~9 wt.% Mn and T87-29B with ~5 wt.% Mn). Both Fe/Al profiles show a clear and distinct enrichment of Fe along with the lower Mn peak, but the fraction of Fe released in the amorphous oxyhydroxide fraction by sequential extraction of the BP18 samples increases at this level whereas there is negligible Fe in the absorbed ion fraction (17.5 cm, Fig. 3).

Casford et al. (2003) reported the presence of benthic foraminiferal fauna throughout S1 for MC562. They postulate predominantly conditions of either continuous dysoxia or intermittent ventilation at this mid-depth. Conversely, benthic foraminifera are absent between ~28 cm (~8.73 kyr; interpolated) and 14 cm (5.5 kyr, direct radiocarbon dating) sediment depth in core BP18, implying extensive anoxia over the period of sapropel formation.

(ii) Large upper Mn peaks above the S1 sapropel in oxic conditions: the Marker Bed area

Box core SL125 with a maximum upper Mn peak content of 2.9 wt.% was retrieved from 1946 m water depth in the diapiric crestal area of the Mediterranean Ridge south/southwest of Crete where previously the high Mn values have been reported (Cita et al., 1989; De Capitani and Cita, 1996). Profiles in this core are very similar to those investigated above (Fig. 2, 3), with the exception that its upper Mn peak is both large and broad (Fig. 4). As in the other examples, this peak is located exactly at the top of the S1 unit.

ODP Leg 160 drilled three different holes at Site 971 around a mud dome feature (Napoli Dome) in the Marker Bed area, with Hole 971C located in the circular depression or "moat" that surrounds this mud dome. The S1 unit in the uppermost hydraulic piston core of Hole 971C is unusual in that it is ~65 cm thick, whereas all
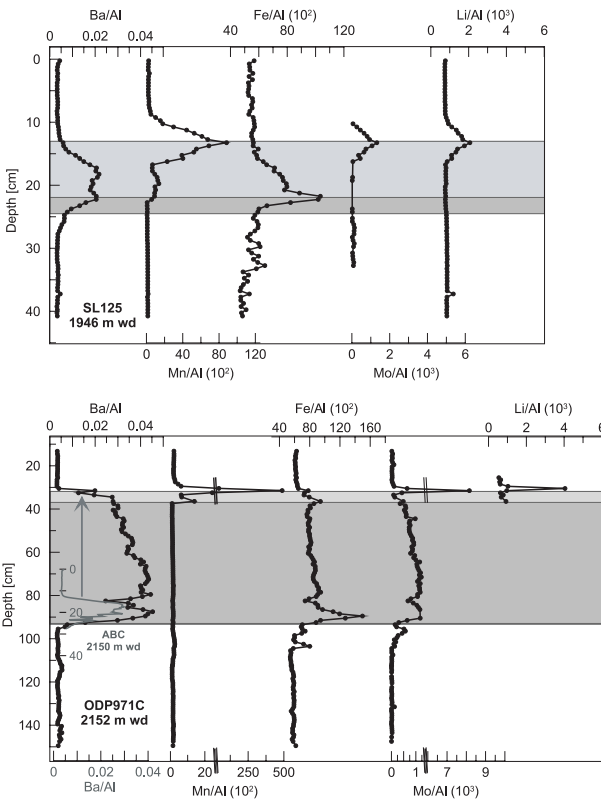
Fig. 4 Upper panel: Elemental ratios versus depth in core SL125. Lower panel: Elemental ratios versus depth in core ODP971C. The Ba/Al profile of nearby core ABC26 is overlain in grey to indicate the inferred position of the original S1 sapropel in this core that is overlain with ~50 cm of redeposited sapropel (arrow) on top. Note that the Mn/Al and Mo/Al plots exhibit an x-axis change of scale. Original element concentrations are in µg/g, 10^2 and 10^3 indicates that the ratio was multiplied by 100 and 1000, respectively. Shadings as in Figure 2 indicate the residual and oxidized S1 zones.

other S1 examples investigated are 15-20 cm thick (Fig. 2, 3, 5). The ODP shipboard description of 971C notes that the S1 unit is "expanded", but our interpretation, based on micropaleontology (E.J Rohling, pers. comm. 2004) and inorganic chemistry is that the extra thickness of this S1 unit is due to a redeposition of ~50 cm of S1 sapropel sediment that occurred towards the end of sapropel times, as indicated in Figure 4. High water contents are commonly associated with high C_{org} contents in sapropel sediments, and down slope displacement of sapropel sediment from the mud dome appears to have occurred unaccompanied by more compact underlying sediments with a lower C_{org} content.

The point of interest of the core 971C S1 for this study is that the upper Mn peak is large and very sharp, with the upper and lower Mn peak maxima containing 14.2 and 0.62 wt.% Mn (Fig. 4). The upper peak is situated at the top of the high Ba/Al values, and the separation of the maxima at 31.5 and 36.5 cm indicate 5 cm of post-depositional oxidation, which is similar to the oxidation depth seen in most other S1 units (e.g. BP10 in Fig. 2). Although different hydrogenetic, diagenetic, or diapiric possibilities for Mn supply could be invoked for a large upper Mn peak in this locality, if the redeposition interpretation (Fig. 4) is correct then this Mn peak must have formed very late in S1 times. It is most likely that the upper Mn peak represents a thin surficial diagenetic MnO_x layer that formed from a pore water flux of Mn^{2+} that was generated from the redeposited sapropel sediment in this unusually thick S1 unit. This interpretation implies that bottom waters must have been oxic. The unusual thickness of the S1 unit by comparison with the other cores from the Marker Bed area (ABC26 and SL125, Fig. 2 and 4) suggest that the inferred redeposition event is the major factor that produced such large upper peak in this case, and its sharpness demonstrates the rapidity of MnO_x remobilization and redistribution.

(iii) Large upper Mn peaks above the S1 sapropel in oxic conditions: Medina Rise

Core T87-29B was retrieved from a water depth of 1530 m depth on Medina Rise and has an upper Mn peak maximum content of 4.7 wt.% Mn (Rasmussen, 1991; Troelstra et al., 1991). The separation of the upper and lower Mn peaks related to post-depositional oxidation is similar to that seen in the other cores, but an important difference is that the upper Mn peak is located in a slightly different position. Its maximum is located 2 cm below the top of the zone of high Ba/Al values that define the full S1 sapropel, rather than exactly on its upper boundary (Fig. 5). On a hydrogenetic explanation for the formation mechanism of upper Mn peaks, this peak must have formed in the sediments before the end of sapropel times. Alternatively, on a diagenetic

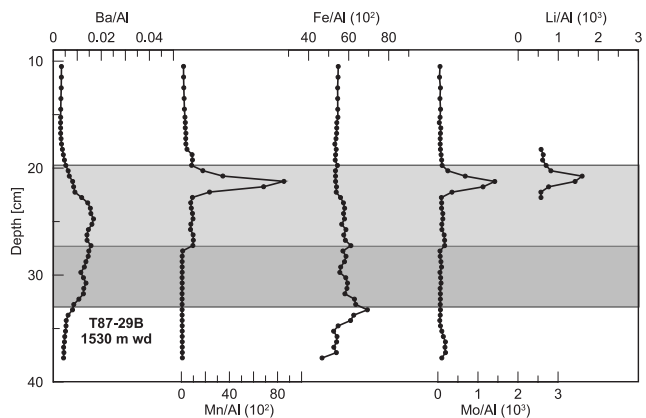Fig. 5 Elemental ratios versus depth in core T87-29B. Original element concentrations are in μg/g, 10^2 and 10^3 indicates that the ratio was multiplied by 100 and 1000, respectively. Shadings as in Figure 2 indicate the residual and oxidized S1 zones.

explanation it must represent a thicker oxic sediment layer at this shallower location during the last phase of sapropel formation.

3.3 Molybdenum sorption on manganese oxyhydroxide (MnO$_x$)

The large Mn peaks discussed above are accompanied not only by enrichments of adsorbed Ba and Fe (section 3.2), but also by variable enrichments of several other redox-sensitive elements. The elements that exhibit the most pronounced and consistent enrichments are Mo and Li. All the cores with large upper high Mn peaks display an exact coincidence of Mn/Al, Mo/Al and Li/Al maxima, with the Mo and Li enrichments clearly dependent on the magnitude of the Mn peaks (Fig. 3, 4, and 5).

Molybdenum is a multivalent element that is present in oxic seawater at relatively high concentration of 10-11 µg l^{-1} (Collier, 1985; Barling et al, 2001), mainly as the stable Mo(VI)O$_4$$^{2-}$ (molybdate) species (Manheim and Landergren, 1978) with the three orders of magnitude less Mo(OH)$_6$ (molybdic acid) (Erickson and Helz, 2000). The main sources of the Mo dissolved in seawater are mobilization during weathering and erosion and subsequent transport by continental runoff, and low temperature hydrothermal input of about 10% of the total (Siebert et al., 2003). Molybdenum can be concentrated from seawater by reduction into strongly reducing or sulfidic sediments, because it is readily incorporated into authigenic sulfides (Huerta-Diaz and Morse, 1992; Crusius et al., 1996; Helz et al., 1996; Vorlicek and Helz, 2002; Sundby et al., 2004). Under these conditions Mo(VI)O$_4$$^{2-}$ is reduced to Mo(IV) (Bertine, 1972; Calvert and Pedersen, 1993). This uptake in sulfidic conditions produces a sufficiently marked increase over the Mo content of detrital material (<1 µg g^{-1}) that Mo has been proposed as an indicator element for sulfidic redox conditions at the time of sediment formation (Piper, 1994; Crusius et al., 1996). High Mo contents are therefore always observed in unoxidized sapropel units along with high S and Fe contents and low Mn contents (e.g. Fig. 3, 4 and 5).

In contrast, an estimated 47-85% of the total Mo removal from the ocean occurs in oxic conditions by pelagic sediments (Bertine and Turekian, 1973; Morford and Emerson, 1999). Shimmield and Price (1986) have summarized evidence for the scavenging and uptake of Mo by oxic Mn-containing sediments, Mn-containing particulate material, and ferromanganese nodules. Although the exact
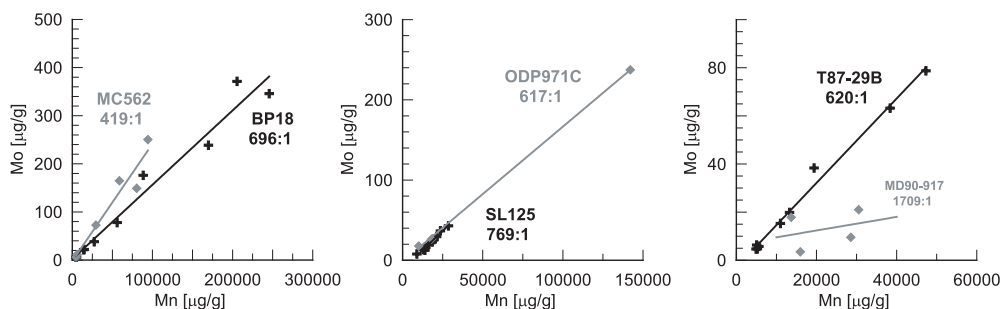

Fig. 6 Correlation of measured Mo and Mn concentrations with mean Mn:Mo ratios shown: left panel core BP018 (black) and MC562 (grey) data, middle panel core SL125 (black) and ODP971C (grey) data, right panel core T87-29B (black) and MD90-917 (grey) data.

mechanism of this Mo uptake remains poorly understood (Barling et al., 2001), Erickson and Helz (2000) suggest that the $Mo(OH)_6$ species is probably involved. Earlier work (Takematsu et al., 1985; Shimmield and Price, 1986; Calvert and Pedersen, 1993), demonstrated that the Mn:Mo mass ratio in Mn-enriched oxic sediments, nodules and crusts is consistently ~500:1 up to 25 wt.% Mn (500 µg g^{-1} Mo). Unlike Mo enrichments with sulfide, burial and preservation of these Mo enrichments in the sedimentary record is not expected because of reductive dissolution of MnO_x on burial. Shimmield and Price (1986) suggest that Mo adsorbed by MnO_x is preferentially released and lost to solution when the Mn[IV] and Mn[III] in MnO_x are reduced to Mn[II]. This contrasts with the behavior of Mn itself, because residual MnO_x can adsorb Mn^{2+} after reductive release to solution.

Most of the Mn in both peaks above the residual S1 is present as MnO_x (see above) and is therefore also expected to adsorb Mo. In the oxic sediments above the residual sapropel, where Mn contents exceed 1500 µg g^{-1} because of the presence of diagenetic MnO_x, Mo is readily measured by ICP-AES and correlates linearly with Mn (Fig. 6). The average enrichments of ~600 (Fig. 6) is slightly higher than the 500:1 ratio reported by Shimmield and Price (1986). The average Mn:Mo ratio of 600:1 appears to be the ratio for Mo adsorbed from eastern Mediterranean bottom waters on to MnO_x.

Molybdenum isotope fractionation was determined for two samples of the upper Mn peak of BP18. The sample with the highest Mn concentration at 12-12.5 cm has a Mo isotope composition of $\delta^{98/95}Mo_{MOMO} = -2.6‰$ (±0.1) and the sample immediately below has a value of -2.4‰ (±0.1). These isotopic compositions are distinctly offset from the values found by Siebert et al. (2003) for ocean waters (of $\delta^{98/95}Mo_{MOMO} = 0‰$) or reducing sediments (of $\delta^{98/95}Mo_{MOMO} = -1.8$ to $-0.5‰$), but lie between the estimated mean crustal input composition (of $\delta^{98/95}Mo_{MOMO} = -2.3$ to $-2‰$) and Fe-Mn crusts and pelagic sediments (of $\delta^{98/95}Mo_{MOMO} = -2.7$ to $-2.9‰$). The preferential sorption of lighter Mo isotopes to the upper Mn peak MnO_x therefore appears consistent with sorption from seawater under oxic conditions (T. Nägler, pers. comm. 2004), although more measurements are required for fuller interpretation.

3.4 Lithium sorption on manganese oxyhydroxide (MnO_x)

Lithium is enriched in the continental crust (Heier and Billings, 1978), and is present in the ocean at the relatively high concentration of ~26 µM (178 µg kg^{-1}). The principal sources for Li are river discharge, hydrothermal fluids, and cold seepage, and the sinks are water column adsorption, low-temperature alteration of basaltic rocks, and silicate weathering (Aloisi et al., 2004b). Alkali elements like lithium are unaffected by redox reactions (James and Palmer, 2000) and most of the uptake of Li into particulate material occurs in the water column before burial in sediments (Zhang et al., 1998). The fraction of Li removed from seawater during early diagenesis of clay minerals is ~8% of the modern riverine flux of Li to the ocean (James and Palmer, 2000; Huh, 1998).

In order to establish the authigenic fraction associated with the large upper Mn peaks, Li_{excess} was calculated as:

$$Li_{excess} = Li_{tot} - (Al_{tot} * (Li/Al)_{det}) \hspace{2cm} (2)$$

because the Li data exhibits a relatively large Li-clay contribution with a constant Li/Al clay ratio. Li_{tot} is the bulk Li concentration determined by ICP-AES and $(Li/Al)_{det}$ is the Li background concentration associated with the clay mineral fraction, determined by sequential extraction as 0.0007. Li_{excess} shows an average Mn:Li correlation of ~750:1 (MC562 652:1; BP18 898:1; SL125 724:1; T87-29B 797:1) within the upper Mn peaks (Fig. 7). This positive correlation of Li_{excess} with
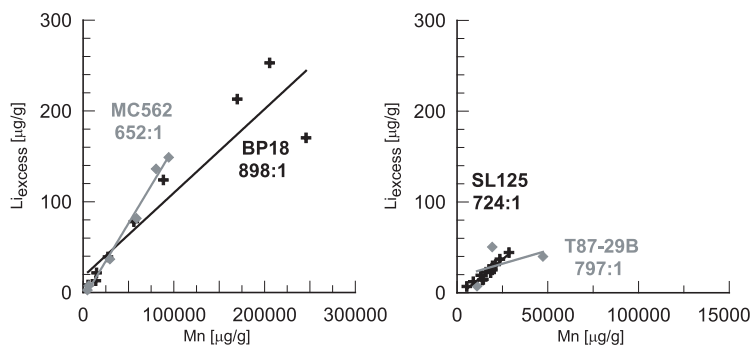
Fig. 7 Correlation of measured Li_{excess} and Mn concentrations with mean Mn:Li ratios shown: left panel core BP18 (black) and MC562 (grey) data; right panel core SL125 (black) and T87-29B (grey) data.

Mn under oxic conditions, comparable to that postulated for Mo above, has not been previously reported to our knowledge. Some but by no means all hydrothermal samples that are rich in Mn-oxides also show distinct enrichments of Li (Hodkinson et al., 1994; Glasby et al., 1997; Koschinsky and Hein, 2003; Dekov et al., 2003). In fresh precipitates from seawater, Sato et al. (1989) found that concentrations of alkali and alkaline earth elements were higher with Mn oxides than with Fe(III) oxides. The ionic radii of Li^+ and Mo^{6+} are the same (0.68 Å), and are believed to substitute for Mn^{4+} with an ionic radii of 0.62 Å (Koschinsky and Hein, 2003). Based on the sequential extraction investigation, the largest Li fraction is released in step 4 that dissolves amorphous oxides (Fig. 3), but a significant fraction is also released in step 3 that dissolves carbonates. According to Koschinsky and Hein (2003), who found similar Li behavior in a leaching investigation, Li might be present either as a loosely bound fraction or as a discrete Li phase. In this work the main fraction of the Li_{excess} is incorporated in or absorbed directly to the amorphous oxide phase and a minor fraction is found as the easily exchangeable phase/absorbed ions. Earlier investigations (Gieskes, 1983; Zhang et al., 1998; James and Palmer, 2000) have shown that Li is a readily exchangeable ion because seawater Li deposited along with marine sediments is readily displaced from the solid to solution by less hydrated cations like NH^{4+}. Thus Li may be direct adsorbed from seawater or from Li released from underlying sediments.

3.5 A large upper Mn peak now located in anoxic conditions: the S1 sapropel in core MD90-917

Mercone et al. (2000, 2001) reported a single large Mn peak of 3.3 wt.% Mn in the S1 sapropel of core MD90-917 recovered from a depth of 1010 m in the Otranto Strait in the Adriatic Sea (Fig. 8). At this locality the sediments accumulate so rapidly that the S1 C_{org} content is low, post-depositional oxidation of the original sapropel is insignificant and there is no lower Mn peak. As a result, the zones of C_{org} and Ba/Al enrichment coincide in this S1 example (Mercone et al., 2001). Like the upper Mn peaks in cores T87-29B (Fig. 5) and BP15 (Fig. 2) that were also retrieved from shallow water depths, the Mn peak in core MD90-917 is within the S1 unit, i.e. it is located in sediments laid down before the end of S1 times, but this S1 unit is now located so deep in the sediments that the pore water condition at this level must now be anoxic.

X-ray diffraction of the sediments from this upper Mn peak revealed a 2.94 Angstrom d-spacing peak characteristic for kutnahorite, the mixed authigenic Mn-Ca carbonate mineral containing trace Mg (Mercone et al., 2001; Fig. 8). Diffusion of Mn^{2+} from reduction of MnO_x is often limited by uptake of Mn^{2+} on to carbonate surfaces in anoxic conditions in oozes and marls (Boyle, 1983;
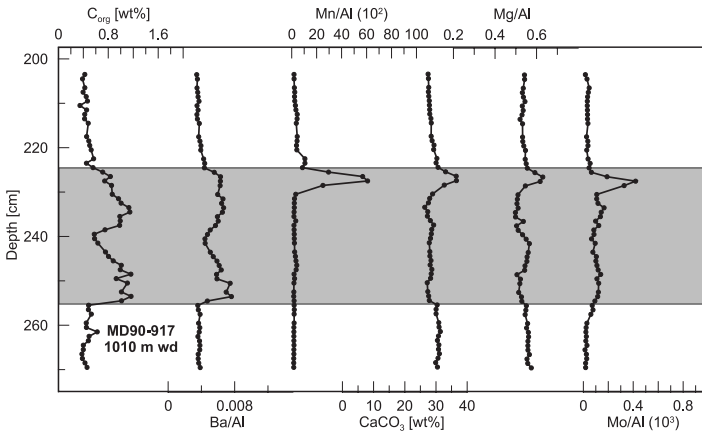
Fig. 8 C_{org} and $CaCO_3$ contents (wt.%) and elemental ratios versus depth in core MD90-917. Original element concentrations are in µg/g, 10^2 and 10^3 indicates that the ratio was multiplied by 100 and 1000, respectively. The residual S1 is indicated by the grey shading (this S1 example is so rapidly accumulated that it has no oxidized section).

Thomson et al., 1986; Middelburg et al., 1987), but formation of kutnahorite is a related and more extreme possibility. A crude estimate of the composition of the authigenic Mn,Ca phase in core MD90-917 was obtained by plotting the Ca and CO_3^{2-} contents (CO_3^{2-} was calculated from total CO_2 released on acid hydrolysis) against Mn content (Fig. 9). Over the 7 upper Mn peak samples with a Mn content >0.5 wt.%, the best-fit lines indicate a molar balance of additional Mn plus Ca versus additional CO_3^{2-} that corresponds to $(Mn_{0.77}Ca_{0.23})CO_3$. This is similar to the Mn molar fraction of 0.7-0.8 found in the authigenic Mn,Ca carbonates that form episodically as chemical laminations in the sediments of the Baltic Sea deeps. It has been concluded that the critical requirement for the formation of these Baltic Mn layers is the development of very high (>0.2 mmol kg^{-1}) pore water Mn^{2+} concentrations from MnO_x reduction in the presence of alkalinity (Kulik et al., 2000; Neumann et al., 2002). The Mn peak in core MD90-917 demonstrates that a similar conversion of MnO_x to kutnahorite also occurs in eastern Mediterranean sediments when large MnO_x peaks are reduced. Given the repetitive nature of sapropel formation, such authigenic Mn, Ca carbonate peaks, probably of smaller magnitude, can also be expected to have formed in the sedimentary record in association with older sapropels, although their long-term persistence is not assured (Van Os et al., 1991, 1994, De Lange et al., 1994, Heiser et al. 2001).
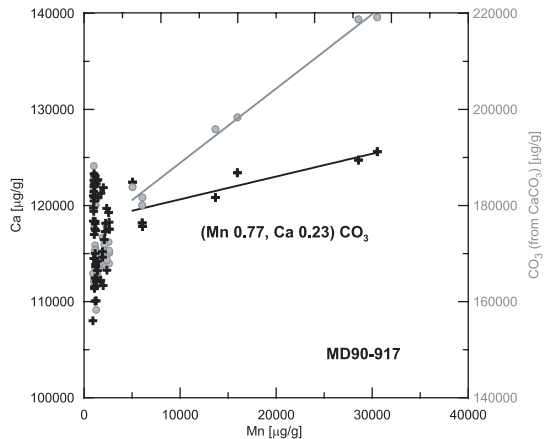

Fig. 9 Correlation of Ca and CO_3 with Mn from core MD90-917 (all data). The two regression lines through the seven samples with Mn >5000 µg g^{-1} indicate a molar balance of additional Mn plus Ca versus additional CO_3^{2-} that corresponds to $(Mn_{0.77}Ca_{0.23})CO_3$.

If adsorbed Mo is lost preferentially when MnO_x is reduced, as suggested by Shimmield and Price (1986), Mo would not be expected to accompany the Mn in kutnahorite. In fact a clear Mo peak does occur in coincidence with the Mn peak, although the Mn/Mo mass ratio at and above this Mn peak averages ~ 1700:1, considerably larger than the Mn/Mo ratios observed for MnO_x in oxic conditions in the cores discussed above where the MnO_x is still in oxic conditions (Figures 6 and 8). Loss of Mo from MnO_x on reduction therefore appears to have been extensive but not complete.

3.6 A conceptual model related to water depth and ventilation to form large upper Mn peaks above sapropel S1.

From the consideration of different S1 sapropel units just discussed with upper peaks of >3 wt.% Mn some generalizations can be drawn. (1) Such large Mn concentrations are found at other eastern Mediterranean localities besides the crestal diapiric ridge (the Marker Bed area), e.g. on the Libyan slope, Medina Rise, and the Straits of Otranto (Fig. 1). (2) Apart from core ODP971C (2152 m), all S1 examples with unusually large upper peak Mn contents occur in sediments retrieved from water depths between 1100-2000 m (Fig. 10). Not all cores in this water depth range exhibit large peaks however, and peak magnitudes are highly variable in the two areas from which multiple cores are available, the Marker Bed area (this work; Cita et al., 1989; De Capitani and Cita, 1996) and the Libyan slope (this work). (3) In the Libyan slope cores studied here, a benthic foraminiferal fauna is present throughout S1 in core MC562 from 1391 m (Casford et al., 2003), but completely absent from the S1 unit of core BP18 from 1850 m indicating that bottom waters at these depth interval could not have been continuously anoxic during S1 formation. (4) The systematics of parallel Mo and Li enrichments with Mn are consistent with all the upper Mn peaks that are still in oxic conditions being present as MnO_x.

Paleoceanographic models for intense solid phase Mn enrichments in sediments envisage that their formation occurs where oxic/anoxic interfaces in the water column intersect bottom topography (e.g. Force and Cannon, 1988; Frakes and Bolton, 1992; Calvert and Pedersen, 1996). Focusing of fine particulate MnO_x precipitated in the water column on to topography also results in variable localized Mn enrichments. Two independent but related lines of evidence suggest that it is likely that during S1 formation eastern Mediterranean sediments in deeper water had less
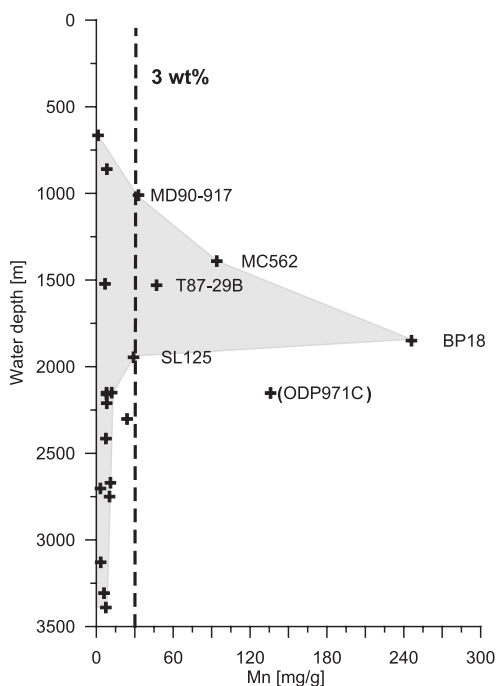

Fig. 10 Maximum Mn content (mg/g) in the upper Mn peaks of the cores studied versus water column depth. Additional data from cores MC12 and 07S (Thomson et al., 1995), UM15, 26 and 35 (Van Santvoort et al., 1996) and LC21, BC12, LC25 and MDVAL90-9502 (Mercone, 2000) are also shown. The dashed line is at 3 wt.% Mn. The shaded area indicates the general trend of Mn-enrichment.

exposure to bottom water oxygen than sediments in shallower water. Murat and Gott (2000) found that the C_{org} of S1 units increased systematically between water depths of 500-4000 m, and inferred that deeper sediments must have experienced lower mean bottom water O_2 levels than shallower sediments. Casford et al. (2003) noted that benthic foraminifera occur throughout S1 sapropel units in several cores retrieved from water depths <2000 m, and inferred that bottom waters must have been dysoxic or at least regularly and intermittently oxic.

The combination of less intense or less frequent bottom water ventilation and higher preserved C_{org} contents in the deepest sediments during sapropel formation would be expected to lead to enhanced sulfide formation that would promote anoxia in the overlying bottom waters and thus allow a loss of Mn^{2+} from the sediments to bottom waters. The presence of O_2 higher in the water column, either continuously or regularly during S1 times as required by the C_{org} and benthic foraminiferal evidence, would be expected to precipitate this Mn^{2+} where and when oxic and anoxic waters met and mixed.

In the present anoxic water column of the Black Sea, the highest dissolved Mn^{2+} contents occur in the few hundred meters below the redox interface that is located at ~200 m (e.g. Lewis and Landing, 1991). This results from precipitation of MnO_x at the oxic/anoxic redox interface in the water column in response to mixing and diffusion, and from the continuous re-dissolution of precipitated MnO_x as it sinks back down into the deeper, anoxic sulfidic water column. Kempe et al. (1991) also reported that a fine particle layer (FPL) with a large increase in dissolved Mn^{2+} below it follows the pycnocline in the Black Sea. This FPL also has higher manganese concentrations towards the shelf where particulate MnO_x deposited in the sediment is exposed to reducing bottom waters. A similar process could be expected for the eastern Mediterranean during S1 times, but the geometry of the oxic/anoxic interface must have been quite different. Some level of ventilation to considerable depth is required to introduce O_2 at depth to react with deep anoxic waters containing Mn^{2+} and form MnO_x.

Differences in oxygenation level with water depth during sapropel S1 formation thus readily provide a mechanism through which both a preferential loss of Mn^{2+} from the deepest sediments and a preferential deposition of MnO_x on higher topography in the basin might occur. The facts that benthic foraminifera occur throughout S1 (Casford et al., 2003), and that the evidence of increasing C_{org} contents with water depth comes from the earlier (residual) parts of S1 units (Murat and Gott, 2000), further indicates that these differences in the mean oxygenation levels must have occurred throughout S1 formation. A single basin-wide ventilation event at the end of S1 times could not have been the cause of the Mn distributions now observed in the sediments nor the cause of upper Mn peaks. The record of multiple hydrogenetic inputs of MnO_x to mid-depth sediments as implied by this mechanism would not be preserved as spikes in Mn content in S1 sediments, however, because anoxic pore water conditions in the sapropel would dissolve them and concentrate them into a single surficial diagenetic MnO_x layer. This process is exemplified by the large narrow upper Mn peak in core ODP971C that sits at the top of the thick, largely redeposited S1 unit. The large upper Mn peak is consistent with a zone refining of Mn from the body of that unusually thick (redeposited) sapropel to the top of the unit to form MnO_x, which implies anew that bottom waters must have been oxic to some degree at the time of its formation late in S1 times.

The large Mn peaks now observed are therefore interpreted as mainly diagenetic, even though the Mn additions to intermediate water depth S1 units were hydrogenetic in nature. Indeed the unusually

large upper Mn peaks occur at and above the depth (~2000 m) at which mud mounds are found in the eastern Mediterranean (Robertson and Kopf, 1998; Kopf et al., 2000). These mounds certainly emit CH_4 and possibly Mn^{2+}, but any Mn^{2+} contribution from this source would be expected to produce fine MnO_x in the water column that would behave similarly to the hydrogenetic MnO_x just discussed (Klinkhammer and Hudson, 1986).

One corollary of the mechanism envisaged is that sediments from the deepest parts of the basin are expected to have experienced the most marked sediment and bottom water anoxia and therefore to have lost most Mn. All published profiles from cores at >2500 m water depth exhibit upper Mn peak contents <1 wt.% (Fig. 10) like the deep-water core SL114 (Fig. 2, Table 1). On the other hand, higher mean O_2 concentrations in bottom waters above shallower-water sites can account for the repeated finding of upper Mn peaks located within, rather than at the tops of S1 units in cores from widely separated but always shallower-water locations (cores BP15, T87-29B, MD90-917; Fig. 2, 5, 8 and 10). Higher bottom water O_2 tensions at these sites during sapropel formation would result in a deeper oxic layer, and the available Mn in the sediments would be diagenetically refined into this deeper oxic layer in the sapropel rather than at the very top as in most examples. Core MD90-917, for example, is located at the outlet to the Adriatic Sea, one of the areas where new eastern Mediterranean bottom water is formed, and where the highest O_2 levels should first be encountered. The large peak in this core also indicates that large Mn enrichments, originally formed as MnO_x, might be found preserved as kutnahorite above older sapropel units.

4. Conclusions

A set of cores with particularly large (>3 wt.%) Mn contents in the uppermost of the two Mn-enriched horizons usually observed above sapropel S1 have been examined in the light of other S1 studies. Although mostly equivalent in time to smaller upper Mn peaks, the magnitude of these large Mn peaks appears very variable in any particular area, and the wide variation in Mn content does not appear to be reflected in other geochemical parameters apart from those trace elements whose concentration is controlled by uptake on to MnO_x. The preferred scenario envisages a diagenetic loss of Mn^{2+} from the deepest (>2000 m water depth) sediments into anoxic bottom waters, a re-precipitation of this Mn^{2+} as MnO_x where it encounters O_2 higher in the water column, and a removal of MnO_x on higher topography in oxic waters. The precipitation step requires that anoxic and oxic waters meet and react at intermediate water depths (1000-2000 m). This mechanism is consistent with higher mean O_2 levels at intermediate depths than at the deepest depths in the basin, that is also required by micropaleontological and C_{org} evidence. This situation must also have occurred regularly during sapropel formation rather than in a single event at the end of the S1 period, because benthic foraminifera and lower C_{org} contents are found throughout S1 units from shallower water depths. The combination of pore water anoxia at shallow depth in the sapropel and some level of oxygen in bottom waters would maintain the excess Mn introduced by this hydrogenetic mechanism as large diagenetic surficial peaks in the sapropel sediments. Molybdenum and lithium become incorporated into this diagenetic MnO_x at fixed Mn/Mo and Mn/Li ratios of ~0.0016 and 0.0013, and a of $\delta^{98/95}Mo_{MOMO}$ ratio of ~-2.5‰ supports this hydrogenetic mechanism.

Acknowledgements

C h a p t e r   5

Effects of the Santorini (Thera) eruption on manganese behavior in Holocene sediments of the eastern Mediterranean

Abstract

The explosive eruption on the island of Santorini in ~1630 B.C. in Minoan times had a large environmental impact over the eastern Mediterranean region. It has even been suggested that a Mn-enriched layer (the "Marker Bed") that lies above the most recent sapropel (S1) in the sediments of a crestal area of the Mediterranean Ridge gained Mn from a hydrothermal source related to the Santorini eruption. Radiocarbon dating of two cores from this area sampled at high resolution demonstrate that this large Mn peak in fact pre-dates the Santorini event by ~2.5 ky and forms part of a pattern seen in Mn profiles from all over the eastern Mediterranean. This same Mn profile shape is altered in areas that experienced substantial deposits of either the tephra layer emitted by the Santorini eruption or the turbidites that were triggered by it. Evidence of both of these perturbations is readily identified from compositional element/Al and Sr/Ca profiles that are distinct from those of the enclosing sediments. In one core with a 37 cm thick Santorini ash layer an oxidation front succeeded in penetrating the whole ash layer after emplacement to form a Mn peak but is now retreating. In cores where thin (<15 cm) Santorini turbidites or ash layers lie above S1, oxidation fronts initially form additional Mn peaks on top of the turbidites and subsequently alter the characteristic double peaked Mn profile shape usually observed above sapropel S1.

1. Introduction

Cita and co-workers have reported the widespread occurrence of a prominent dark layer in the near-surface sediments of a diapiric area on the crest of the Mediterranean Ridge south of Crete (Cita et al., 1989; Camerlenghi et al., 1992; De Capitani and Cita, 1996; Hieke et al., 1996). This layer lies above the most recent eastern Mediterranean sapropel (S1) that formed in the Holocene between 9.8 and 5.7 ^{14}C ky (De Lange et al., submitted for publication), and its coloration is due to variable Mn contents of up to 25 wt.% of the total sediment (Cita et al., 1989; De Capitani and Cita, 1996; chapter 4). Formation of this Mn-enriched "Marker Bed" layer was ascribed to an expulsion of hydrothermal fluid, possibly related in some manner to the catastrophic explosive eruption of Santorini that occurred between 1599 and 1633 B.C. in the late Bronze Age (Ramsey et al., 2004).

Recent work (De Lange et al., submitted for publication; chapter 4) has shown that similar layers with Mn contents of >3 wt.% occur at other eastern Mediterranean localities besides the Marker Bed area, but apparently always at water depths between 1000-2000 meters. Reitz et al. (chapter 4) consider that all these high Mn peaks are principally diagenetic in nature even though the large amount of Mn involved probably results from multiple earlier hydrogenous input events.

Two distinctly separated Mn peaks, generally both with concentrations of <1 wt.% Mn, occur in the sediments above the S1 sapropel in the eastern Mediterranean basin (Higgs et al., 1994; Thomson et al., 1995, 1999; Van Santvoort et al., 1996). The *upper* peak marks the position of the oxic layer that was present at the top of the sapropel at the end of S1 times (chapter 4; Van Santvoort et al., 1996), while the *lower* of the two Mn peaks is forming actively as a consequence of early diagenesis (Van Santvoort et al., 1996). In this latter case, O_2 diffusing downwards from oxygenated bottom waters reacts with Mn^{2+} diffusing upwards in the sediments from anoxic conditions at depth to precipitate MnO_x. The maximum Mn content at the lower face of this lower peak therefore marks the present limit of oxic conditions in the sediments, and is located immediately above the dark C_{org}- and sulfide-rich visual (residual) S1 unit. This same high mobility of Mn during early diagenesis leads to the expectation that Santorini's Minoan eruption might have had some influence on Mn profiles. This work investigates the Mn peaks observed in sediments from the Marker Bed area and from other areas where the S1 sapropel is overlain either by the ash layer or turbidites resultant from the Santorini eruption.

2. Sedimentological expressions of the Santorini eruption

The explosive Minoan eruption of Santorini was an event of considerable environmental significance (LaMoreaux, 1995; Pyle, 1997), and two distinct expressions of the event are found in the eastern Mediterranean deep-sea sediment record. The ash emitted, also known as Mediterranean tephra Z2, is distinctive in geochemistry and mineralogy (Keller et al., 1978) and is present as a cm-dm thick layer in the south-eastern Aegean Sea and in the north-western Levantine Sea (e.g. Sparks et al., 1983; Narcisi and Vezzoli, 1999; McCoy and Heiken, 2000).

In other deep regions of the eastern Mediterranean, turbidites interpreted to have been triggered by the tsunami induced by the collapse of the Santorini caldera are found (Kastens and Cita, 1981; Cita et al., 1984, 1996; Hieke, 1984; Cita and Aloisi, 2000). These turbidites have all been termed "homogenites" (Cita et al., 1984), later subdivided into two basic types A and B and two specific types C and D (Cita et al., 1996; Cita and Aloisi, 2000). Type A is a pelagic turbidite of local provenance that is found at the bottom of small ponded basins of the Calabrian and Mediterranean Ridges. Type B is an abyssal turbidite of distal provenance most likely sourced from the Libyan coast in the Gulf of Sirte that has been found on the Ionian Abyssal Plain and Sirte Abyssal Plains. This Type B homogenite has also been termed the Augias turbidite by Hieke (1984; 2000). The Sirte and Ionian Abyssal Plains are linked through the Ionian Gap, and this turbidite is >10 m thick on the floors of both plains. Type B homogenites often have a thick sandy base (Cita and Aloisi, 2000). Where present, homogenite and the Z2 tephra intervals are always located above sapropel S1.

Deposition of either an ash or a turbidite in a sufficiently thick layer at the sea floor will influence the redox profile in the pore waters of the underlying sediment. The diffusive penetration of bottom water O_2 into the newly deposited surficial sediment layer over time will depend on the rate of O_2

consumption by reduced species within it (Jahnke, 1998). In the case of turbidites, the main reductants are expected to be C_{org} and sulfides (Wilson and Thomson, 1998), although ash from Mount Pinatubo has also been shown to consume O_2 (Haeckel et al., 2001). The loss of oxygen tension in the sediments at depth under the turbidite that occurs as a consequence of this surface blanketing can be expected to affect Mn speciation and distribution, because MnO_x at depth will be reduced by reductants like Fe^{2+} that are present in anoxic pore waters (Postma, 1985). The Mn^{2+} so produced is then free to diffuse to produce new near-surface diagenetic MnO_x peaks where pore water O_2 is re-encountered in the upwards direction (Wilson et al., 1985; Thomson et al., 1993; Mucci and Edenborn, 1992; Deflandre et al., 2002; Mucci et al., 2003). It has been found in the Madeira Abyssal Plain turbidite succession (Wilson et al., 1985; Thomson et al., 1993) and elsewhere (Mucci and Edenborn, 1992; Jung et al., 1997; Haeckel et al., 2001; Deflandre et al., 2002) that such oxidation fronts advance rapidly over dm into the redeposited units, depending on the concentrations of reductants present (solid phase C_{org} and sulfide, pore water Fe^{2+} and Mn^{2+}), but rarely achieve >1 m penetration. Since the Type B homogenite found on eastern Mediterranean abyssal plains is 10-20 m thick, it follows that the active oxidation front will be located somewhere in the uppermost few dm of this unit.

3. Methods

Locations and water depths of the cores discussed are presented in Table 1, and their positions in the eastern Mediterranean basin are illustrated in Figure 1.

The analytical data discussed were obtained at different times on different Inductively-Coupled Plasma Atomic Emission Spectroscopy (ICP-AES) instruments in different laboratories; comparison of methods and techniques used were done on selected cores. Data for cores MC12, SL60, SL125, SL139, and BC19 were collected after total dissolution with HF by methods similar to that reported by van Santvoort et al. (1996), while those for core T87-19B were collected after a 1:5 fusion with $LiBO_2$ by the method of Totland et al. (1992). To monitor precision and accuracy of the methods used, sample duplicates and international as well as in-house standards were applied.

Table 1. Positions and water depths of the cores investigated.

Core	Latitude [°N]	Longitude [°E]	Type of corer	ship / year	Water depth [m]	Upper Mn peak maximum [mg/g]
SL60	35°39.7′	26°35.0′	Piston	Prof. Logachev 1999 (Smilable)	1522	7.7
SL125	33°39.4′	24°33.0′	Box	Prof. Logachev 1999(Smilable)	1946	28.6
MC12	33°23.7′	25°01.3′	Multi	Marion Dufresne 69 / 1991	2211	8.1
BC19	33°47.9′	28°36.5′	Box	Marion Dufresne 69 / 1991	2750	10.3
SL139	34°16.1′	19°49.8′	Box	Prof. Logachev / 1999 (Smilable)	3293	8.6
T87-19B	36°48.9′	19°10.7′	Box	Tyro / 1987	3483	4.3
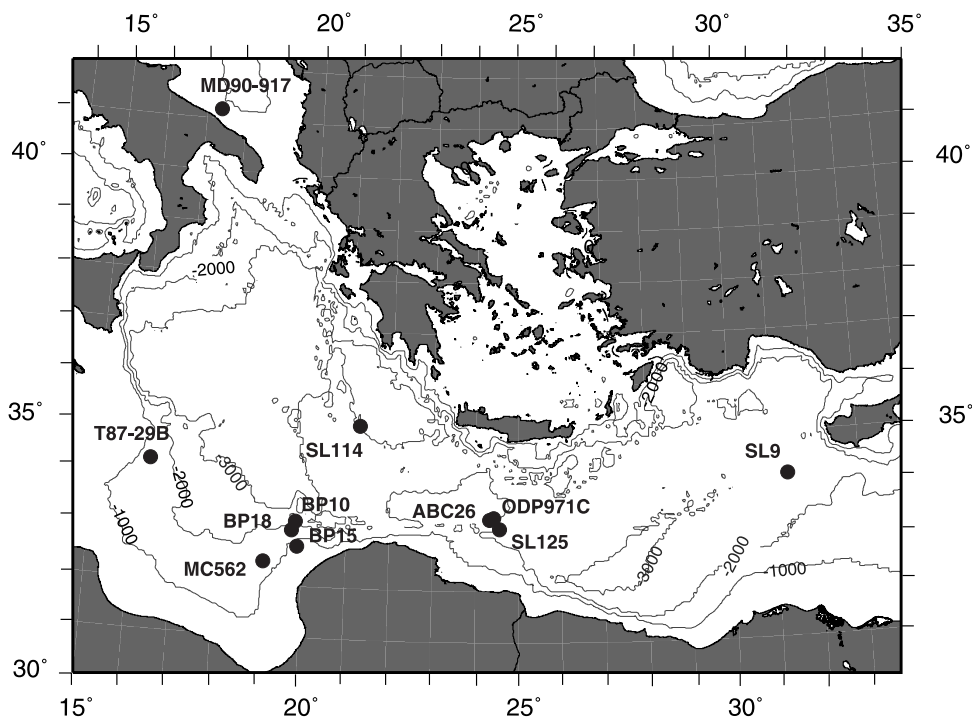
Fig. 1 Map of the eastern Mediterranean with locations of the cores investigated. Bathymetric contours are at 1000 m intervals.

Pore water analyses of Fe and Mn of BC19 and SL139 were made by Atomic Adsorption Spectrometry (AAS), after onboard sampling according to the method described by van Santvoort et al. (1996). Each sample solution was analyzed in triplicate, and a deviation of less than 10% was accepted.

CaCO$_3$ was determined after analyzing the total carbon of bulk samples and organic carbon of the decarbonated samples on a Fisons Instruments CNS NA analyzer using dry combustion at 1030°C.

$$CaCO_3 \text{ wt\%} = (C_{tot} \text{ wt\%} - C_{org} \text{ wt\%}) / 12.01 * 100.09 \qquad (1)$$

where C$_{tot}$ is the measured total total carbon, C$_{org}$ is the organic carbon measured in decarbonated samples and 12.01 and 100.09 are the molar weights of C and CaCO$_3$. Removal of inorganic carbon (C$_{tot}$ − C$_{inorg}$) was achieved by adding 7.5 ml 1M HCl to ~300 mg of sediment, shaking for 12 hours than centrifuging off the acid; this step was repeated with a shaking time of 4 hours and subsequently the sediment was washed twice with demineralized water and dried before the C$_{org}$ analysis. International and in-house standards and duplicates were processed at the same time to monitor the accuracy and precession of the analyses.

Bulk element concentrations (e.g. Fe, Mn and Ba) are normalized to Al to take account of fluctuations in aluminosilicate content, on the assumptions that the element/Al ratio in detrital material should be relatively constant, and that increases in these ratios indicate where diagenetic enhancements of these redox-sensitive elements occur (Van Os et al., 1991).

4. Results and discussion

4.1 A comparison of Mn profiles in the Marker Bed locality

Box core SL125 was retrieved from the Marker Bed locality on the diapiric crestal area of the Mediterranean Ridge south/southwest of Crete where Cita and co-workers reported the highest Mn values. Earlier geochemical investigations (Cita et al., 1989; De Capitani and Cita, 1996) compared spot samples from the Marker Bed with samples taken a few cm above and below, so that SL125 is the first core from the area with an unusually large Mn peak for which detailed and continuous inorganic geochemical profiles have been gathered. These profiles are compared with similar data from nearby core MC12 (Fig. 2) that have been used to elucidate the post-depositional diagenetic modifications experienced by sapropel S1 (Thomson et al., 1995, 1999). Although the upper Mn peak maximum in core SL125 is at the lower end of the wide range of values reported by De Capitani and Cita (1996), the Mn enhancement is substantial at 2.9 wt.% Mn compared with 0.8 wt.% Mn at the corresponding Mn maximum in core MC12.

The original and visible boundaries of sapropel S1 are defined by criteria described by Thomson et al. (1999) from variations of element/Al ratios (Fig. 2). The Mn/Al profile in both cores shows the typical double peak feature with the upper peak exactly on top of the zone of high Ba/Al values that accompany high initial C_{org} values in sapropels, while the lower peak is situated immediately above the dark residual S1 unit. The coincidence of the upper Mn maximum with the point at which Ba/Al values return to the low constant detrital value from the high Ba/Al values characteristic of sapropel S1 times has also been reported in several other eastern Mediterranean cores (Thomson et al., 1995; Van Santvoort et al., 1996; Mercone et al., 2000; Slomp et al., 2002; chapter 4). The position of the lower Mn peaks mark the limit of the post-depositional oxidation of sapropel organic matter that has occurred since formation of the upper Mn peak at the end of S1 times (Fig. 2).

The sapropel Ba/Al levels are higher in core MC12 than in core SL125, while the upper Mn/Al peak in SL125 is much larger than that in MC12. The Sr/Ca levels are high in and around the sapropel in both cores. This has been attributed to diagenetic aragonite formation that accompanies sulfate reduction in sapropels (Thomson et al., 2004), whereas recent results suggest that a near coastal source may be more important (chapter 6). The $CaCO_3$ and element/Al profiles (K, Ti, Zr) are similar in both cores. This comparison of the elemental profiles in the two cores demonstrates both the compositional variability that is found in different S1 examples and the consistent evidence of the post-depositional oxidation that has been experienced by S1 units since their formation (Fig. 2).

Radiocarbon dating undertaken on planktonic foraminifera separated from a few levels in and around sapropel S1 in several eastern Mediterranean cores including SL125 and MC12 confirms the synchronicity of the age of the S1 units at ~9.8 ky to ~5.7 ky ^{14}C convention years B.P. (De Lange et al., submitted for publication). Recognizing that marine radiocarbon convention ages underestimate calibrated or dendrochronological time by 350-600 years in the time range 5.0 to 9.0 ky B.P. (Stuiver and Braziuas, 1993), the age of the sediments that host the upper Mn peak is ~5.7 ky ^{14}C convention years B.P. which corresponds to a calibrated age of ~6.1 ky B.P. The tephra layer of box core BC19 has an age of about 3.65 ky [14]C B.P. (G. de Lange, pers. comm. 2005). Accordingly, the upper Mn (Marker Bed) peak pre-dates the Santorini eruption ~3.6 ky ago by ~2.5 ky, so that a direct association with the Santorini event can be discounted.
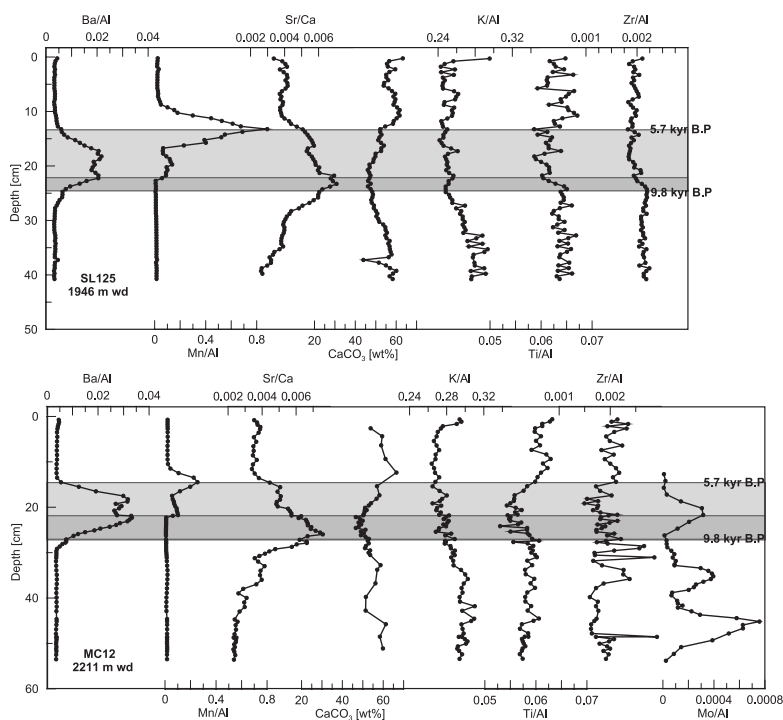
Fig. 2 Element ratios (Ba/Al, Mn/Al, Sr/Ca, K/Al, Ti/Al, and Zr/Al) and CaCO$_3$ concentration in the sediment versus depth in core SL125 from 1946 m water depth (upper panel) and MC12 from 2211 m water depth (lower panel). The residual S1 and the oxidized S1 zones are illustrated by the dark and light grey shadings, respectively. Original element concentrations are μg/g unless otherwise indicated. The time of the beginning and end of sapropel formation is indicated on the boundaries.

4.2 The effect of the Santorini tephra layer on Mn diagenesis

Core SL60 was recovered in the south-east Aegean Sea at 1522 m water depth, and Santorini tephra Z2 is present between 20 and 57 cm, well above the original S1 sapropel at 70-105 cm (Fig. 3). Mercone et al. (2000) reported the ash layer from the Santorini explosion above S1 in another core (MD81-LC21) taken close to the SL60 position, and confirmed the timing of the event with radiocarbon dating to be between ~3.3-3.4 ky ^{14}C convention B.P. Core BC19 was retrieved from an abyssal hill at 2750 m in the western Levantine Basin and is thus more distant from Santorini (Fig. 1). The tephra layer at 6-9 cm depth in this core is much thinner, but well above the original sapropel S1 at 16-28 cm. High Ba/Al, K/Al, Zr/Al and low Fe/Al, Ti/Al, Cr/Al, and Ni/Al ratio values differentiate the distinct dark Z2 tephra layers on compositional grounds from the marl sediments that enclose them in both cores. The ash does not contain biogenic CaCO$_3$ so that its CaCO$_3$ contents are expected to be negligible (Fig. 3). Although the Santorini ash is considered to be very homogenous in composition (e.g. Schmid et al., 2000), the profiles of the element/Al ratios are not "square wave" in shape through the 37 cm thick ash layer in core SL60. It is not immediately evident whether this inhomogeneity is due to an evolution in the composition of the emitted ash over the period of the eruption, or to a differentiation of the ash as it settled from the sea surface through the
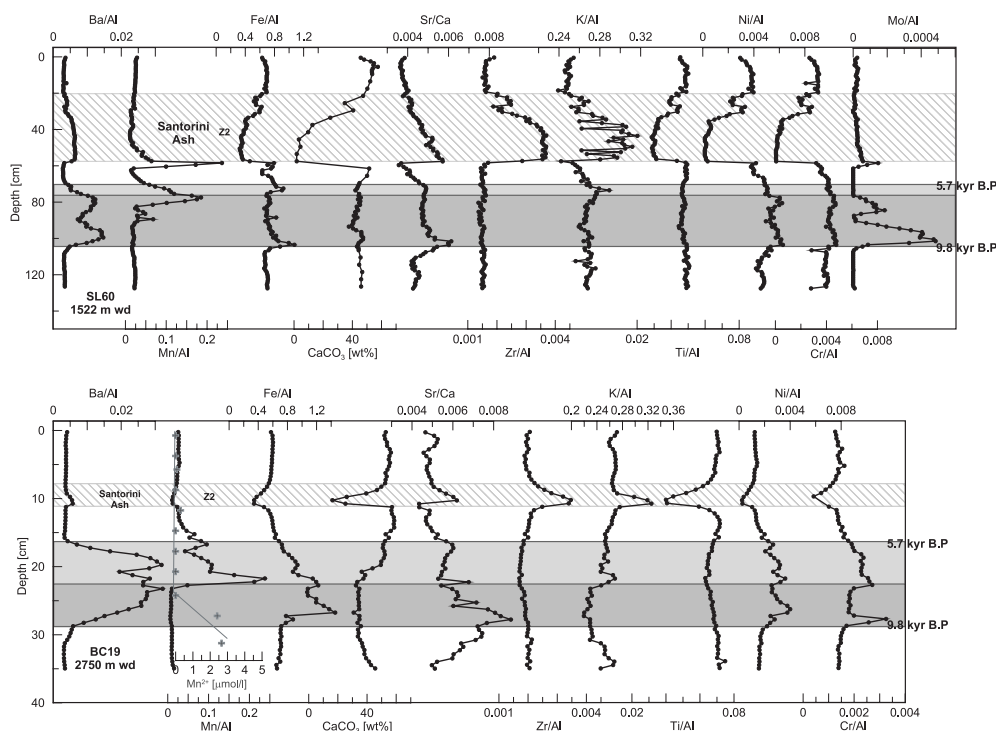
Fig. 3 Element ratios of Ba/Al, Mn/Al, Fe/Al, Sr/Ca, Zr/Al, K/Al, Ti/Al, Ni/Al, Cr/Al, and Mo/Al (core SL60 only) and CaCO₃ concentration in the sediment and pore water Mn²⁺ concentration (core BC19 only) versus depth in cores SL60 from 1522 m water depth (upper panel) and BC19 from 2750 m water depth (lower panel). The residual S1 and the oxidized S1 zones are illustrated by the dark and light grey shadings, respectively. Original element concentrations are µg/g unless otherwise indicated. The Santorini ash layers are indicated by diagonal shading.

water column to the sea floor, or to a contamination of the ash with other sedimentary material introduced either during settling or after emplacement by bioturbation. In order to examine these possibilities, two end-members were calculated from the core SL60 analyses. One of these is an average of the sediment composition above and below the ash layer, and the other is the mean of three contiguous analyses taken near the base of the ash layer that display the most extreme compositional contrasts (highest Ba/Al and Zr/Al, lowest Cr/Al and Ni/Al ratios, and lowest CaCO₃ contents; Fig. 3; Table 2).

Geochemical analyses aimed at confirming a Santorini origin for ashes from different locations tend to compare the compositions of glass fractions that have been cleaned before analysis so as to be free from crystalline components and other contamination (e.g. Schmid et al., 2000; Saminger et al., 2000; Pearce et al., 2002, 2004). By contrast, the core analyses here were bulk geochemical analyses, gathered by sequentially cutting wet sediment from the core, and analyzing dried and ground total sediment that included pore water salt. Comparison of the published glass analyses with the core SL60 ash end-member (Table 2) indicate that the latter is likely to be slightly contaminated with CaCO₃ because its Ca, Mg and Sr contents are all higher than published ash compositions. The higher Mn content is due to post-depositional formation of MnOₓ that is present as a peak at the base of the ash

Element	unit	SL60 Z2 Bulk ICP-AES	BC19 Z2 Bulk ICP-AES	T87-19B turbidite base	SL60 background sediment Bulk ICP-AES	BC19 background sediment Bulk ICP-AES	Bulk pumice Schmidt et al. (2000) XRF	Glass fraction Schmidt et al. (2000) XRF	Ash analysis Peltz et al. (2001)	Minoan Bo-1 Santorini glass Hammer et al. (2003)
		n=3	n=3	n=4	n=30	n=52				
CaCO3	%	1.86	20.75		50.7	55.5				
Al		7.92	6.34	1.06	4.1	3.3	7.44	7.00	7.52	7.32
Mg		0.70	0.99	1.93	2.9	1.9	0.48	0.28		0.21
K		2.28	2.04	3.36	1.0	0.9	2.40	2.70	2.5	3.10
Na		3.84	3.06	5.41	1.3	1.2	3.40	3.30	3.57	2.40
Fe		2.73	2.18	3.12	2.9	2.0	2.22	1.64	2.12	1.73
Mn		0.33	0.07	0.09	0.2	0.1	0.07	0.05	0.06	0.14
S		0.07	0.15		0.1	0.2				
Ti		0.23	0.26	0.28	0.2	0.2	0.27	0.19	0.26	0.36
Ca		2.46	8.31	4.94	19.2	22.2	1.60	1.10	1.45	1.3
Sr	ppm	134.33	421.77	674.4	754.2	1086.5				72
Cu		15.67	27.22	92.9	37.6	44.6				
V		39.68	40.11		68.2	55.7			23	13
Zn		67.45		74.0	63.4				55	
P		376.80	392.58	1298.7	407.7	427.3				
Ba		510.56	358.22	734.9	127.5	120.7	479.00		556	690
Cr		3.79	10.13	18.5	142.1	47.0				1.7
Co		8.16			19.6	15.0			4	
Ni		12.74	15.60	27.8	163.2	46.5				
Y		38.16	36.23	16.0	14.9	16.5				32.5
Zr		217.72	249.73	280.1	64.8	65.9	286.00		271	292

Table 2 Element end-member concentrations of the ash layers and the background sediments in cores SL60 and BC19 as well as of the turbidite base of T87-19B. For piston core SL60 the Z2 ash composition was calculated from the samples at 52.0-54.5 cm, and the background sediment composition from the samples at 0-18.5 and 58-69.5 cm. For box core BC19 the Z2 ash composition was calculated from the samples at 10.25-10.88 cm and the background sediment composition was calculated from the samples at 0-8.38 and 11.5-16.13 cm. For box core T87-19B the composition of the turbidite base was calculated from samples at 16.25-17.75 cm. For comparison published element concentrations of Santorini ash are listed.

bed as discussed below (Fig. 3), and the higher Na content is likely due to pore water salt. When the data are plotted in a ternary diagram with Ca, Ti, and Zr apices selected to separate the end-member ash and background sediment compositions (Fig. 4), data from the visual ash layer in cores SL60 and BC19 plot on a mixing line between the calculated SL60 ash end-member composition and the background sediment composition. This suggests that the visual ash layers in the cores (Fig. 3) are actually a mixture of Santorini ash and sediment, although the question remains open as to whether this mixing occurred during deposition of the layer, or after deposition by bioturbation mixing.

The ash layer of SL60 consists of two sub layers that are clearly distinguishable by the apparent interruption (at ~28 cm core depth) of the characteristic elemental profiles (Fig. 3). The upper layer could be the Kolomvos ash layer that was emitted about 2000 years ago from a volcanic eruption in the South Aegean Sea (McCoy, 1980, 1981). However, from the average element concentration of this layer it is obvious that there is a good agreement of some elements (Al, Zr, Ba; Table 2) with the Z2 in SL60 and BC19 but there is as well a good agreement of some elements (Mg, Sr, Cr, Co, Ni) with the background sediments, so that it is impossible to group this layer clearly to the Z2 or deny a sort of unity. The data points of this upper layer follow in fact the mixing line of the ash-endmember and the background sediment of the SL60 yet they plot much closer to the background data (Fig. 4). It could thus be that it is a secondary and possibly additionally, bioturbated phase of the Z2 ash layer that took much longer to settle through the water column, a minor turbidite of upper ash composition or later wash in of Santorini ash from land surfaces rather than ash material from a different volcanic eruption. However, these possibilities are rather speculative and it is not the target of this paper to classify the ash layers above S1 but to study their effects on the manganese behavior.

In the S1 layers of cores SL60 and BC19 the Ba/Al, Fe/Al, and Sr/Ca ratios are high, particularly in the residual (visual) units. The Mn/Al profiles in these two cores are more complex than the Mn profiles of cores MC12 and SL125. In the core SL60 Mn profile two large peaks are present, one that gradually increases with depth near the base of the turbidite with a sharp maximum immediately under the turbidite base at 59 cm, and a distinct but broader peak that lies in the top of the S1 unit. All 37 cm (20-57 cm) of the coarse ash layer in core SL60 appears to have been penetrated by bottom water O_2 at some time since its emplacement. The evidence for this
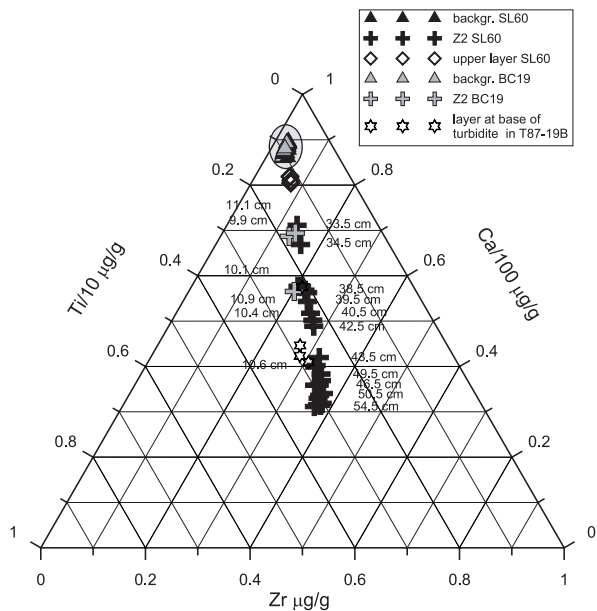

Fig. 4 Ternary plot of Ca/100 μg/g (main element in biogenic carbonates), Ti/10 μg/g (mainly introduced by terrigenous material and the ash), and Zr μg/g (enriched in the ash). Labels on the right are sediment depths in SL60 and those on the left are from BC19. The background composition is indicated by the shading.

penetration is the Mn peak that begins at ~50 cm depth in the ash with the Mn maximum at 59 cm and a sharp cut-off at 61 cm. This peak shape, with a marked increase with depth and a sharp basal cut-off, is that expected to develop at a progressive oxidation front when a diffusive downwards flux of O_2 from bottom waters reacts with an upwards flux of Mn^{2+} to form MnO_x (Wilson et al., 1986; Jung et al., 1997) and is also a shape that can be recognized in many lower Mn peaks in sapropel S1 (e.g. that of MC12 in Fig. 2). Haeckel et al. (2001) found that bottom water O_2 had penetrated ~5 cm into the tephra layer deposited from the 1991 Mount Pinatubo explosion in only 7 years, so both Santorini ash layers here are expected to have been fully oxidized in the 3600 years since their emplacement.

The S1 sapropel at the shallower water location of core SL60 is in the form of two lobes between 70-105 cm, and these sediments were deposited so rapidly that the post-depositional oxidation experienced by most other S1 sapropels is very limited (Mercone et al., 2001). The Mn peak that sits inside but just below the top of the sapropel unit is no longer expected to be present as MnO_x (Mercone et al., 2000, 2001) because it is located so deep in the sediment that pore water conditions must now be anoxic.

Reitz et al. (chapter 4) have demonstrated that Mo is sorbed from bottom waters on to MnO_x in eastern Mediterranean sediments at a Mn:Mo ratio of ~600:1, and have suggested that this value increases as Mo is preferentially lost from MnO_x on reduction (Shimmield and Price, 1986). Where Mo is measurable in core SL60 (only concentrations >1.5 µg g^{-1} appear to be reliable), the Mo/Al ratio displays 3 peaks; the upper two of which are coincident with the two Mn peaks and the lowest coincides with sulfides in the residual sapropel. The Mn:Mo ratio is ~1500:1 at the shallower Mn peak and ~1900:1 at the deeper Mn peak. These Mn:Mo ratios are similar to the ratio of ~1700:1 measured in an Adriatic core where Mo had been lost when MnO_x was reduced and converted to kutnahorite [$(Mn,Ca)CO_3$] (chapter 4). From the Mn:Mo ratios in core SL60, it is inferred that the active oxidation front may now be around 45 cm depth because Mn/Mo values of >500 are found at all greater depths.

The Mn profile of core BC19 has similarities with the general pattern seen elsewhere in the eastern Mediterranean (e.g. Fig. 2), with two distinct Mn peaks (Fig. 3). The upper Mn peak maximum is located at the top of the high Ba/Al values that mark the original S1, while the lower Mn peak has its maximum with an abrupt cut off just above the residual S1 unit. Pore water data for this core reveal that Mn^{2+} from depth in the sediments is being supplied to the base of the lower Mn peak, which in this case is the larger of the two Mn peaks. It is expected that bottom water O_2 would rapidly penetrate the thin ash layer in this core after its deposition. Nevertheless, the additional material added at the sediment surface by the ash layer must have decreased the flux of O_2 available at depth that is consumed in oxidation of either sapropel C_{org} or pore water Mn^{2+}. This corresponds to the change in slope seen in the shape of the lower Mn peak, more of the available O_2 flux has been consumed in Mn^{2+} precipitation rather than C_{org} oxidation since the ash fall event, which consequently slows down the downward oxidation.

4.3 The effect of Santorini turbidites on Mn diagenesis

As described above, a post-emplacement oxidation front must now be located in the upper reaches of the Augias turbidite on the abyssal plains because of its considerable thickness (section 2). Cores SL139 and T87-19B were retrieved well above the floors of the Sirte and Ionian Plains, respectively

(unpublished cruise report, G. de Lange et al., 1999; Troelstra et al., 1991), and in both cores the Augias turbidite is present as a much thinner but compositionally distinct unit. In the nomenclature of Cita et al. (1996), both these examples are type C homogenites that are formed from upslope flow of the material that mainly deposited on the abyssal plains as type B homogenites. Core SL139 was retrieved from 3293 m water depth and the original sapropel S1 lies at 22-30 cm with the turbidite at 4-14 cm, while core T87-19B was retrieved from 3483 m water depth and the original sapropel S1 is at 30-43 cm and the turbidite is at 6-18 cm. Excluding the turbidite thickness, overall accumulation rates based on an age of ~10 ky at the base of S1 are ~2.2 cm ky^{-1} for SL139 and ~3.0 cm ky^{-1} for T87-19B.

The unusual feature of the Augias turbidite is its high concentration of detrital aragonite in a deep water setting (Hieke 1984, 2000), and in cores SL139 and T87-19B this aragonite is evident through Sr/Ca values that are much higher than those found in biogenic low-Mg calcite or pteropod aragonite (Thomson et al., 2004; Rutten et al., 2000). In both cores the Sr/Ca, Mn/Al, Ca/Al and
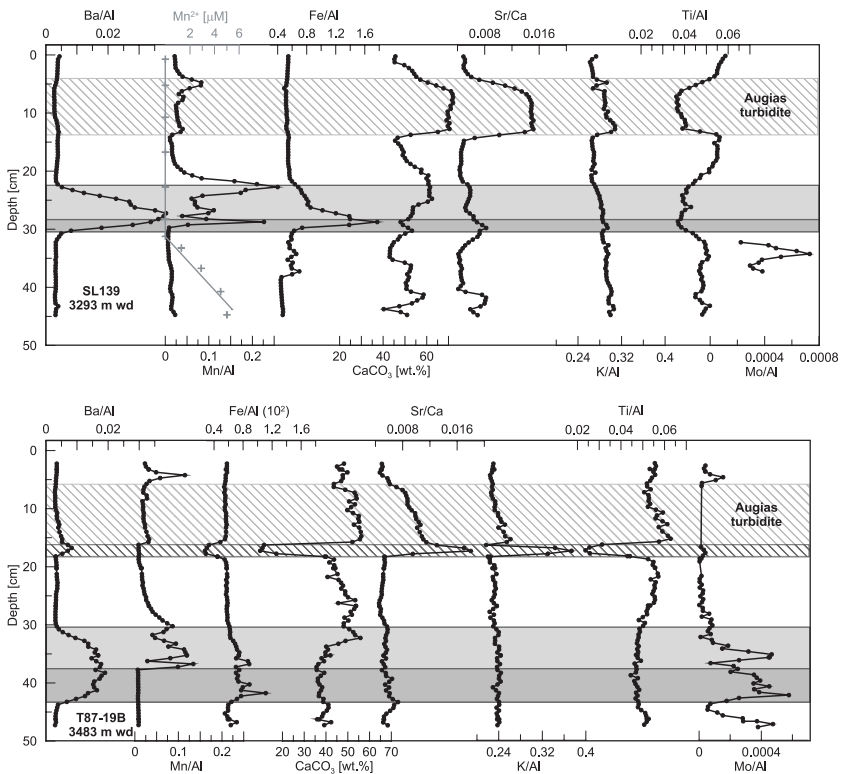
Fig. 5 Element ratios (Ba/Al, Mn/Al, Fe/Al, Sr/Ca, K/Al, Ti/Al, and Mo/Al) and concentration of C$_{org}$, CaCO$_3$, and pore water Mn^{2+} (SL139 only) versus depth in cores SL139 from 3293 m water depth (upper panel) and T87-19B from 3483 m water depth (lower panel). The residual S1 and the oxidized S1 zones are illustrated by the dark and light grey shadings, respectively. Original element concentrations are µg/g unless otherwise indicated. The Augias turbidite is indicated by a light grey diagonal shading and in core T87-19B a layer of different composition is indicated by darker grey diagonal shading; the Sr/Ca peak in this layer is caused by the extreme low CaCO$_3$ content.

Ti/Al profiles show a grading from the coarser bases of the turbidite units to the finer tops (Fig. 5). The compositional characteristics of this turbidite are inherited from its shallow water source sediments, with the high Sr/Ca ratio derived from a high algal aragonite content and heavy minerals delivering high Ti and Zr contents (Hieke and Werner, 2000). The compositions of the Augias turbidite and the background sediments in cores SL139 and T87-19B are not identical, as can be seen in the Ca, Sr and Ti ternary data plot (Fig. 6 a). Some lateral as well as vertical inhomogeneity might be expected in such a large turbidite with an estimated volume as up to 162 km³ (Rebesco et al., 2000).

The ~2 cm thick layer at the base of the turbidite in core T87-19B has a distinctly different composition from the remainder of the turbidite. These compositional differences might be caused by a heavy mineral component contributed from the shallow water source of the turbidite, but the composition of this layer has similarities with the Z2 ash discussed above (i.e. high Ba and Zr, low Ca and Cr; Table 2). Plotting the three data points from this layer on the Ca, Ti, Zr ternary diagram, constructed to display the mixing of Santorini ash and the background sediments of cores SL60 and BC19, shows that the basal layer of the turbidite in core T87-19B may in fact be Santorini ash underlying the Augias turbidite (Fig. 4).

The Mn profiles in both cores are complex but very similar, with small Mn/Al peaks on top of both turbidite layers at 4-5 cm, an increase Mn/Al towards the base of the units, and three Mn maxima in the oxidized zone of the S1 sapropel (Fig. 5) rather than two as seen in other cores (e.g. Fig. 2). These Mn profiles are best considered in the context of the diagenetic readjustments that have been demonstrated to occur in response to the deposition of recent turbidites. That work (Mucci and Edenborn, 1992; Deflandre et al., 2002; Mucci et al., 2003) demonstrates that Mn from the sediment surface that was buried by the turbidite is reduced and migrates as Mn^{2+} up through the turbidite body to form MnO_x at the new sediment/water interface at the turbidite top. This is the likely cause of the Mn peaks at 4-5 cm in both cores. The length of time required for bottom water O_2 to penetrate the 10-12 cm thick Augias turbidite layer in these two cores will depend on the reductant content in the redeposited sediment (Wilson and Thomson, 1998). The Mn content increases with depth into both turbidite units, but it is not clear whether this is a consequence of the passage of the oxidation front through the turbidite with precipitation of MnO_x (as expected from a diffusive oxidation front and observed in the Santorini ash of core SL60), or whether it is a grading effect in the turbidite body (note that Sr/Ca, Ti/Al
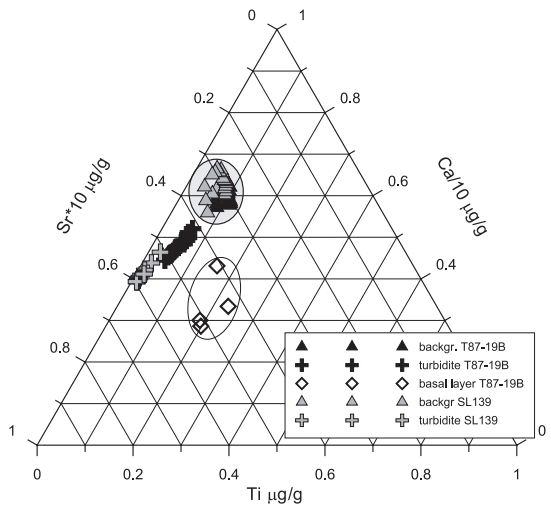

Fig. 6 Ternary plot of Ca/10 µg/g (main element in biogenic carbonates), Ti µg/g (mainly introduced by terrigenous material), and Sr*10 µg/g (enriched in 'Augias turbidite' aragonite). The background composition is indicated by the shading and the open ellipse indicates the divergent composition of the basal layer of T87-19B.

and Zr/Al profiles also plot with a gradient in both turbidites; Fig. 5). The Mn profile shape now observed in both cores may represent some combination of these two effects.

The Mn peaks in the oxidized S1 units are at 23, 27, and 29 cm depth in core SL139 and 30, 35 and 37 cm depth in core T87-19B. In both cores the uppermost of the three Mn peaks is coincident with the upper limit of the high sapropel Ba/Al values and thus corresponds to the upper Mn peak in other S1 units (Fig. 2). It is then likely that one of the other two Mn peaks must mark the penetration depth of O_2 at the time of turbidite emplacement, while the other must mark the present locus of oxidation (usually the lower Mn peak maximum in other S1 units). Pore water data for SL139 reveal that the lowest peak is actively forming through supply of pore water Mn^{2+} from deeper sediments (Fig. 5). For T87-19B it is similarly believed that the lower of the three Mn peaks marks the current limit of oxidation. As in the case of the Santorini ash layer in core BC19, it can be assumed that the turbidite layer was rapidly penetrated by bottom water O_2, but that the O_2 flux from bottom water available to resume oxidation of the sapropel C_{org} must have been less than the flux available before turbidite emplacement because of the new longer diffusion distance from the sediment/water interface to the C_{org} of the sapropel.

Where Mo was measurable in core T87-19B, the Mn:Mo ratio over the Mn peak at the top of the turbidite is ~660, similar to the Mn:Mo ratio of 600 that has been established for MnO_x precipitating under oxic conditions (chapter 4). The Mn:Mo ratios at the three Mn maxima are ~1020, 320, and 480 from the top of the original S1 to the top of the remaining S1. It therefore seems that the upper Mn peak experienced some loss of Mo during the time that it took O_2 to penetrate through the Augias Turbidite. The ratios of the middle and deepest of the three peak appear to have either lost Mn or gained Mo compared with that usually observed for MnO_x precipitated in oxic conditions, or it may be that Mo has redistributed in some fashion between the three Mn peaks.

5. Conclusions

It has been demonstrated that the Mn enrichment in the sediments of the diapiric crestal Mediterranean Ridge crest that has been termed the Marker Bed is hosted in sediments that are ~2500 years older than the Santorini eruption. Such Mn peaks were formed at the end of the period of sapropel S1 deposition, and thus clearly predate the Santorini event and cannot be related to it. However, if ash or turbidites initiated by the Santorini explosion are present in sediments as sufficiently thick layers, they influence diagenesis modifying Mn profiles at and below the sediment surface that was blanketed by the ash or turbidite.

Acknowledgements

C h a p t e r   6

Enhanced Sr-rich aragonite in eastern Mediterranean sapropel (S1): diagenetic versus detrital/biogenic origin

Abstract

CaCO$_3$ contents in eastern Mediterranean sapropels are generally lower than in the enclosing marl sediments. In sediments of a transect from ~650 to 2100 m water depth at the Sirte continental slope the opposite feature was observed. Although the increased Sr/Ca ratios observed in these sediments agree with such feature observed in other eastern Mediterranean S1 sediments, their absolute magnitude is much higher. The enhanced Sr/Ca ratio in these sediments is associated with their aragonite content, which for the Sirte transect reaches levels of up to ~40 wt.%. The aragonite content and Sr/Ca ratios in the S1 sediments of this transect decrease with increasing water depth and decrease with distance to the African coast for all eastern Mediterranean cores. In view of the lack of a coherent relationship with sedimentary reduced sulphur contents and porosity, and considering the major amount of aragonite found specifically in the sediments of the Sirte transect, authigenic precipitation can contribute only a limited fraction at most. SEM observation and electron-microprobe analyses showed that the needles and needle clusters are morphologically aragonite, contain the highest Sr/Ca ratio, and are similar to skeleton fragments of the green alga *Halimeda*. Consequently, a detrital/biogenic source is the likely mechanism for the major part of the aragonite enrichments found in S1 sediments of the Sirte transect and by inference must also play an important role for other sites. Possibly, upwelling and run-off related offshore directed surface water flows, consistent with enhanced precipitation during sapropel S1, may have assisted in the transport of near-coastal aragonitic organisms to more coast-remote areas.

1. Introduction

Export of Carbon may either occur via precipitation of calcium carbonate by pelagic organisms or by photosynthesis and formation of organic carbon (e.g. Jahnke, 1996; Mucci et al., 2000). Generally, only a small proportion of the C$_{org}$ is accumulated on the sea floor, as most of it is converted back to CO$_2$ in the water column due to bacterial oxidation. Enhanced preservation of C$_{org}$ in the sedimentary record may point to dysoxic or anoxic conditions in the water column (e.g. Arthur and Dean, 1998; Sachs and Repeta, 1999) and/or increased productivity (e.g. Calvert and

Pedersen, 1992; Rohling and Hilgen, 1991). However, on a global scale a variable portion of inorganic carbon as $CaCO_3$ reaches the sea floor depending on the saturation state of the water column with respect to calcium carbonate.

The Holocene sediment record of the eastern Mediterranean Sea is characterized by C_{org}-poor sediments (0.1-0.2 wt.%; e.g. Van Santvoort et al., 1996, 2002) that are interrupted by a distinct interval of C_{org}-rich sediments (> ~2 wt.%); the so called sapropel S1. This sapropel formed at the time of maximum northern hemisphere summer insolation when the intensity of the African monsoon was enhanced (e.g. Rossignol-Strick, 1985). Numerous authors have reported on the humid sapropel intervals in general and the S1 in specific (e.g. Rossignol-Strick, 1983; Gasse, 2000) suggesting a major flooding of water from Africa (Rossignol-Strick et al., 1982). The relatively light ocean surface δ18O values of G. ruber during S1 (e.g. Fontugne and Calvert, 1992;) as well as the decreased Ti/Al ratio (e.g. Nijenhuis et al., 2001) all support enhanced precipitation. Additionally, Meier et al. (2004) reported a decrease in the halophylic calcareous dinoflagellate species *Lebessphaera urania* deducing that salinity of surface water was definitely decreased induced by freshwater input.

The C_{org}-poor sediments enclosing the S1 horizon are a consequence of intensive remineralization of C_{org} in a well oxygenated water column, like that of the present oligotrophic eastern Mediterranean (Bethoux, 1993; Roether and Well, 2001). However, C_{org}-poor and light brown sediments directly overlying the S1 unit are in origin part of the S1. The loss of C_{org} in these sediments is a secondary feature induced by post-depositional oxidation that the upper S1 unit has been experienced since their formation (De Lange et al., 1989; Higgs et al., 1994; Thomson et al., 1995, 1999; Van Santvoort et al., 1996). Although the original C_{org} signal is oxidized, it is possible to estimate the full primary S1 horizon as the biogenic Ba that accompanies the settling C_{org} is preserved (Thomson et al., 1995, 1999; Van Santvoort et al, 1996). The characteristic geochemical signatures evoked by this post-depositional progressing oxidation front, as the Mn double-peak one of the most conspicuous, have been described in earlier publications (Thomson et al., 1995; Van Santvoort et al., 1996; Mercone et al., 2000).

In general, the C_{org}-poor nannofossil marls have higher total carbonate contents than the S1 sediments that are enclosed by them. This generally lower carbonate contents within sapropel sediments has been observed for most sapropels from Pliocene to Holocene. The origin for this difference has been suggested to be due to dilution, dissolution, or dominant opal rather than carbonate production during sapropel formation (Van Os et al., 1994; Aksu et al., 1995; Nijenhuis et al., 1996; Schenau et al., 1999; Kemp et al., 2000; Corselli et al., 2002). In contrast, Weldeab et al. (2003) reported on an increase in carbonate contents for sapropel S6 sediments and explained this by a favored dominance of non-opportunistic calcareous plankton due to moderate productivity increase.

The major fraction of the $CaCO_3$ record usually consists of three mineral polymorphs, (i) low-Mg calcite that is generally formed by surface dwelling organisms and commonly the only form that is preserved in deepwater sediments, (ii) aragonite, and (iii) high-Mg calcite. The latter two are generally not typically found in deep-ocean sediments because they tend to dissolve before or after deposition since oceanic deepwater is strongly undersaturated with respect to aragonite and high Mg-calcite (Berner and Honjo, 1981; Fabry and Deuser, 1991). However, eastern Mediterranean sediments do contain these more soluble $CaCO_3$ polymorphs (Rutten, 2001). In open ocean areas, aragonite and high-Mg calcite are found predominantly in sediments at shallow water depth and/or

at low latitudes (Wilkinson and Given, 1986, Tucker and Wright, 1990). The high-Mg calcite found in the marls above and below the S1 unit has been interpreted as diagenetic (Milliman and Müller, 1973; Aksu et al., 1995; Calvert and Fontugne, 2001).

Thomson et al. (2004) found that eastern Mediterranean sapropel S1 shows high Sr/Ca ratios and explained the Sr enrichment by the enrichment of aragonite because samples with the highest aragonite content also had the highest Sr contents. They proposed three potential mechanisms that could lead to higher aragonite contents in S1 sediments: (i) aragonite production in surface waters, (ii) detrital aragonite, and (iii) diagenetic aragonite formation due to sulphate reduction. In view of the good correlation between the amount of sulphur, the Sr/Ca ratio, and the aragonite content, the latter mechanism was suggested as the most likely principal source for the aragonite enrichment. At the same time, they state not to be able to fully exclude a potential detrital source.

The present study particularly investigates Sirte continental slope sediments that have Sr/Ca ratio and aragonite enrichments that are much higher than ever reported for deep eastern Mediterranean sediments.

2. Methods

The investigated box core transect of BP15 (32.778 N, 19.876 E), BP18 (33.100 N, 19.733 E), and BP10 (33.222 N, 19.767 E) has been recovered north west of Cape Sirte during BioPass cruise in 2001 with RV Pelagia, from water depth of 665 m, 1850 m, and 2108 m, respectively.

All box cores were sub-sampled in 0.5 cm resolution directly after the cruise. Inorganic bulk element concentrations were performed by Inductively Coupled Plasma-Atomic Emission Spectrometry (ICP-AES) after total digestion described in chapter 4. Organic carbon and $CaCO_3$ contents were obtain on a Fisons Instruments CNS NA analyzer using dry combustion at 1030°C.

Oxygen and carbon stable isotopes were performed on the planktonic foraminifer species *Globigerinoides ruber* with a size between 300 and 400 µm using a VG SIRA-24 mass spectrometer equipped with an isocarb phosphoric acid bath. Prior to analyzes, the samples were roasted at 380°C for 30 minutes under vacuum to remove any organic remains. Analytical reproducibility of the laboratory standard was better than 0.1‰ for δ18O and better than 0.05 ‰ for δ13C. Species specific Acceleration Mass Spectrometry (AMS) radiocarbon analysis were carried out on cleaned and handpicked planktonic foraminifera (*G. ruber*) >150 µm in size at the Utrecht University AMS facility (G.J. van de Graaff laboratorium).

Selected samples of BP18 were investigated for element concentrations in the carbonate fraction. To remove inorganic carbon, a 2-step 1M HCl leach was used. The leached solution was filtered over a 0.2 µm filter prior to analyses by ICP-AES. Each sample solution was analyzed in triplicate; a deviation of less than 3% was accepted. The sample residual was freeze-dried, grinded and dissolved by total digestion and subsequently analyzed by ICP-AES. On these same samples a semi-quantitative determination of the different carbonate fractions (e.g. low-Mg calcite, high-Mg calcite, aragonite etc.) was done using a XRD full pattern analyses performed at the University of Bremen (Emmermann and Lauterjung, 1990; Vogt et al., 2002). The full pattern results of sample BP18 12-12.5 cm that contains 40% MnOOH, has been corrected for this amorphous phase that is not detectable by XRD full pattern analyses.

Selected samples of box core BP15 and BP18 were examined by scanning electron microscopy

(SEM) at the Christan-Albrechts University in Kiel and electron microprobe at the IfM-GEOMAR in Kiel. Sample preparation was done similar to the method described by Thomson et al. (2004). Grain size analyses were carried out in the sedimentology laboratory of Utrecht on a Malvern Instruments Mastersizer.

3. Results and discussion

3.1 Geochemical characteristics of Sirte continental slope sediments

Sapropel S1 sediments are characterized by relatively light ocean surface $\delta^{18}O$ values, decreased Ti/Al ratios, distinctly smaller grain sizes (D50 distribution), and increased Ba/Al ratios (Figure 1), reported to indicate enhanced precipitation, reduced dust flux due to more dense Sahara vegetation and increased productivity/preservation, respectively (Rossignol-Strick, 1983; Fontugne and Calvert, 1992; Thomson et al., 1995, 1999; Van Santvoort et al., 1996; Gasse, 2000; Nijenhuis et al., 2001). The limits of the original S1 formation period has been determined by plotting the Ba/Al ratio versus radiocarbon analyses on *G. ruber* for the investigated box cores of the Sirte continental slope transect; the residual S1 is established by the C_{org} content (Fig. 1).

The cores of this study show $CaCO_3$ concentrations of 55-65 wt.% for the marl sediments (excluding turbidite horizons) and ~60-80 wt.% for the S1 sediments (Fig. 1). In contrast to other sapropel horizons an increase of 5-15 wt.% $CaCO_3$ within the S1 sediments is found. Generally, a $CaCO_3$ content decrease is observed within the sapropel horizon (e.g. Van Os et al., 1994). The high $CaCO_3$ values between ~1.5 and 3.5 kyr B.P. of the deeper cores (BP18 and 10) reflect distinct thin turbidite horizons. This concerns most likely the Augias turbidite that has been triggered by the tsunami that resulted from the collapse of the Santorini caldera about 3.6 ky B.P. (Kastens and Cita, 1981; Hieke, 1984; Cita et al., 1984, 1996; Cita and Aloisi, 2000).

The enhanced Sr/Ca ratio within the S1 sediments (Fig. 1), corresponds to similar enrichments found in other cores from the eastern Mediterranean (e.g. Thomson et al., 2004). XRD full-pattern analyses of selected samples of BP18 indicate that the elevated Sr/Ca ratio is related to an increase in Sr-rich aragonite (Fig. 2 and 1). Sr/Ca ratios in HCl leached samples of S1 with high bulk Sr/Ca ratios, plotted versus aragonite/sum of carbonates (XRD full pattern analyses) have similar aragonite end-member values as found by Thomson et al. (2004). These authors determined a Sr/Ca ratio of 0.027 for a pure aragonite end-member and a zero aragonite end-member with a Sr/Ca ratio of 0.0033. According to these Sr/Ca ratio end-members the aragonite content for the transect cores was calculated on the base of the terrigenous corrected Sr/Ca ratio (Fig. 2); Sr and Ca were corrected with a terrigenous Sr/Al ratio of 0.0015 and a terrigenous Ca/Al ratio of 0.0377 gained by total digestion of decarbonated samples of BP18. These aluminosilicate background ratios obtained for eastern Mediterranean Holocene sediments are distinctly lower than those proposed by Wedepohl (1995; Sr/Al = 0.0051 and Ca/Al = 0.4059), but are in the same range as those of another study (0.0011 and 0.052 for Sr/Al and Ca/Al, respectively; unpublished data A. Rutten). Differences in the calculated aragonite concentrations obtained after applying one or the other correction factor were negligible.

The correspondence between aragonite content obtained from full pattern analyses and from calculation is convincing even though the calculated values are somewhat higher where Sr/Ca is most enriched (Fig. 2). These higher values might be related to an additional source of Sr, which cannot
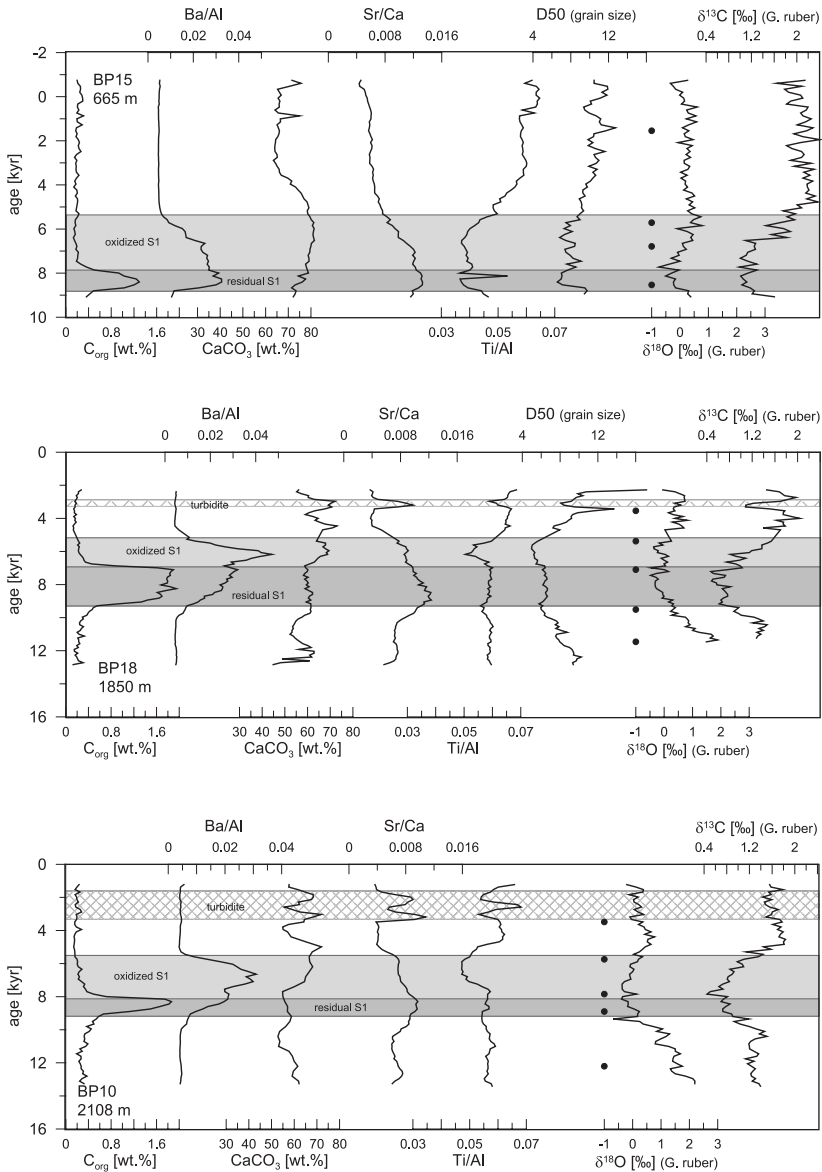
Fig. 1 Concentrations of C_{org}, $CaCO_3$, stable carbon and oxygen isotopes, element ratios (Ba/Al, Sr/Ca, Ti/Al), and D50 grain size distribution (except for BP10) versus radiocarbon convention age in cores BP15 from 665 m water depth (upper panel), BP18 from 1850 m water depth (middle panel; samples from the major Mn-peak characterizing the end of S1 have not been plotted), and BP10 from 2108 m water depth (lower panel). The residual and oxidized S1 zones are illustrated by the dark and light grey shadings, respectively. Original element concentrations are μg/g unless otherwise indicated. The turbidite horizons are indicated by a cross-hatched shading. Radiocarbon ages have been extrapolated from the ^{14}C-controled intervals of 2-12 kyr (black dots), which may have lead to erroneous ages for the upper sector of the cores.

be aluminosilicate but which might be related to a small, possibly diagenetic component similar to the two particles reported by Thomson et al. (2004; Sr/Ca of 0.13).

In the core top, XRD full-pattern aragonite values are higher than those calculated from Sr/Ca ratio, which is related to observe enhanced levels of pteropods being aragonitic but with low Sr/Ca ratios (Sr/Ca 0.0036; Rutten et al., 2000). In summary, a clear enrichment of a Sr-rich aragonite is present in all S1 sapropels but particularly in those of the Sirte transect.

3.2 Potential sources of increased aragonite concentrations in S1 sediments

Two potential mechanisms have recently been suggested for the occurrence of high Sr-rich aragonite contents in the most recent sapropel S1 (Thomson et al., 2004, see introduction), namely a) diagenetic formation of aragonite and b) a detrital/biogenic source.

a) diagenetic aragonite

Although Thomson et al. (2004) could not rule out a potential near-coastal source, they concluded that the higher Sr/Ca ratios and inferred aragonite contents in Eastern Mediterranean sediments can be best explained by authigenic re-crystallization due to an increase in alkalinity generated by sulphate reduction. This conclusion was mainly based on the good correlation between the amount of reduced S as pyrite and the inferred amount of Sr-rich aragonite. Early diagenesis could produce substantial amounts of carbonate provided that sufficiently enhanced sulphate reduction rates would occur to produce a sufficient amount of alkalinity, relatively close to the sediment water interface to ensure the supply of the potentially limiting Ca and Sr ions.

Theoretically, the amount of authigenic carbonate that may have been formed due to increased alkalinity induced by iron or sulfate reduction processes can be estimated (e.g. Berelson et al., 1996; Mucci et al., 2000; Pfeifer et al., 2002). The amount of potential aragonite formed in this way was estimated by Thomson et al. (2004) to ~10% for their core LC25 having up to 15 wt.% aragonite. In view of the total reduced S, its $\delta^{34}S$ (suggesting an 'open' system; Passier et al., 1996), and C_{org} contents, and assuming realistic sulphate reduction rates, then the estimate of Thomson et al. (2004) is at the upper limit of
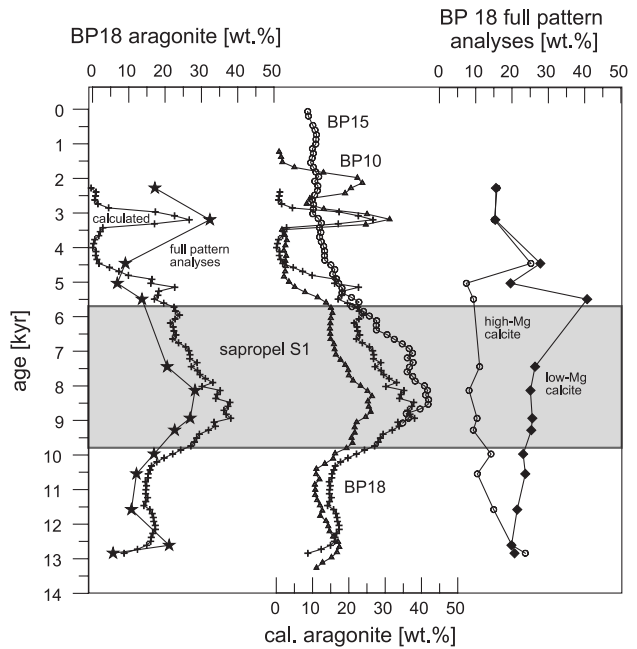
Fig. 2 XRD full-pattern analysis of selected samples of core BP18 and calculated aragonite contents of BP15, 18, and 10 versus radiocarbon convention age.

being realistic. Moreover, the S1 sediments from the Sirte transect contain up to 40 wt.% aragonite and have relatively low organic C and S contents (maximal 1.3-2.0 and 0.4-0.7 wt.%, respectively).

Even though theoretically possible, these processes have never been observed to contribute significantly to the CaCO$_3$ inventory in marine surface sediments. Significant amounts of diagenetic carbonate formations have conversely been reported under specific environmental conditions that support the enhancement of precipitation rates e.g. by anaerobic decomposition of organic matter in lagoonal systems or by advection of methane saturated fluids at cold seeps (Middelburg et al., 1990; Luff and Wallmann, 2003; Luff et al., 2004; Aloisi et al., 2004a). However, the formation of a substantial portion of authigenic carbonate would significantly reduce the pore space, but the reverse is observed.

Furthermore, enhanced degradation of organic matter as anticipated for diagenetic aragonite formation would lead to a significantly lower pore water $\delta^{13}C_{HCO_3^-}$, hence to a lighter $\delta^{13}C_{bulk\ carbonate}$ signal. In contrast a $\delta^{13}C$ of 1.55 to 2.10 ‰ is observed here, which is more typical for eastern Mediterranean surface water precipitation (Aloisi et al., 2000).

In view of the limited potential amount of diagenetic aragonite that may form, and the lack of consistent variation with porosity and bulk carbonate $\delta^{13}C$, it is unlikely that the major fraction of aragonite found in S1 sediments of this study can be attributed to diagenetic formation.

b) biogenic/detrital aragonite

The aragonite contents in S1 sediments of the transect, thus all located within the same small area show a distinct decrease with increasing water depth (Fig. 2). With an Aragonite Compensation
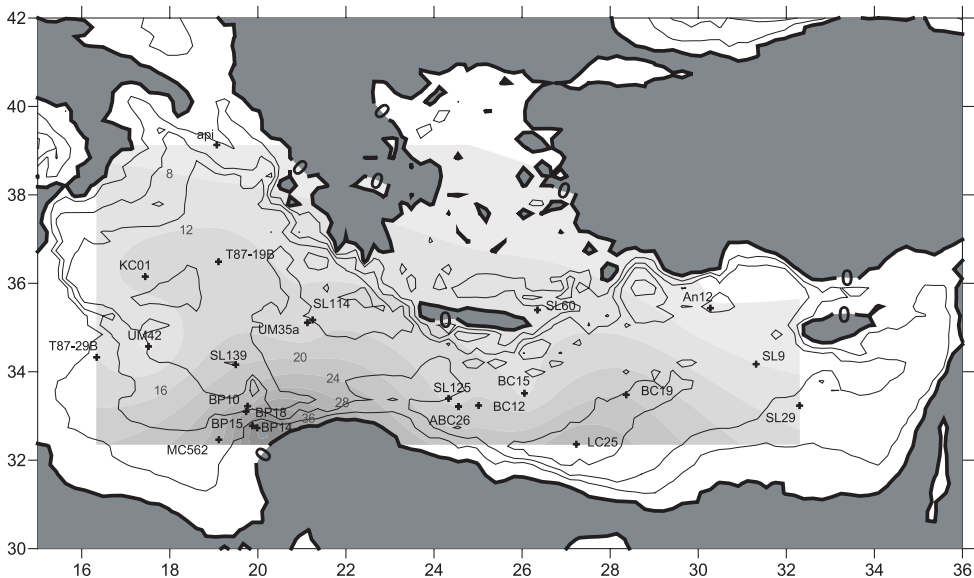
Fig. 3 Contour map showing the interpolated (kriging) maximum aragonite distribution in eastern Mediterranean S1 sediments at various core locations. All aragonite values used were calculated on base of terrigenous corrected Sr/Ca values; grey numbers on contour boundaries indicate maximal aragonite values. Bathymetric contours are at 1000 m intervals.

Depth (ACD) at >3000 m water depth for the S1 period to the Present (pteropods have been determined in 3 km deep S1 sediments), ACD-related dissolution is particularly unlikely to have influenced any of the sediments discussed here. This decrease of Sr-rich aragonite with increasing water depth, thus distance to the coast suggests that the Sr-rich aragonite may have been introduced from the shelf.

All cores studied by Thomson et al. (2004) show distinctly lower aragonite values (max. ~15 wt.%) than those of the transect along the Libyan continental slope (max. ~35-40 wt.%). The distribution of the calculated maximum aragonite concentrations over the eastern Mediterranean indicates a dependency of aragonite to (i) distance from the African shelf (Fig. 3) and (ii) related water depth (Fig. 4). The dependency of water depth is most obvious for that cores which are from different water depth of one area. The relationship observed earlier between aragonite and reduced S (Thomson et al., 2004) may also indicate a relationship with water depth. The observed relationship, therefore, must reflect a primary source on the North African continental shelf (Fig. 3).

By comparing the carbonate fractions in two cores, one from the Sirte near-coastal transect and another from the more coast-remote deep basin (ABC26), the following observation can be made: (i) their calcite content is nearly identical, but (ii) the S1 sapropel aragonite content is much higher in the near-coastal than in the distant core (Fig. 5). This indicates that carbonate productivity at both sites must have been similar, making it unlikely that the increased aragonite contents come from surface water production but rather must come from the African shelf.

The relatively lighter $\delta^{13}C$ values of *G. ruber* during S1 suggest that enhanced wind mixing, possibly induced by stronger western wind (Tuenter et al., 2003) and enhanced runoff, may have been a more pronounced feature for the Sirte area than for other sites studied thus far. Such wind mixing and an increased runoff due to enhanced precipitation during S1 all contribute to seaward moving
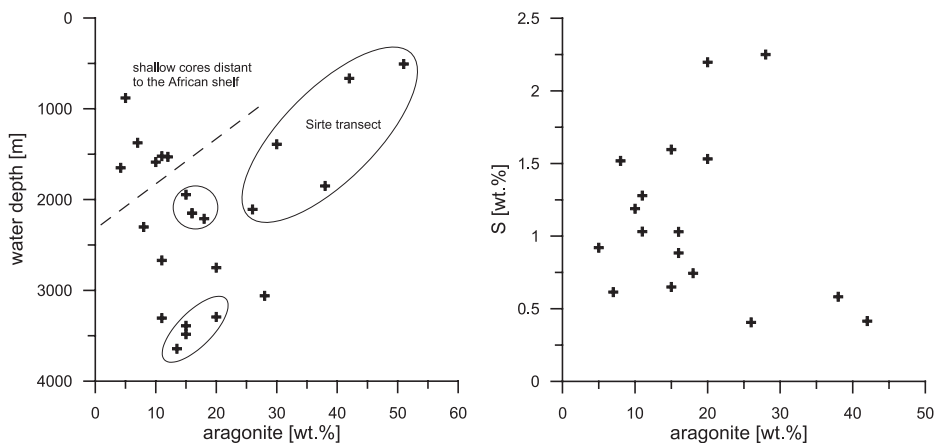
Fig. 4 left panel: calculate aragonite content versus water depth of all cores shown in Fig. 3. The dashed line separates the shallow but distant to the African shelf cores from the rest of the cores. Cores of the same area are enclosed by a circle or ellipse (compare Fig. 3; large ellipse: BP10, 14, 15, 18, MC562, second-largest: KC1, T87-19B, SL114, SL139, smallest: BC12, ABC26, SL125). Right panel: calculated aragonite content versus sulfur content for all cores where S data were available.

shallow water masses potentially entraining shallow-living near-coastal aragonitic organisms such as *Halimeda*.

3.3 SEM observation

If most of the aragonite is detrital/biogenic then this should be recognizable under the scanning electron microscope (SEM). In the oxidized as well as in the remaining part of the S1 horizon of BP15 (665 m water depth) and BP18 (1850 m water depth) a lot of needle debris and faecal pellet like needle aggregates of about 10-20 μm, with variable needle lengths but a conspicuously constant needle diameter of ~0.2 μm, were observed. Some of the aggregates seem to be loosely packed and others seem to be quite compact, some are composed only of needles but others are made of needle and coccolithophorid fragments; no distinct difference was observed between the oxidized and remaining S1 sediments regarding this observations (Fig. 6 a and b, image A-I). The pure needle aggregates seem to be very similar to skeletal fragments of the calcareous green algae *Halimeda* that is an important biological and geological component of tropical and temperate shallow waters (to 150 m; e.g. Hillis, 1991) and that is still living in the Mediterranean (Hillis, 2001). Precipitation in *Halimeda* occurs as Sr-rich aragonite (Sr/Ca of about 0.024; Beck et al., 1992) within intercellular spaces but outside the cell walls (e.g. Lowenstam, 1955; Hillis-Colinvaux, 1980). The needles of the aggregates or clusters that were found in all samples look most similar to these described and shown by Macintyre and Reid (1995) who investigated the crystal alteration in living *Halimeda*. Most of the needle aggregates in the S1 sediments show a combination of primary aragonite needles of 1-3 μm and needles that are altered to anhedral equant aragonite of 0.1-0.5 μm (Fig. 6 a and b, image A-G, I; Macintyre and Reid, 1995) which is best observed in the close up image F (Fig. 6 a). Even though from the pointed terminations it is apparent that this aragonite needles are physiochemical precipitates, however, variations in size do not clearly suggest that these are *Halimeda* grains. The aggregates that are made of a mixture of needles and coccolithophorid fragments (Fig. 6 b, image H) seem to be faecal pellets that have been produced by grazing organisms.

Electron-microprobe analyses of needle aggregates (pure needle and needle/coccolithophorid aggregates) in the oxidized and residual S1 sediments gave an average Sr/Ca ratio of ~0.0119, the average Sr/Ca ratio of aggregates from the residual S1 sediments of both cores is ~0.0139. Accordingly, the needle cluster and faecal pellets that are highly abundant in the investigated sediments seem to be the source of Sr-rich aragonite.

A further potential source of Sr-rich aragonite the didemnid ascidian specules that can have Sr levels up to 6.5 ‰ (Matthews, 1966) were found infrequently in different preservation states as the genus Bonetia (Osman Varol pers. comm., 2005) in oxidized and residual S1 sediments (Fig. 6 b,
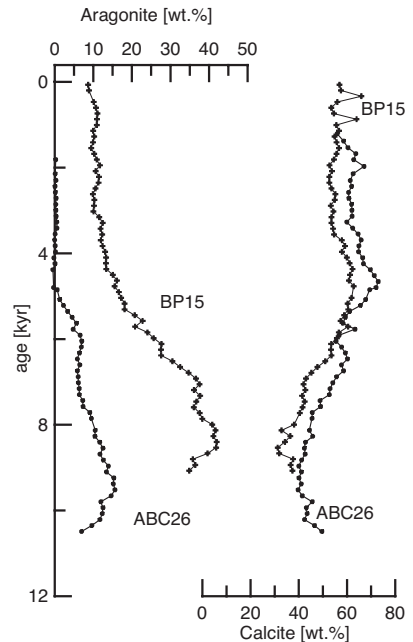
Fig. 5 Concentrations of aragonite and calcite in a shallow core from the Libyan continental slope BP15 (crosses) and a deep water core distant to the African shelf ABC26 (dots).
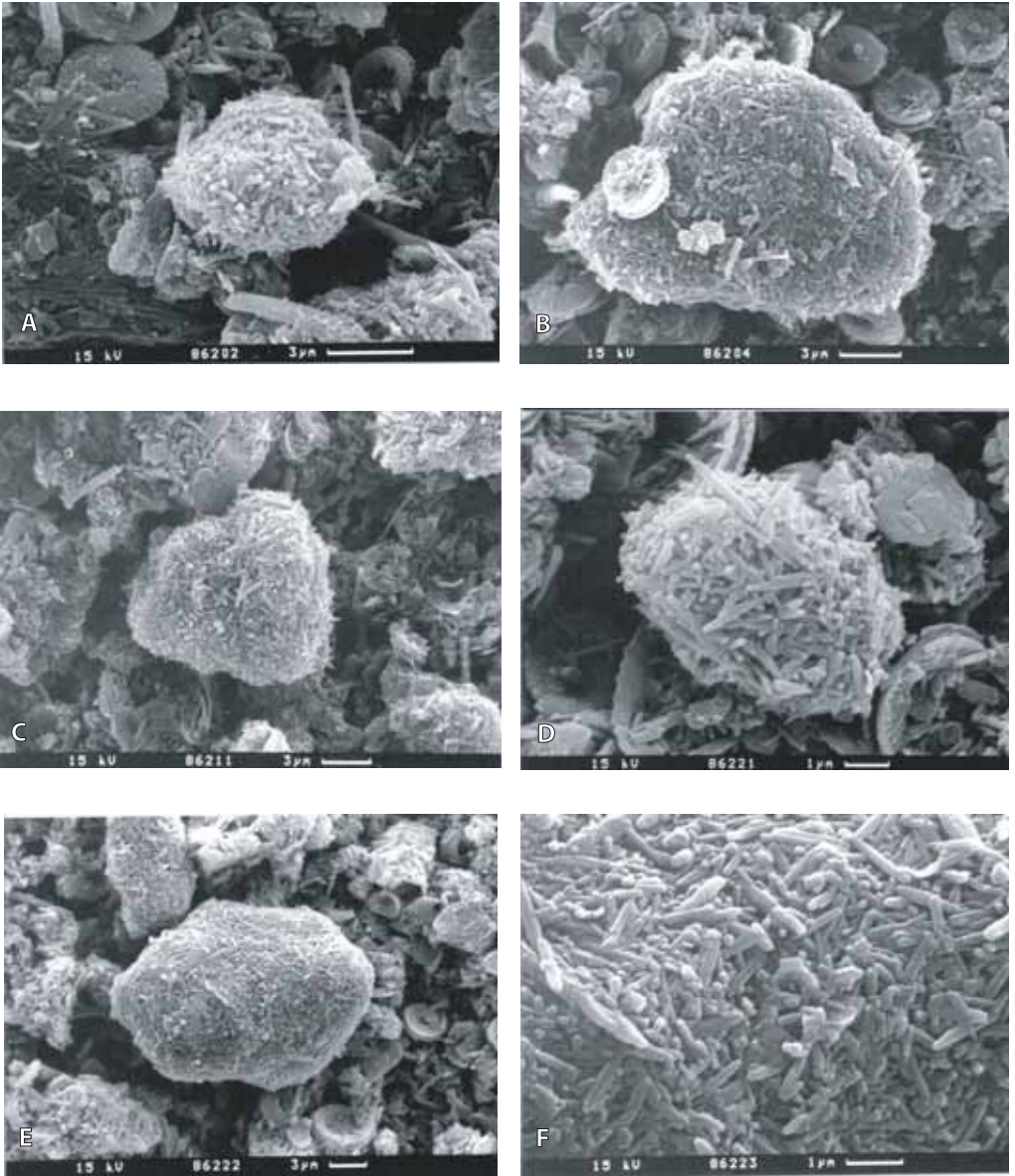
Figure 6a and b SEM images of Sr-rich aragonite needles and objects from S1 sediments of a shallow (BP15) and deep water (BP18) core from the Sirte continental slope. (A) Relatively small (~8 µm) and loosely packed aragonite needle cluster and needle debris from the oxidized S1 of BP15. (B) Larger and more compacted cluster with relatively short needles form the same sample. (C) Relatively compact aragonite needle cluster and needle debris from the unoxidized S1 of BP15. (D) Small (~8 µm) loosely packed agaronite needle cluster with mainly long needles (1-3 µm); pointed terminations are clearly visible. (E) Compact faecal pellet like needle cluster from the unoxidized S1 of BP15. (F) Close-up of (E) many of altered needles (0.1-0.5 µm); the pointed terminations are clearly visible.
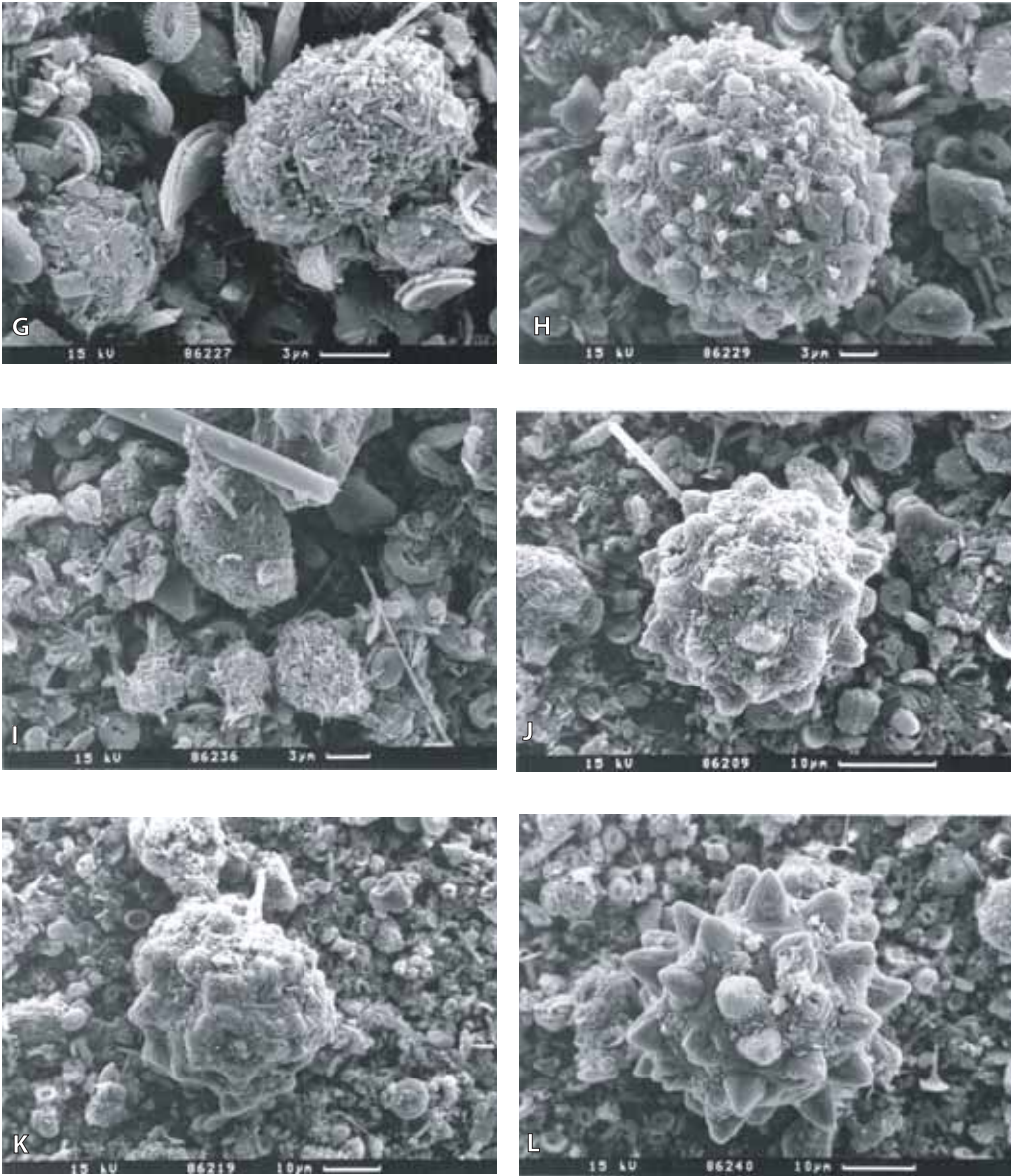
Fig. 6 a and b (continued); (G) Loosely packed faecal pellet like aragonite needle object from the oxidized S1 of BP18; many fragments of coccolithophorids are in the background. (H) Faecal pellet like cluster of mainly aragonite needles and coccolithophorid fragments. (I) Compact (bigger object in the middle) and loose (little objects at the lower margin) aragonite needle clusters from the unoxidized S1 of BP18. (J) Poorly preserved ascidian *Bonetia* from the oxidized S1 of BP15. (K) Poorly preserved ascidian of the same genus form the relatively thin unoxidized S1 of BP15. (L) Well preserved ascidian *Bonetia* from the unoxidized S1 of BP18.

image J-L). Ascidians are well known from continental shelves throughout the world but they are rarely found in deep water (Varol and Houghton, 1996). It might be that the needle clusters are fragments of ascidians, yet, no fragmental ascidian clusters like these have been published so far. However, ascidians are sensitive to fresh water influences. It has been reported that large colonies close to the Australian coastline are regularly killed by heavy cyclonic rainfalls (Varol and Houghton, 1996). Freshwater input was enhanced during S1 and could regularly (during summer) have killed large amounts of ascidians which then would have drifted on the surface and settled as feacal pellets or via hyperpycnal flows. Such flows might have occurred periodically, possibly as 'flash flooding' from Saharan rivers during most intense precipitation similar to the hyperpycnal flows triggered by medium to small size rivers described by (Mulder et al., 2003).

3.4 Preservation of Sr-rich aragonite

The ascidians observed in the sediment carry extremely valuable information about the preservation state of Sr-rich aragonite in oxidized and residual S1 sediments. The best preserved example was observed in the center of the 10 cm thick residual S1 of BP18 (Fig. 6 b, image J). The examples from BP15 (oxidized and residual S1) are all poorly preserved, however, it has to be mentioned that the residual S1 of this core is only 2.5 cm thick and the sample was taken from the upper cm of this 2.5 cm section. Accordingly, this sample was already exposed to further oxidation of organic matter and consequently $CaCO_3$ alteration. From the ascidian observation it is apparent that Sr-rich aragonite is better preserved within the residual S1 than in the oxidized S1. The initial aragonite contents of the upper, now oxidized part of S1 may, therefore, have been higher than it is at present. Possibly, the oxic degradation of organic matter in the upper S1 interval has resulted in the partial dissolution/re-crystallization of aragonite into calcite. This would correspond to aragonite values being highest in the lower part of the S1 (the residual part; Fig. 2) and total carbonate values being highest in the upper part of the S1 (oxidized part; Fig. 1). This assumption is supported by the observation that during post-depositional oxidation the pore water Mg/Ca ratio may be lowered by dissolution of aragonite in marine-derived pore fluids that start early precipitation of low-Mg calcite cements (Sanders et al., 2003).

4. Conclusions

The Sr/Ca ratio enrichment in S1 sediments is shown to be related to Sr-rich aragonite, which is mainly present as aragonite needle clusters and faecal pellet like objects with an average Sr/Ca ratio of 0.0119. The highest Sr-rich aragonite contents of up to 40 wt.% have been found in cores on the Sirte continental slope, while values appear to decrease with distance to the North African margin and consequently with water depth.

In consideration of the limited potential amount of diagenetic aragonite that may form, the lack of consistent variation with porosity, and the clear relation of aragonite to the distance to the African shelf and water depth, the major fraction of Sr-rich aragonite cannot be attributed to diagenetic formation but rather to a detrital/biogenic near-coastal source.

In sapropel S1 sediments of the Sirte transect we have observed ascidians, needle debris and faecal pellet like needle aggregates, containing variable needle lengths but having a conspicuously constant needle diameter ~0.2 μm, resembling that of *Halimeda*, all pointing to a near-coastal source area.

Acknowledgement

Chapter 7

Outlook and perspective related to S1 studies

During sapropel S1 formation the bottom water of the eastern Mediterranean may have been regularly anoxic below 2000 m water depth (chapter 4). On the base of this observation it can be assumed that bottom waters of more shallow locations might have been regularly dysoxic, possibly up to 300 m water depth were the shallowest S1 sapropels are found. The observation of anoxic bottom waters below 2000 m water depth could be taken as one major evidence, supporting the anoxia hypothesis as the most likely triggering mechanism for sapropel formation, at least for S1 formation.

However, the exact development of bottom water anoxia and the related redox changes in the water column during the entire formation period are not certain. A potential tool to unravel the development of bottom water anoxia/dysoxia might be the analyses of the isotopic ratio of $\delta^{98/95}Mo_{MOMO}$. Molybdenum has a homogenous and constant isotopic seawater composition over the last 60 Myr, whereas oxic Mo sinks have lighter and suboxic sinks show heavier isotopic values. Consequently, the sedimentary record is an archive for the isotopic fractionation of molybdenum between these different sinks, which might make the $\delta^{98/95}Mo_{MOMO}$ a suitable tool to trace back the development of the bottom water redox conditions during S1 formation. However, particularly in the eastern Mediterranean S1 sediments, which have certainly been heavily overprinted by post-depositional diagenesis due to oxygen penetration, the molybdenum isotope application might be treacherous because not much is known about its fractionation due to diagenetic overprinting. Yet, if the secondary diagenetic fractionation systematics could be established this would certainly be a widely applicable indicator for paleo-redox conditions. Besides, it would be certainly valuable for a reliable assessment of paleo-redox conditions because some sediments experienced several secondary diagenetic overprintings e.g. due to ash layer and turbidite deposition and to oxygen penetration (see chapter 5). The combination of high resolution bulk geochemical and rock-magnetic analyses as applied in chapter 3 seem to be an appropriate device to get a better understanding of the possible effect and influence that a secondary relocation of the redox boundary might have on 'secondary' fractionation of the molybdenum isotopic signal.

Nevertheless, the hypothesis of anoxia during S1 formation is not only supported by the observations in chapter 4 (i.e. the major Mn peak at mid-water depth) but also by the findings in chapter 6 (i.e. constant calcite production signal), from which it seems obvious that primary production of calcareous organisms was most likely not distinctively enhanced (Fig. 5; chapter 6). In contrast, it has been shown that near-coastal aragonite production may have been enhanced. To further support the hypothesis that primary production was not significantly enhanced during S1 formation, a systematic comparison of the isotopic carbon signal ($\delta^{13}C$) of surface dwelling calcareous organisms with that of the bulk sediment and that of the organic matter should be carried out. It has been shown in chapter 6 that the $\delta^{13}C$ signal of the surface dwelling foraminifer G. ruber is distinctly lighter during S1 in cores of the Sirte continental slope than in other eastern Mediterranean cores.

These lighter values might be induced by enhanced wind mixing, which would also explain the transport of shelf-produced aragonite to the more coastal-remote areas, but which might also be induced by enhanced runoff. A comparison with the isotopic carbon signal of organic matter could clarify the possibility of enhanced runoff because the land-derived organic matter has a distinct lighter isotopic signal (-26 to -28‰) than that produced by marine organisms (-20 to -22‰; Meyers, 1994). Furthermore, there is still the possibility that the lighter $\delta^{13}C$ signal of G. ruber is caused by diagenetic overprinting; this question could be solved by a comparison with the isotopic signal of the bulk material that can be seen as a combination of all the different carbon sources accumulating the different information they carry. If diagenetic overprinting occurred, than it should be displayed in the bulk signal as well. However, ideally the isotopic carbon values of pore water should be determined, if possible, to exclude or support the possibility of diagenetic alteration.

Finally, if primary production was not significantly enhanced during S1 formation, than it has to be questioned if biogenic barium is certainly a proxy for paleo-productivity or rather one for first order preservation of organic carbon.

References

Aksu, A.E., Yasar, D., Mudie, P.J. (1995). Oringin of late glacial-Holocene hemipelagic sediments in the Aegean Sea: Clay mineralogy and carbonate cementation. *Mar. Geol. 123*, 33-59.

Aloisi, G., Pierre, C., Rouchy, J.-M., Foucher, J.-P., Woodside, J., the MEDINAUT Scientific Party (2000). Methan-related authigenic carbonates of eastern Mediterranean Sea mud volcanoes and their possible relation to gas hydrate destabilisation. *Earth Planet. Sci. Lett. 184*, 321-338.

Aloisi, G., Wallmann, K., Haese, R., Saliège, J.-F. (2004a). Chemical, bilogical and hydrological controls on the ^{14}C content of cold seep carbonate crusts: numerical modeling and implications for convection at cold seeps. *Chem. Geol. 213*, 359-383.

Aloisi, G., Wallmann, K., Drews, M. (2004b). Evidence for the submarine weathering of silicate minerals in Black Sea sediments: Possible implications for the marine Li and B cycles. *Geochem. Geophys. Geosyst. 5*, Q04007, doi: 10.1029/2003GC000639.S.

Antoine, D., André, J.-M., Morel, A. (1996). Oceanic primary production 2. Estimation at global scale from satellite (coastal zone color scanner) chlorophyll. *Global Biogeochem. Cycle 10(1)*, 57-69.

Archer, D.E. (1996). A data-driven model of the global calcite lysocline. *Global Biochem. Cycles 10*, 511-526.

Arthur, M.A., Dean, W.E., Stow, D.A.V. (1984). Models for the deposition of Mesozoic-Cenozoic fine-grained, organic-carbon-rich, sediment in the deep-sea. In: Stow, D.A.V., Piper, D.J.W. (Eds.), Fine-Grained Sediments: Deep-water Processes and Facies. *Geol. Soc. London, Spec. Publ. 15*, 527-560.

Arthur, M.A., Dean, W.E. (1998). Organic-matter production and preservation and evolution of anoxia in the Holocene Black Sea. *Paleoceanography 13(4)*, 395-411.

Balzer, W. (1982). On the distribution of iron and manganese at the sediment water interface - thermodynamic versus kinetic control. *Geochim. Cosmochim. Acta 46*, 1153-1162.

Barling, J., Arnold, G.L., Anbar, A.D. (2001). Natural mass-dependent variations in the isotopic composition of molybdenum. *Earth Planet. Sci. Lett. 193*, 447-457.

Baumann, K.-H., Henning, R., Meggers, H. (1995). Carbonate Contents. In: Schulz, H., Bleil, U., Henrich, R., Segl, M. (Eds.). *Geo Bremen SOUTH ATLANTIC 1994*, *Cruise No. 29*, 17 Juni – 5 September 1994. METEOR-Berichte, Universität Hamburg, pp. 248-252.

Beck, J.W., Edwards, R.L., Ito, E., Taylor, F.W., Recy, J., Rougerie, F., Joannot, P., Henin, C. (1992). Sea-surface temperature from coral skeletal strontium calcium ratios. *Science 257*, 644-647.

Berelson, W.M., McManus, J., Coale, K.H., Johnson, K.S., Kilgore, T., Burdige, D., Pilskaln, C. (1996). Biogenic matter diagenesis on the sea floor: a comparison between two continental margin transects. *J. Mar. Research 54*, 731-762.

Berger, W.H., Smetacek, V., Wefer, G. (1989). Ocean productivity and paleoproductivity – an overview. In: Berger, W.H., Smetacek, V., Wefer G. (Eds.), Productivity of the ocean: present and past. *Dahlem Workshop Rep, Life Sci. Res. Rep. 44*, Wiley & Sons, Chichester, pp. 1-34.

Berger, W.H., Herguera, J.C., Lange, C.B., Schneider, R. (1994). Paleoproductivity: Flux proxies versus nutrient proxies and other problems concerning the Quaternary productivity record. In: Zahn, R., Pedersen, T.F., Kaminski, M.A., Labeyrie, L. (Eds.), Carbon Cycling in the Glacial Ocean: Constraints on the Ocean's Role in Global Change. *NATO ASI Series 17*, Springer, Berlin, Heidelberg, pp. 385-412.

Berner, R.A. (1980). Early Diagenesis: a Theoretical Approach. Princeton University Press, Princeton, New York.

Berner, R.A., Honjo, S. (1981). Pelagic sedimentation of aragonite: Its geochemical significance. *Science 211*, 940-942.

Bernstein, R.E., Byrne, R.H., Betzer, P.R., Greco, A.M. (1992). Morphologies and transformations of celestite in seawater: the role of acantharians in strontium and barium geochemistry. *Geochim. Cosmochim. Acta 56*, 3273-3279.

Bertine, K.K. (1972). The deposition of molybdenum in anoxic waters. *Mar. Chem. 1*, 43-53.

Bertine, K.K., Turekian, K.K. (1973). Molybdenum in marine deposits. *Geochim. Cosmochim. Acta 37*, 1415-1434.

Béthoux, J.P. (1993). Mediterranean sapropel formation, dynamic and climatic viewpoints. *Oceanologica Acta 16*, 127-133.

Bishop, J.K.B. (1988). The barite-opal-organic carbon association in oceanic particulate matter. *Nature 332*, 341-343.

Bloemendal, J., Lamb, B., King, J.W. (1988). Palaeoenvironmental implications of rock-magnetic properties of late Quaternary sediment cores from the eastern equatorial Atlantic. *Paleoceanography 3*, 61-87.

Bloemendal, J., King, J.W., Tauxe, L., Valet, J.P. (1989). Rock magnetic stratigraphy of Leg 108 (eastern tropical Atlantic) Sites 658, 659, 661 and 665. *Proc. ODP, Sci. Results 108*, 415-428.

Bloemendal, J., King, J.W., Hall, F.R., Doh, S.-J. (1992). Rock magnetism of late Neogene and Pleistocene deep-sea sediments: relationship to sediment source, diagenetic processes, and sediment lithology. *J. Geophys. Res. 97*, 4361-4375.

Bowen, H.J.M. (1979). Environmental chemistry of the elements. Academic Press, London.

Boyle, E.A. (1983). Manganese carbonate overgrowths on foraminifera tests. *Geochim. Cosmochim. Acta 47*, 1815-1819.

Brown, E.T., Callonnec, L.L., German, C.R. (2000). Geochemical cycling of redox-sensitive metals in sediments from Lake Malawi: A diagnostic paleotracer for episodic changes in mixing depth. *Geochim. Cosmochim. Acta 64*, 3515-3523.

Brummer, G.J.A., Van Eijden, A.J.M. (1992). "Blue ocean" paleoproductivity estimates from pelagic carbonate mass accumulation rates. *Mar. Micropaleontol. 19*, 99-117.

Burdige, D.J. (1993). The biogeochemistry of Mn and Fe reduction in marine sediments. *Earth Sci. Rev. 35*, 249-284.

Burdige, D.J., Gieskes, J.M. (1983). A pore water/solid phase diagenetic model for manganese in marine sediments. *Am. J. Sci. 283*, 29-47.

Calvert, S.E. (1983). Geochemistry of Pleistocene sapropels and associated sediments from the eastern Mediterranean. *Oceanol. Acta. 6*, 255-267.

Calvert, S.E., Pedersen, T.F. (1992). Organic carbon accumulation and preservation in marine sediments: How important is anoxia? In: Whelan, J., Farrington, J.W. (Eds.), *Organic Matter*, University Press, New York, pp. 231-263.

Calvert, S.E., Pedersen, T.F. (1993). Geochemistry of Recent oxic and anoxic marine sediments: Implications for the geological record. *Mar. Geol. 113*, 67-88.

Calvert, S.E., Pedersen, T.F. (1996). Sedimentary geochemistry of manganese: Implications for the environment of formation of manganiferous black shales. *Econ. Geol. Bull. Soc. 91*, 36-47.

Calvert, S.E., Fontugne, M.R. (2001). On the late Pleistocene-Holocene sapropel of climatic and oceanographic variability in the eastern Mediterranean. *Paleoceanography 16*, 78-94.

Camerlenghi, A., Cita, M.B., Hieke, W., Ricchiuto, T. (1992). Geological evidence for mud diapirism on the Mediterranean Ridge accretionary complex. *Earth Planet Sci. Lett. 109*, 493-504.

Cardinal, D., Fagel, N., Luc, A., Dehairs, F. (1999). Ba Repartition in Surface Sediment and Trap Material: A Sequential Leaching Approach. *J. Conf. Abstr. EUG X, 4*, 425.

Casford, J.S.L., Rohling, E.J., Abu-Zied, R.H., Fontanier, C., Jorissen, F.J., Leng, M.J., Schmiedl, G., Thomson, J. (2003). A dynamic concept for eastern Mediterranean circulation and oxygenation during sapropel formation. *Palaeogeogr. Palaeoclimatol. Palaeoecol. 190*, 103-119.

Chow, T.J., Goldberg, E.D. (1960). On the marine geochemistry of barium. *Geochim. Cosmochim. Acta 20*, 192-198.

Church T.M. (1970). Marine barite. Ph.D. Thesis, University of California, USA.

Cita, M.B., Camerlenghi, A., Kastens, K.A., McCoy, F.W. (1984). New findings of Bronze Age homogenites in the Ionian Sea - geodynamical implications for the Mediterranean. *Mar. Geol. 55*, 47-62.

Cita, M.B., Aghib, F., Arosio, S., Folco, S., Sarto, L., Erba, E., Rizzi, A. (1989). Bacterial colonies and manganese micronodules related to fluid escape on the crest of the Mediterranean Ridge. *Riv. It. Paleontol. Stratigr. 95*, 315-336.

Cita, M.B., Camerlenghi, A., Rimoldi, B. (1996). Deep-sea tsunami deposits in the eastern Mediterranean: New evidence and depositional models. *Sediment. Geol. 104*, 155-173.

Cita, M.B., Aloisi, G. (2000). Deep-sea tsunami deposits triggered by the explosion of Santorini (3500 y BP), eastern Mediterranean. *Sediment. Geol. 135*, 181-203.

Colley, S., Thomson, J., Wilson, T.R.S., Higgs, N.C. (1984). Post-depositional migration of elements during diagenesis in brown clay and turbidite sequences in the North East Atlantic. *Geochem. Cosmochim. Acta 48*, 1223-1235.

Collier, R.W. (1985). Molybdenum in the Northeast Pacific Ocean. *Limnol. Oceanogr. 30*, 1351-1354.

Corselli, C., Principato, M.S., Maffioli, P., Crudeli, D. (2002). Changes in planktonic assemblages during sapropel S5 deposition: Evidence from Urania Basin area, eastern Mediterranean. *Paleoceanography 17(3),* 1029, doi:10.1029/2000PA000536.

Crusius, J., Calvert, S., Pedersen, T., Sage, D. (1996). Rhenium and molybdenum enrichments in sediments as an indicator of oxic, suboxic and sulfidic conditions of deposition. *Earth Planet. Sci. Lett. 145*, 65-78.

Curtis, C. (1983). Microorganisms and diagenesis of sediments. In: Krumbein, W.E. (Ed.), *Microbial Geochemistry*. Blackwell, Oxford, pp. 263-286.

Day, R., Fuller, M., Schmidt, V.A. (1977). Hysteresis Properties of Titanomagnetites: Grain-Size and Compositional Dependence. *Physics of the Earth and Planetary Interiors 13*, 260-267.

Dean, W.E., Gardner, J.V., Piper, D.Z. (1997). Inorganic geochemical indicators of glacial-interglacial changes in productivity and anoxia on the Californian continental margin. *Geochim. Cosmochim. Acta 61*, 4507-4518.

De Capitani, L., Cita, M.B. (1996). The "marker Bed" of the Mediterranean Ridge diapiric belt: Geochemical characteristics. *Mar. Geol. 132*, 215-225.

Deflandre, B., Mucci, A., Gagné, J.-P., Guignard, C., Sundby, B. (2002). Early diagenetic processes in coastal marine sediments disturbed by a catastrophic sedimentation event. *Geochim. Cosmochim. Acta 66*, 2547-2558.

Dehairs, F., Chesselet, R., Jedwab, J. (1980). Discrete suspended particles of barite and the barium cycle in the open ocean. *Earth Planet. Sci. Lett. 49*, 528-550.

Dehairs, F., Fagel, N., Antia, A.N., Peinert, R., Elskens, M., Goeyens, L. (2000). Export production in the Bay of Biscay as estimated from barium – barite in settling material: a comparison with new production. *Deep-Sea Research I 47*, 583-601.

Dekov, V.M., Marchig, V., Rajta, I., Uzonyi, I. (2003). Fe-Mn micronodules born in the metalliferous sediments of two spreading centres: the East Pacific Rise and Mid-Atlantic Ridge. *Mar. Geol. 199*, 101-121.

De Lange, G.J. (1992). Distribution of various extracted phosphorus compounds in the interbedded turbiditic/pelagic sediments of the Madeira Abyssal Plain, eastern North Atlantic. *Mar. Geol. 109*, 115-139.

De Lange, G.J., Middelburg, J.J., Pruysers, P.A. (1989). Discussion: Middle and Late Quarternary depositional sequences and cycles in the eastern Mediterranean. *Sedimentology 36*, 151-158.

De Lange, G.J., Catalano, G., Klinkhammer, G.P., Luther III, G.W. (1990). The interface between oxic seawater and the anoxic Bannock brine; its sharpness and the consequences for the redox-related cycling of Mn and Ba. *Mar. Chem. 31*, 205-217.

De Lange, G.J., Van Os, B., Pruysers, P.A., Middelburg, J.J., Castradori, D., Van Santvoort, P., Müller, P.J., Eggenkamp, H., Prahl, F.G. (1994). Possible early diagenetic alteration of palaeo proxies. *NATO ASI Series I 17*, 225-258.

De Lange, G.J., Van Santvoort, P.J.M., Langereis, C., Thomson, J., Corselli, C., Michard, A., Rossignol-Strick, M., Paterne, M., Anastasakis, G. (1999). Palaeo-environmental variations in eastern Mediterranean sediments: a multidisciplinary approach in a prehistoric setting. *Prog. Oceanogr. 44*, 369-386.

De Lange, G.J., Thomson, J., Reitz, A., Slomp, C.P, Principato, S., Erba, E., Corselli, C. (submitted for publication). Wax and wane of the formation of the most recent eastern Mediterranean sapropel: implications for black shale formation.

De Master, D.J., Dunbar, R.B., Gorson, L.I., Leventer, A.R., Morrison, J.M., Nelson, D.M., Nittrouer, C.A., Smith WO, Jr. (1992). Cycling and accumulation of biogenic silica and organic matter in high latitude environments: the Ross sea. *Oceanography 5*, 146-153.

Dunlop, D.J. (2002a). Theory and application of the Day plot (M_{rs}/M_s versus H_{cr}/H_c) 1. Theoretical curves and tests using titanomagnetite data. *J. Geophys. Res. 107*, 10.1029/2001JB000486.

Dunlop, D.J. (2002b). Theory and application of the Day plot (M_{rs}/M_s versus H_{cr}/H_c) 2. Application to data for rocks, sediments, and soils. *J. Geophys. Res. 107*, 10.1029/2001JB000487.

Dymond, J. (1981). Geochemistry of the Nazca Plate surface sediments: an evaluation of hydrothermal, biogenic, detrital, and hydrogenous sources. Nazca Plate: crustal formation and Andean convergence. *Mem. Geol. Soc. Am. 154*, 133-174.

Dymond, J., Lyle, M., Finney, B., Piper, D.Z., Murphy, K., Conard, R., Pisias, N.G. (1984). Ferromanganese nodules from MANOP Site HS, and R – control of mineralogical and chemical composition by multiple accretionary processes. *Geochim. Cosmochim. Acta 48*, 931-949.

Dymond, J., Suess, E., Lyle, M. (1992). Barium in deep-sea sediment: a geochemical proxy for paleoproductivity. *Paleoceanography 7*, 163-181.

Emeis, K.C. (1993). Geochemische Auftriebsindikatoren in Sedimenten des Nordwestlichen Arabischen Meeres. Pers. Commun. In: Rutsch et al. (1995) [10]Be and Ba concentrations in West Africa sediments trace productivity in the past. *Earth Planet. Sci. Lett. 133*, 129-143.

Emerson, S., Hedges, J.I. (1988). Processes controlling the organic carbon content of open ocean sediments. *Paleoceanography 3*, 621-634.

Emmermann, R., Lauterjung, J. (1990). Double X-ray analysis of cuttings and rock flour: A powerful tool for rapid and reliable determination of borehole lithostratigraphy. *Scientific Drilling 1*, 269-282.

Erickson, B.E., Helz, G.R. (2000). Molybdenum (VI) speciation in sulfidic waters. Stability and lability of thiomolybdates. *Geochim. Cosmochim. Acta 64*, 1149-1158.

Fabry, V.J., Deuser, W.G. (1991). Aragonite and magnesian calcite fluxes to the deep Sargasso Sea. *Deep-Sea Res. I 38*, 713-728.

Fagel, N., André, L., Dehairs, F. (1999). Advective excess Ba transport as shown from sediment and trap geochemical signatures. *Geochim. Cosmochim. Acta 63*, 2353-2367.

Fischer, G., Wefer. G. (Eds.), (1999). Use of Proxis in Paleoceanography: Examples from the South Atlantic. Springer-Verlag, Berlin, Heidelberg, 735 pp.

Fontugne, M.R., Calvert, S.E. (1992). Late Pleistocene variability of the carbon isotopic composition of organic matter in the eastern Mediterranean: Monitor of changes in carbon sources and atmospheric CO_2 concentrations. *Paleoceanography 7*, 1-20.

Force, E.R., Cannon, W.F. (1988). Depositional model for shallow-marine manganese deposits around black shale deposits. *Econ. Geol. Bull. Soc. 83*, 93-117.

Frakes, L., Bolton, B. (1992). Effects of ocean chemistry, sea-level and climate on the formation of primary sedimentary manganese ore deposits. *Econ. Geol. Bull. Soc. 87*, 1207-1217.

François, R., Honjo, S., Manganini, S.J., Ravizza, G.E. (1995). Biogenic barium fluxes to the deep sea: implications for paleoproductivity reconstruction. *Global Biogeochem. Cycles 9*, 289-303.

Frederichs, T., Bleil, U., Däumler, K., von Dobeneck, T., Schmidt, A.M. (1999). The Magnetic View on the Marine Paleoenvironment: Parameters, Techniques and Potentials of Rock Magnetic Studies as a Key to Paleoclimatic and Paleoceanographic Changes. In: Fischer, G., Wefer, G. (Eds.), *Use of Proxies in Paleoceanography: Examples from the South Atlantic.* Springer-Verlag, Berlin, Heidelberg, pp. 575-599.

Froelich, P.N., Klinkhammer, G.P., Bender, M.L., Luedtke, N.A., Heath, G.R., Cullen, D., Dauphin, P., Hammond, D., Hartman, B., Maynard, V. (1979). Early oxidation of organic matter in pelagic sediments of the eastern equatorial Atlantic: suboxic diagenesis. *Geochim. Cosmochim. Acta 43*, 1075-1090.

Funk, J.A., von Dobeneck, T., Wagner, T., Kasten, S. (2003a). Late Quaternary Sedimentation and Early Diagenesis in the Equatorial Atlantic Ocean: Patterns, Trends and Processes Deduced from Rock Magnetic and Geochemical Records. In: Wefer, G., Mulitza, S., Ratmeyer, V. (Eds.), *The South Atlantic in the Late Quaternary: Reconstruction of Material Budget and Current Systems.* Springer-Verlag, Berlin, 461-497.

Funk, J.A., von Dobeneck, T., Reitz, A. (2003b). Integrated Rock Magnetic and Geochemical Quantification of Redoxomorphic Iron Mineral Diagenesis in Late Quaternary Sediments from the Equatorial Atlantic. In: Wefer, G., Mulitza, S., Ratmeyer, V. (Eds.), *The South Atlantic in the Late Quaternary: Reconstruction of Material Budget and Current Systems.* Springer-Verlag, Berlin, 237-260.

Gasse, F. (2000). Hydrological changes in the African tropics since the Last Glacial Maximum. *Quat. Sci. Rev. 19*, 189-211.

Gieskes, J.M. (1983). The chemistry of interstitial waters of deep sea sediments: Interpretation of deep sea drilling data. In: Riley, J.P., Chester, R. (Eds.), *Chemical Oceanography 8.* Academic Press, 221-269.

Gingele, F., Dahmke, A. (1994). Discrete barite particles and barium as tracers of paleoproductivity in South Atlantic sediments. *Paleoceanography 9*, 151-168.

Gingele, F., Zabel, M., Kasten, S., Bonn, W.J., Nürnberg, C.C. (1999). Biogenic barium as a proxy for paleoproductivity: Methods and implications of application. In: Fischer, G., Wefer, G. (Eds.), *Use of Proxies in Paleoceanography: Examples from the South Atlantic,* Springer Verlag, Berlin, pp. 345-364.

Gladney, E.S., Roelandts, I. (1988). 1987 compilation of elemental concentration data for USGS BHVO-1, MAG-1, QLO-1, RGM-1, SCO-1, SDC-1, SGR-1 and STM-1. *Geostandards Newsletters 12*, 253-362.

Glasby, G.P., Stüben, D., Jeschke, G., Stoffers, P., Garbe-Schönberg, C.-D. (1997). A model for the formation of hydrothermal manganese crusts from the Pitcairn Island hotspot. *Geochim. Cosmochim. Acta 61*, 4583-4597.

Goldberg, E., Arrhenius, G. (1958). Chemistry of pelagic sediments. *Geochim. Cosmochim. Acta 13*, 153-212.

Haeckel, M., Van Beusekom, J., Wiesner, M.G., König, I. (2001). The impact of the 1991 Mount Pinatubo tephra fallout on the geochemical environment of the deep-sea sediments in the South China Sea. *Earth Planet. Sci. Lett. 193*, 151-166.

Hammer, C.U., Kurat, G., Hoppe, P., Grum, W., Clausen, H.B. (2003). Thera eruption date 1645 BC confirmed by new ice core data? *Paper presented at the SCIEM 2000 – EuroConference,* SCIEM, Vienna.

Hastings, D., Emerson, S., Mix, A. (1996). Vanadium in foraminiferal calcite as a tracer for changes in the areal extent of reducing sediments. *Paleoceanography 11*, 665-678.

Hebbeln, D., Marchant, M., Freudenthal, T. (2000). Surface sediment distribution along the Chilean continental slope related to upwelling and productivitiy. *Mar. Geol. 164*, 119-137.

Hedges, J.I, Keil, R.G. (1995). Sedimentary organic matter preservation: an assessment and speculative synthesis. *Mar. Chem.* 49, 81-115.

Heier, N.S., Billings, G.K. (1978). Lithium. In: Wedephol, K.H. (Ed.), *Handbook of Geochemistry,* Springer-Verlag, Heidelberg, pp. 3-G-13-H-1.

Heiser, U., Neumann, T., Scholten, J., Stüben, D. (2001). Recycling of manganese from anoxic sediments in stagnant basins by seawater inflow: a study of surface sediments from the Gotland Basin, Baltic Sea. *Mar. Geol. 177*, 151-166.

Helz, G.R., Miller, C.V., Charnock, J.M., Mosselmans, J.F.M., Pattrick, R.A.D., Gardner, C.D., Vaughan, D.J. (1996). Mechanism of molybdenum removal from the sea and its concentration in black shales: EXAFS evidence. *Geochim. Cosmochim. Acta 60*, 3631-3642.

Hieke, W. (1984). A thick Holocene homogenite from the Ionian Abyssal Plain (eastern Mediterranean). *Mar. Geol. 55*, 63-78.

Hieke, W., Cita, M.B., Mirabile, G.L., Negri, A., Werner, F. (1996). The summit area (Antaeus/Pan di Zucchero) of the Mediterranean Ridge: A mud diaper field? *Mar. Geol. 132*, 113-129.

Hieke, W., Werner, F. (2000). The Augias megaturbidite in the central Ionian Sea (central Mediterranean) and its relation to the Holocene Santorini event. *Sediment. Geol. 135*, 205-218.

Higgs, N.C., Thomson, J., Wilson, T.R.S., Croudace, I.W. (1994). Modification and complete removal of eastern Mediterranean sapropel by postdepositional oxidation. *Geology 22*, 423-426.

Hilgen, F.J. (1991). Astronomical calibration of Gauss to Matuyama sapropels in the Mediterranean and implication for the Geomagnetic Polarity Time Scale. *Earth Planet. Sci. Lett. 104*, 226-244.

Hillis, L. (1991). Recent calcified Halimedaceae. In: Riding, R. (Ed.), *Calcareous Algae and Stromatolites.* Springer, Berlin, pp. 167-188.

Hillis, L.W. (2001). The calcareous reef alga *Halimeda* (Chlorophyta, Bryopsidales): a cretaceous genus that diversified in the Cenozoic. *Palaeogeogr. Palaeoclimatol. Palaeoecol. 166*, 89-100.

Hillis-Colinvaux, L. (1980). Ecology and taxonomy of *Halimeda*: primary producer of coral reefs. *Adv. Mar. Biol. 17*, 1-327.

Hodkinson, R.A., Stoffers, P., Scholten, J., Cronan, D.S., Jeschke, G., Rogers, T.D.S. (1994). Geochemistry of hydrothermal manganese deposits from the Pitcairn Island hotspot, southeastern Pacific. *Geochim. Cosmochim. Acta 58*, 5011-5029.

Holstein, J. (2002). Effekt benthischer Mineralisationsprozesse auf die Lösung von biogenem Opal. Diplomarbeit, Universität Bremen, Germany.

Huckriede, H., Meischner, D. (1996). Origin and environment of manganese-rich sediments within black-shale basins. *Geochim. Cosmochim Acta 60*, 1399-1413.

Huerta-Diaz, M.A., Morse, J.W. (1992). Pyritization of trace metals in anoxic marine sediments. *Geochim. Cosmochim. Acta 56*, 2681-2702.

Huh, Y., Lui-Heung, C., Zhang, L., Edmond, J.M. (1998). Lithium and its isotopes in major world rivers: Implications for weathering and the oceanic budget. *Geochim. Cosmochim. Acta 62(12)*, 2039-2051.

Imbrie, J., Palmer Imbrie, K., 1998. Ice Ages: Solving the Mystery. Seventh printing. Harvard University Press, Cambridge Massachusetts London, 224 pp.

Jahnke, R.A. (1996). The global ocean flux of particulate organic carbon: Areal distribution and magnitude. *Glob. Biogeochem. Cycle 10*, 71-88.

Jahnke, R.A. (1998). Geochemical impacts of waste disposal on the abyssal seafloor. *J. Mar. Syst. 14*, 355–375.

Jahnke, R.A., Craven, D.B., Gaillard, J.-F. (1994). The influence of organic matter diagenesis on $CaCO_3$ dissolution at the deep-sea floor. *Geochim. Cosmochim. Acta 58*, 2799-2809.

James, R.H., Palmer, M.R. (2000). Marine geochemical cycles of the alkali elements and boron: The role of sediments. *Geochim. Cosmochim. Acta 64(18)*, 3111-3122.

Josey, S.A. (2003). Changes in the heat and freshwater forcing of the eastern Mediterranean and their influence on deep water formation. *J. Geophys. Res. 108(C7)*, doi:10.1029/2003JC001778.

Jung, M., Ilmberger, J., Mangini, A., Emeis, K.C. (1997). Why some Mediterranean sapropels survived burn-down (and others did not). *Mar. Geol. 141*, 51-60.

Kadko, D., Cochran, J.K., Lyle, M. (1987). The effect of bioturbation and adsorption gradients on solid and dissolved radium profiles in sediments from the eastern equatorial Pacific. *Geochim. Cosmochim. Acta 51*, 1613-1623.

Karlin, R., Lyle, M., Heath, G.R. (1987). Authigenic magnetite formation in suboxic marine sediments. *Nature 326*, 490-493.

Kasten, S., Haese, R.R., Zabel, M., Rühlemann, C., Schulz, H.D. (2001). Barium peaks at glacial terminations in sediments of the equatorial Atlantic Ocean – relicts of deglacial productivity pulses? *Chem. Geol. 175*, 635-651.

Kastens, K.A., Cita, M.B. (1981). Tsunami-induced sediment transport in the abyssal Mediterranean Sea. *Geol. Soc. Amer. Bull. 92*, 845-857.

Keller, J., Ryan, W.B.F., Ninkovich, D., Altherr, R. (1978). Explosive volcanic activity in the Mediterranean over the past 200,000 yr as recorded in deep-sea sediments. *Geol. Soc. Amer. Bull. 89*, 591-604.

Kemp, A.E.S., Pike, J., Pearce, R.B., Lange, C.B. (2000). The "Fall dump" – A new perspective on the role of a "shade flora" in the annual cycle of diatom production and export flux. *Deep-Sea Res. II 47*, 2129-2154.

Kempe, S., Diercks, A.-R., Liebezeit, G., Prange, A. (1991). Geochemical and structural aspects of the pycnocline in the Black Sea (R/V Knorr 134-8 Leg 1, 1988). In: Izdar, E., Murray, J.W. (Eds.), *Black Sea Oceanography*, Kluwer Academic Publishers, Dordrecht, 89-110.

Kidd, R.B., Cita, M.B., Ryan, W.B.F. (1978). Stratigraphy of eastern Mediterranean sapropel sequences recovered during DSDP Leg 42A and their paleoenbironmental significance. *Initail Rep. Deep Sea Drill. Proj. 42A*, 421-443.

Klinkhammer, G., Hudson, A. (1986). Dispersal patterns for hydrothermal plumes in the south-Pacific using manganese as a tracer. *Earth Planet. Sci. Lett. 79*, 241-249.

Klinkhammer, G.P., Palmer, M.R. (1991). Uranium in the oceans: where it goes and why. *Geochim. Cosmochim. Acta 55*, 1799-1806.

Klump, J., Hebbeln, D., Wefer, G. (2000). The impact of sediment provenance on barium-based productivity estimates. *Mar. Geol. 169(3-4)*, 259-271.

König, I., Drodt, M., Suess, E., Trautwein, A.X. (1997). Iron reduction through the tan-green color transition in deep-sea sediments. *Geochim. Cosmochim. Acta, 61*, 1679-1683.

König, I., Haeckel, M., Drodt, M., Suess, E., Trautwein, A.X. (1999). Reactive Fe(II) layers in deep-sea sediments. *Geochim. Cosmochim. Acta 63*, 1517-1526.

Kopf, A., Robertson, A.H.F., Volkmann, N. (2000). Origin of mud breccia from the Mediterranean Ridge accretionary complex based on evidence of the maturity of organic matter and related petrographic and regional tectonic evidence. *Mar. Geol. 166*, 65-82.

Koschinsky, A., Halbach, P. (1995). Sequential leaching of marine ferromanganese precipitates: Genetic implications. *Geochim. Cosmochim. Acta 59(24)*, 5113-5132.

Koschinsky, A., Hein, J.R. (2003). Uptake of elements from seawater by ferromanganese crusts: solid-phase associations and seawater speciation. *Mar. Geol. 198*, 331-351.

Kostka, J.E., Luther III, G.W. (1994). Partitioning and speciation of solid phase iron in saltmarsh sediments. *Geochim. Cosmochim. Acta 58*, 1701-1710.

Krauskopf, K.B. (1967). Introduction to geochemistry. McGraw-Hill, Inc., New York.

Kristensen, E., Kristiansen, K.D., Jensen, M.H. (2003). Temporal behavior of manganese and iron in a sandy coastal sediment exposed to water column anoxia. *Estuaries 26(3)*, 690-699.

Kulik, D.A., Kersten, M., Heiser, U., Neumann, T. (2000). Application of Gibbs Energy minimization to model early-diagenetic solid-solution aqueous-solution equilibria involving authigenic rhodochrosites in anoxic Baltic Sea sediments. *Aquatic Geochem. 6*, 147-199.

LaMoreaux, P.E. (1995). Worldwide environmental impacts from the eruption of Thera. *Environ. Geol. 26(3)*, 172-181.

Lamy, F., Hebbeln, D., Wefer, G. (1998). Terrigenous sediment supply along the Chilean continental margin: modern regional patterns of texture and compostion. *Geol. Rundsch. 87*, 477-494.

Lea, D.W., Boyle, E.A. (1989). Barium content of benthic foraminifera controlled by bottom-water composition. *Nature 338*, 751-753.

Lewis, B.L., Landing, W.M. (1991). The Biogeochemistry of Manganese and Iron in the Black-Sea. *Deep-Sea Res. Part A 38*, 773-803.

Lord III, C.J. (1982). A selective and precise method for pyrite determination in sedimentary materials. *J. Sediment. Petrol. 52*, 664-666.

Lototskaya, A.A. (1999). Mid-latitude North Atlantic climate between 150,000 and 100,000 years BP. Amsterdam University, PhD thesis, 171 pp.

Lourens, L.J., Hilgen, F.J., Gudjonsson, L., Zachariasse, W.J. (1992). Late Pliocene to Early Pleistocene Astronomically Forced Sea-Surface Productivity and Temperature-Variations in the Mediterranean. *Mar. Micropaleontol. 19*, 49-78.

Lourens, L.J., Antonarakou, A., Hilgen, F.J., Van Hoof, A.A.M. (1996). Evaluation of the Plio-Pleistocene astronomical timescale. *Paleoceanography 11*, 391-413.

Lowenstam, H. (1955). Aragonite needles secreted by algae and some sedimentary implications. *J. Sed. Petrol. 25*, 270-272.

Luff, R., Wallmann, K. (2003). Fluid flow, methane fluxes, carbonate precipitation and biogeochemical turnover in gas hydrate-bearing sediments at Hydrate Ridge, Cascadia Margin: Numerical modeling and mass balances. *Geochim. Cosmochim. Acta 67(18)*, 3403-3421.

Luff, R., Wallmann, K., Aloisi, G. (2004). Numerical modeling of carbonate crust formation at cold vent sites: significance for fluid and methane budgets and chemosynthetic biological communities. *Earth Planet. Sci. Lett. 221*, 337-353.

Lyle, M. (1983). The brown-green colour transition in marine sediments: a marker for the Fe(III)-Fe(II) redox boundary. *Limnol. Oceanogr. 28*, 1026-1033.

Lynn, D. C., Bonatti, E. (1965). Mobility of manganese in diagenesis of deep-sea sediments. *Mar. Geol. 3*, 457-474.

Macintyre, I.G., Reid, R.P. (1995). Crystal alteration in a living calcareous alga (*Halimeda*): implications for studies in skeletal diagenesis. *J. Sediment. Res., Sect. A 65(1)*, 143-153.

Mangini, A., Jung, M., Laukenmann, S. (2001). What do we learn from peaks of uranium and of manganese in deep sea sediments? In: Kasten, S. and Hensen, C. (Eds.), *Mar. Geol. 177*, 63-78.

Manheim, F.T., Landergren, S. (1978). *Handbook of Geochemistry II, Section 42. B-O*. Springer-Verlag, Berlin.

Martin, W.R., Bender, M., Leinen, M., Orchardo, J. (1991). Benthic organic carbon degradation and biogenic silica dissolution in the central equatorial Pacific. *Deep-Sea Res. 38*, 1481-1516.

Matthews, R.K. (1966). Genesis of recent lime mud in southern British Honduras. *J. Sed. Petrol. 36(2)*, 428-454.

McCoy, F.W. (1980). The upper Thera (Minoan) ash in deep-sea sediments: distribution and comparison with other ash layers. In: Dumas, C. (Ed.), Thera and the Aegean world. *Proceedings 2nd International Scientific Congress on the Volcano Thera*, Greece 2, 57-78.

McCoy, F.W. (1981). Areal distribution, redeposition and mixing of tephra within deep-sea sediments of the Eastern Mediterranean sea. In: Self, S., Sparks, R.S.J. (Eds.), Tephra Studies, *Nato Advanced Study Institutes Series C 75*, Reidel, Dordrecht, pp. 245-254.

McCoy, F. W., Heiken, G. (2000). Tsunami generated by the Late Bronze Age eruption of Thera (Santorini), Greece. *Pure Appl. Geophys. 157*, 1227-1256.

Meier, K.J.S., Zonneveld, K.A.F., Kasten, S., Willems, H. (2004). Different nutrient sources forcing increased productivity during eastern Mediterranean S1 sapropel formation as reflected by calcareous dinoflagellate cysts. *Paleoceanography 19*, PA1012, doi:10.1029/2003PA000895.

Mercier, H., Speer, K.G., Honnorez, J. (1994). Flow pathways of bottom water through the Romanche and Chain Fracture Zones. *Deep-Sea Res. I 41*, 1457-1477.

Mercone, D., Thomson, J., Croudace, I.W., Siani, G., Paterne, M., Troelstra, S. (2000). Duration of S1, the most recent sapropel in the eastern Mediterranean Sea, as indicated by AMS radiocarbon and geochemical evidence. *Paleoceanography 15*, 336-347.

Mercone, D., Thomson, J., Abu-Zied, R.H., Croudace, I.W., Rohling, E.J. (2001). High-resolution geochemical and micropalaeontological profiling of the most recent eastern Mediterranean sapropel. *Mar. Geol. 177*, 25-44.

Meyers, P.A. (1994). Preservation of elemental and isotopic source identification of sedimentaty organic matter. *Chem. Geol. 114*, 289-302.

Middelburg, J.J., De Lange, G.J., Van der Weijden, C.H. (1987). Manganese solubility control in marine pore waters. *Geochim. Cosmochim. Acta 51*, 759-763.

Middelburg, J.J., De Lange, G.J., Kreulen, R. (1990). Dolomite formations in anoxic sediments of Kau Bay, Indonesia. *Geology 18*, 399-402.

Milliman, J.D., Müller, J. (1973). Precipitation and lithification of magnesium calcite in the deep-sea sediments of the eastern Mediterranean Sea. *Sedimentology 20*, 29-45.

Milliman, J.D., Troy, P.J., Balch, W.M., Adams, A.K., Li, Y.-H., Mackenzie, F.T. (1999). Biologically mediated dissolution of calcium carbonate above the chemical lysocline? *Deep Sea Research Part I 46*, 1653-1669.

Mills, R.A., Elderfield, H. (1995). Hydrothermal activity and the geochemistry of metalliferous sediment. In: Humphris, S. et al. (Eds.), Seafloor hydrothermal systems: physical, chemical, biological and geological interactions, *A.G.U. Geophysical Monograph 91*, 392-407.

Morford, J.J., Emerson, S.R. (1999). The geochemistry of redox sensitive trace metals in sediments. *Geochim. Cosmochim. Acta 63*, 1735-1750.

Mucci, A., Edenborn, H.M. (1992). Influence of an organic-poor landslide deposit on the early diagenesis of iron and manganese in a coastal marine sediment. *Geochim. Cosmochim. Acta 56*, 3909-3921.

Mucci, A., Sundby, B., Gehlen, M., Arakaki, T., Zhong, S., Silverberg, N. (2000). The fate of carbon in continental shelf sediments of eastern Canada: a case study. *Deep-Sea Res. II 47*, 733-760.

Mucci, A., Boudreau, B., Guignard, C. (2003). Diagenetic mobility of trace elements in sediments covered by a flash flood deposit: Mn, Fe and As. *Appl. Geochem. 18*, 1011-1026.

Mulder, T., Syvitski, J.P.M., Migeon, S., Faugères, J.-C., Savoye, B. (2003). Marine hyperpycnal flows: initiation, behavior and related deposits. A review. *Mar. Petrol. Geol. 20*, 861-882.

Murat, A., Got, H. (2000). Organic carbon variations of the eastern Mediterranean Holocene sapropel: a key for understanding formation processes. *Palaeogeog. Palaeoclimatol. Palaeoecol. 158*, 241-257.

Murray, R.W., Leinen, M. (1996). Scavenged excess aluminium and its relationship to bulk titanium in biogenic sediments from the central equatorial Pacific Ocean. *Geochim. Cosmochim. Acta 60*, 3869-3878.

Narcisi, B., Vezzoli, L. (1999). Quaternary stratigraphy of distal tephra layers in the Mediterranean – an overview. *Global Planet. Change 21*, 31-50.

Neinhuis, P.H. (1981). Distribution of organic matter in living marine organisms. In: Duursma, E.K., Dawson, R. (Eds.), *Marine Organic Chemistry*, Elsevier, Amsterdam, 31-69.

Neumann, T., Heiser, U., Leosson, M.A., Kersten, M. (2002). Early diagenetic processes during Mn-carbonate formation: Evidence from the isotopic composition of authigenic Ca-rhodochrosite of the Baltic Sea, *Geochim. Cosmochim. Acta 66(5)*, 867-879.

Nijenhuis, I.A., Schenau, S.J., Van der Wijden, C,H., Hilgen, F.J., Lourens, L.J., Zachariasse, W.J. (1996). On the origin of upper Miocene sapropelites: A case study from the Faneromeni section, Crete (Greece). *Paleoceanography 11(5)*, 633-645.

Nijenhuis, I.A., Becker, J., De Lange, G.J. (2001). Geochemistry of coeval marine sediments in Mediterranean ODP cores and a land section: implications for sapropel formation models. *Palaeogeogr. Palaeoclimatol. Palaeoecol. 165*, 97-112.

Nürnberg, C.C. (1995). Bariumfluss und Sedimentation im südlichen Südatlantik – Hinweise auf Produktivitätsveränderungen im Quartär. Ph.D. Thesis, *Geomar Report 38*, Kiel, Germany.

Nürnberg, C.C., Bohrmann, G., Schlüter, M., Frank, M. (1997). Barium accumulation in the Atlantic sector of the Southern Ocean: results from 190,000-year records. *Paleoceanography 2*, 63-77.

Olausson, E. (1961). Studies of deep-sea cores. *Rep. Swed. Deep-Sea Exped. 1947-1948 8*, 353-391.

Passier, H.F., Middelburg, J.J., Van Os, B.J.H., De Lange, G.J. (1996). Diagenetic pyritisation under eastern Mediterranean sapropels caused by downward sulphide diffusion. *Geochim. Cosmochim. Acta 60*, 751-763.

Passier, H.F., Dekkers, M.J., De Lange, G.J. (1998). Sediment chemistry and magnetic properties in an anomalously reducing core from the eastern Mediterranean Sea. *Chem. Geol. 152*, 287-306.

Passier, H.F., De Lange, G.J., Dekkers, M.J. (2001). Magnetic properties and geochemistry of the active oxidation front and the youngest sapropel in the eastern Mediterranean Sea. *Geophys. J. Int. 145*, 604-614.

Paytan, A., Kastner, M., Martin, E.E., Macdougall, J.D., Herbert, T. (1993). Marine barite as a monitor of seawater strontium isotope composition. *Nature 366*, 445-449.

Paytan, A., Kastner, M. (1996). Benthic Ba fluxes in the central Equatorial Pacific, implications for the oceanic Ba cycle. *Earth Planet. Sci. Lett. 142*, 439-450.

Pearce, N.J.G., Eastwood, W.J., Westgate, J.A., Perkins, W.T. (2002). Trace-element composition of single glass shards in distal Minoan tephra from SW Turkey. *J. Geol. Soc. Lond. 159*, 545-556.

Pearce, N.J.G., Westgate, J.A., Perkins, W.T., Preece, S.T. (2004). The application of ICP-MS methods to tephrochronological problems. *Appl. Geochem. 19*, 289-322.

Pedersen, T.F., Calvert, S.E. (1990). Anoxia versus productivity: what controls the formation of organic carbon rich sediments and sedimentary rocks? *AAPG Bull. V.74*, 454-466.

Peltz, C., Bichler, M. (2001). Classification of archaeologically stratified pumice by INAA. *J. Radioanal. Nucl. Chem. 248*, 81-87.

Pfeifer, K. (1998). Rekonstruktion der Primärproduktion aus Bariumgehalten in Oberflächensedimenten des Südatlantik. Diplomarbeit, Universität Bremen, Germany.

Pfeifer, K., Kasten, S., Hensen, C., Schulz, H. (2001). Reconstruction of primary productivity from the barium contents in surface sediments of the South Atlantic Ocean. *Mar. Geol. 177*, 13-24.

Pfeifer, K., Hensen, C., Adler, M., Wenzhöfer, F., Weber, B., Schulz, H.D. (2002). Modeling of subsurface calcite dissolution, including the respiration and reoxidation processes of marine sediments in the region of equatorial upwelling off Gabon. *Geochim. Cosmochim. Acta 66(24)*, 4247-4259.

Pfeifer, K., Kasten, S., Hensen, C., Schulz, H.D. (submitted for publication). Ba preservation and re-dissolution in the surface sediments of various oceanic regions of the South Atlantic.

Pinardi, N., Masetti, E. (2000). Variablility of the large scale general circulation of the Mediterranean Sea from observations and modeling: a review. *Palaeogeogr. Palaeoclimatol. Palaeoecol. 158*, 153-173.

Piper, D.Z. (1994). Seawater as the source of minor elements in black shales, phosphorites and other sedimentary rocks. *Chem. Geol. 114*, 95-114.

Postma, D. (1985). Concentration of Mn and separation from Fe in sediments. 1. Kinetics and stoichiometry of the reaction between birnessite and dissolved Fe(II) at 10 degrees C. *Geochim. Cosmochim. Acta 49*, 1023-1033.

Prahl, F.G., De Lange, G.J., Lyle, M., Sparrow, M.A. (1989). Post-depositional stability of long-chain alkenones under oxic and suboxic conditions. *Nature 341*, 434-437.

Pruysers, P.A., De Lange, G.J., Middelburg, J.J., Hydes, D.J. (1993). The diagenetic formation of metal-rich layers in sapropel-containing sediments in the eastern Mediterranean. *Geochim. Cosmochim. Acta 57*, 527-526.

Pyle, D.M. (1997). The global impact of the Minoan eruption of Santorini, Greece, Environ. *Geol. 30(1/2)*, 59-61.

Ramsey, C.B., Manning, S.W., Galimberti, M. (2004). Dating the volcanic eruption at Thera. *Radiocarbon 46(1)*, 325-344.

Rasmussen, T.L. (1991). Benthonic and planktonic foraminifera in relation to the early Holocene stagnation in the Ionian Basin, central Mediterranean. *Boreas 20*, 357-376.

Raymo, M.E. (1997). The timing of major climate terminations. *Paleoceanography 12*, 577-585.

Reading, H.G., Levell, B.K. (1996). Controls on the sedimentary rock record. In: Reading, H.G. (Ed.), *Sedimentary Environments: Processes, Facies and Stratigraphy*. Third edition. Blackwell Science, Oxford, London, pp. 5-36.

Rebesco, M., Della Vedova, B., Cernobori, L., Aloisi, G. (2000). Acoustic facies of Holocene megaturbidites in the Eastern Mediterranean. *Sediment. Geol. 135*, 65-74.

Reitz, A., Hensen, C., Kasten, S., Funk, J.A., De Lange, G.J. (2004a). A combined geochemical and rock-magnetic investigation of a redox horizon at the last glacial/interglacial transition. In: Bohnel, H., Hounslow, M., Morris, A., Petrovsky, E. (Eds.), Paleo, Rock and Environmental Magnetism. *Phys. Chem. Earth 29*, 921-931.

Reitz, A., Pfeifer, K., De Lange, G.J., Klump, J. (2004b). Biogenic barium and the detrital Ba/Al ratio: a comparison of their direct and indirect determination. *Mar. Geol. 204*, 289-300.

Rhoads, D.C., Mulsow, S.G., Gutschick, R., Baldwin, C.T., Stolz, J.F. (1991). The dysaerobic zone revisited: a magnetic facies? In: Tyson, R.V., Pearson, T.H. (Eds.), Modern and Ancient Continental Shelf Anoxia. *Geol. Soc. London, Spec. Publ. 58*, 187-199.

Robertson, A.H.F., Kopf, A. (1998). Tectonic setting and processes of mud volcanism on the Mediterranean Ridge accretionary complex: Evidence from Leg 160. In: Robertson, A.H.F. et al. (Eds.), *Proc. ODP Sci. Res. 160*, Ocean Drilling Program, College Station, Texas, 665-680.

Robinson, S.G., Sahota, J.T.S., Oldfield, F. (2000). Early diagenesis in North Atlantic abyssal plain sediments characterized by rock-magnetic and geochemical indices. *Mar. Geol. 163*, 77-107.

Rösler, H.J., Lange, H. (1972). Geochemical tables. Elsevier, New York. pp. 1-468.

Roether, W., Manca, B., Klein, B., Bregant, D., Georgolpoulos, D., Beitzel, V., Kovacevic, V., Luccetta, A. (1996). Recent changes in eastern Mediterranean deep water. *Science 271*, 333-335.

Roether, W., Well, R. (2001). Oxygen consumption in the Eastern Mediterranean. *Deep-Sea Res. I 48*, 1535-1551.

Rohling, E.J. (1994). Review and new aspects concerning the formation of eastern Mediterranean sapropels. *Mar. Geol. 122*, 1-28.

Rohling, E.J., Hilgen, F.J. (1991). The eastern Mediterranean climate at times of sapropel formation: A review. *Geol. Mijnb. 70*, 253-264.

Rossignol-Strick, M. (1983). African monsoon, an immediate climate response to orbital insolation. *Nature 304*, 46-49.

Rossignol-Strick, M. (1985). Mediterranean Quarternary sapropels, an immediate response to orbital insolation. *Nature 304*, 46-49.

Rossignol-Strick, M., Nesteroff, W.D., Olive, P., Vergnaud-Grazzini, C. (1982). After the leluge: Mediterranean stagnation and sapropel formation, *Nature 295*, 105-110.

Roy, S. (1992). Environments and processes of manganese deposition. *Econ. Geol. Bull. Soc. 87*, 1218-1236.

Rühlemann, C., Mulitza, S., Müller, P.J., Wefer, G., Zahn, R. (1999a). Warming of the tropical Atlantic Ocean and slowdown of thermohaline circulation during the last deglaciation. *Nature 402*, 511-514.

Rühlemann, C., Müller, P.J., Schneider, R.R. (1999b). Organic Carbon and Carbonate as Paleoproductivity Proxies: Examples from High and Low Productivity Areas of the Tropical Atlantic. In: Fischer, G., Wefer. G. (Eds.), *Use of Proxies in Paleoceanography: Examples from the South Atlantic*. Springer-Verlag, Berlin, Heidelberg, 315-344.

Rutsch, H.-J., Mangini, A., Bonani, G., Dittrich-Hannen, B., Kubik, P.W., Suter, M., Segl M. (1995). ^{10}Be and Ba concentrations in West Africa sediments trace productivity in the past. *Earth Planet. Sci. Lett. 133*, 129-143.

Rutten, A. (2001). Fluxes, diagenesis and preservation of recent and Holocene sediments in the eastern Mediterranean. Ph.D. Thesis, *Geol. Ultraiect. 202*, Utrecht, The Netherlands.

Rutten, A., De Lange, G.J., Hayes, A., Rohling, E.J., De Jong, A.F.M., Van der Borg, K. (1999). Deposition of sapropel S1 sediments in oxic pelagic and anoxic brine environments in the eastern Mediterranean: differences in diagenesis and preservation. *Mar. Geol. 153*, 319-335.

Rutten, A., De Lange, G.J., Ziveri, P., Thomson, J., Van Santvoort, P.J.M., Colley, S., Corselli, C. (2000). Recent terrestrial and carbonate fluxes in the pelagic eastern Mediterranean; a comparison between sediment trap and surface sediment. *Palaeogeogr. Palaeoclimatol. Palaeoecol. 158*, 197-213.

Rutten, A., De Lange, G.J. (2002). A novel selective extraction of barite, and its application to eastern Mediterranean sediments. *Earth and Planet. Sci. Lett. 198*, 11-24.

Rutten, A., De Lange, G.J. (2003). Sequential extraction of iron, manganese and related elements in S1 sapropel sediments, eastern Mediterranean. *Palaeogeog. Palaeoclimatol. Palaeoecol. 190*, 79-101.

Ruttenberg, K.C. (1992). Development of a sequential extraction method of different forms of phosphorus in marine sediments. *Limnol. Oceanogr. 37*, 1460-1482.

Sachs, J.P., Repta, D.J. (1999). Oligotrophy and Nitrogene fixation during Eastern Mediterranean sapropel events. *Science 286*, 2485-2488.

Saminger, S., Peltz, C., Bichler, M. (2000). South Aegean volcanic glass: Separation and analysis by INAA and EPMA. *J. Radioanal. Nucl. Chem. 245*, 375-383.

Sanders, D. (2003). Syndepositional dissolution of calcium carbonate in neritic carbonate environments: geological recognition, processes, potential significance. *J. African Earth Sci. 36*, 99-134.

Sarnthein, M., Tetzlaff, G., Koopmann, B., Wolter, K., Pflaumann, U. (1981). Glacial and interglacial wind regimes over the eastern subtropical Atlantic and North-West Africa. *Nature 293*, 193-196.

Sato, Y., Okabe, S., Takematsu, N. (1989). Major elements in manganese and iron oxides precipitated from seawater. *Geochim. Cosmochim. Acta 53*, 1883-1887.

Schenau, S.J, Antonarakou, A., Hilgen, F.J., Lourens, L.J., Nijenhuis, I.A., Van der Weijden, C.H., Zachariasse, W.J. (1999). Organic-rich layers in the Metochia section (Gavdos, Greece): Evidence for a single mechanism of sapropel formation during the past 10 My. *Mar. Geol. 153*, 117-135.

Schenau, S.J., Prins, M.A., De Lange, G.J., Monnin, C. (2001). Barium accumulation in the Arabian Sea: Controls on barite preservation in marine sediments. *Geochim. Cosmochim. Acta 65*, 1545-1556.

Schenau, S.J., Reichart, G.J., De Lange, G.J. (2002). Oxygen minimum zone controlled Mn redistribution in Arabian Sea sediments during the late Quaternary. *Paleoceanography 17*, doi:10.1029/2000PA000621.

Schlitzer, R., Roether, W., Oster, H., Junghaus, H.-G., Hausmann, M., Johannesen, J., Michelato, A. (1991). Chlorofluoro methane and oxygen in the Eastern Mediterranean. *Deep Sea Res.* 38, 1531-1551.

Schmid, P., Peltz, C., Hammer, V.M.F., Halwax, E., Ntaflos, T., Nagl, P., Bichler, M. (2000). Separation and Analysis of Theran Volcanic Glass by INAA, XRF and EPMA. *Mikrochim. Acta 133*, 143-149.

Shaw, T.J., Gieskes, J.M., Jahnke, R.A. (1990). Early diagenesis in differing depositional environments: The response of transition metals in porewater. *Geochim. Cosmochim. Acta 54*, 1233-1246.

Shimmield, G.B., Price, N.B. (1986). The behaviour of molybdenum and manganese during early sediment diagenesis – offshore Baja California, Mexico. *Mar. Chem. 19*, 261-280.

Siebert, C., Nägler, T.F., Kramers, J.D. (2001). Determination of molybdenum isotope fractionation by double-spike multicollector inductively coupled plasma mass spectrometry. *Geochem. Geophys. Geosyst. 2*, 2000GC000124.

Siebert, C., Nägler, T.F., von Blanckenburg, F., Kramers, J.D. (2003). Molybdenum isotope record as a potential new proxy for paleoceanography. *Earth Planet. Sci. Lett. 211*, 159-171.

Slomp, C.P., Thomson, J., De Lange, G.J. (2002). Enhanced regeneration of phosphorous during formation of the most recent eastern Mediterranean sapropel (S1). *Geochim. Cosmochim. Acta 66*, 1171-1184.

Sparks, R.S.J., Brazier, S., Huang, T.C., Muerdter, D. (1983). Sedimentology of the Minoan deep-sea tephra layer in the Aegean and Eastern Mediterranean. *Mar. Geol. 54*, 131-167.

Sternbeck, J., Sohlenius, G. (1997). Authigenic sulfide and carbonate mineral formation in Holocene sediments of the Baltic Sea. *Chem. Geol. 135*, 55-73.

Stuiver, M., Braziunas, T.F. (1993). Modeling atmospheric ^{14}C influences and ^{14}C ages of marine samples to 10,000 BC. *Radiocarbon 35*, 137-189.

Sundby, B., Martinez, P., Gobeil, C. (2004). Comparative geochemistry of cadmium, rhenium, uranium, and molybdenum in continental margin sediments. *Geochim. Cosmochim. Acta 68*, 2485-2493.

Takematsu, N., Sato, Y., Okabe, S., Nakayama, E. (1985). The partition of vanadium and molybdenum between manganese oxides and sea water. *Geochim. Cosmochim. Acta 49*, 2395-2399.

Tang, C., Scott, L.D. (1993). Seasonal salinity changes during Mediterranean sapropel deposition 9000 years B.P.: Evidence from isotopic analyses of individual planktonic foraminifera. *Paleoceanography* 8, 473-493.

Tarduno, J.A., Wilkison, S.L. (1996). Non-steady state magnetic mineral reduction, chemical lock-in, and delayed remanence acquisition in pelagic sediments. *Earth Planet. Sci. Lett. 144*, 315-326.

Taylor, S.R. (1964). Abundance of chemical elements in the continental crust: a new table. *Geochim. Cosmochim. Acta 28*, 1273-1285.

Taylor, S.R., McLennan, S.M. (1985). The continental crust: its composition and evolution. Blackwell Scientific Publications, Oxford.

Tendal, O.S. (1972). A monograph of the Xenophyophoria. Galathea Rep. 12, 8.

Thomson, J., Wilson, T.R.S., Culkin, F., Hydes, D.J. (1984). Non-steady state diagenetic record in eastern equatorial Atlantic sediments. *Earth Planet. Sci. Lett. 71*, 23-30.

Thomson, J., Higgs, N.C., Jarvis, I., Hydes, D.J., Colley, S., Wilson, T.R.S. (1986). The behaviour of manganese in Atlantic carbonate sediments. *Geochim. Cosmochim. Acta 50*, 1807-1818.

Thomson, J., Higgs, N.C., Croudace, I.W., Colley, S., Hydes, D.J. (1993). Redox zonation of elements at an oxic / post-oxic boundary in deep-sea sediments. *Geochim. Cosmochim. Acta 57*, 579-595.

Thomson, J., Higgs, N.C., Wilson, T.R.S., Croudace, I.W., De Lange, G.J., Van Santvoort, P.J.M. (1995). Redistribution and geochemical behaviour of redox-sensitive elements around S1, the most recent eastern Mediterranean sapropel. *Geochim. Cosmochim. Acta 59*, 3487-3501.

Thomson, J., Higgs, N.C., Colley, S. (1996). Diagenetic redistributions of redox-sensitive elements in northeast Atlantic glacial/interglacial transition sediments. *Earth Planet. Sci. Lett. 139*, 365-377.

Thomson, J., Jarvis, I., Green, D.R.H., Green, D.A., Clayton, T. (1998). Mobility and immobility of redox-sensitive elements in deep-sea turbidites during shallow burial. *Geochim. Cosmochim. Acta 62*, 643-656.

Thomson, J., Mercone, D., De Lange, G.J., Van Santvoort, P.J.M. (1999). Review of recent advances in the interpretation of Eastern Mediterranean sapropel S1 from geochemical evidence. *Mar. Geol. 153*, 77-89.

Thomson, J., Crudeli, D., De Lange, G.J., Slomp, C.P., Erba, E., Corselli, C. (2004). *Florisphaera profunda* and the origin and diagenesis of carbonate phases in eastern Mediterranean sapropel units. *Paleoceanography 9*, PA3003, doi:10.1029/2003PA000976.

Torres, M.E., Brumsack, H.J., Bohrmann, G., Emeis, K.-C. (1996). Barite fronts in continental margin sediments: A new look at barium remobilization in the zone of sulfate reduction and formation of heavy barites in diagenetic fronts. *Chem. Geol. 127(1-3)*, 125-139.

Totland, M., Jarvis, I., Jarvis, K.E. (1992). An assessment of dissolution techniques for the analysis of geological samples by plasma spectroscopy. *Chem. Geol. 95*, 35-62.

Troelstra, S.R., Ganssen, G.M., Van der Borg, K., De Jong, A.F.M. (1991). A late Quaternary stratigraphic framework for eastern Mediterranean sapropel S1 based on AMS ^{14}C dates and stable oxygen isotopes. *Radiocarbon 33(1)*, 15-21.

Tucker, M.E., Wright, V.P. (1990). Carbonate Sedimentology. Blackwell Science, Oxford.

Tuenter, E., Weber, S.L., Hilgen, F.J., Lourens, L.J. (2003). The response of the African summer monsoon to remote and local forcing due to precession and obliquity. *Glob. Planet. Change 36*, 219-235.

Turekian, K.K., Wedepohl, K.H. (1961). Distribution of the elements in some major units of the earth's crust. *Geol. Soc. Amer. Bull. 72*, 175-192.

Tyson, R.V., Pearson, T.H. (1991). Modern and ancient continental shelf anoxia: an overview. In: Tyson, R.V., Pearson, T.H. (Ed.), Modern and Ancient Continental Shelf Anoxia. *Geol. Soc. London, Spec. Publ. 58*, 1-24.

Van der Weijden, C.H. (2002). Pitfalls of normalization of marine geochemical data using a common divisor. *Mar. Geol. 184*, 167-187.

Van Hoof, A.A.M., Van Os, B.J.H., Rademakers, J.G., Langereis, C.G., De Lange, G.J. (1993). A paleomagnetic and geochemical record of the upper Cochiti reversal and two subsequent precessional cycles from Southern Sicily (Italy). *Earth Planet. Sci. Lett. 117*, 235-250.

Van Os, B.J.H., Middelburg, J.J., De Lange, G.J. (1991). Possible diagenetic mobilization of barium in sapropelic sediments from the eastern Mediterranean. *Mar. Geol. 100*, 125-136.

Van Os, B.J.H., Lourens, L., Hilgen, F.J., De Lange, G.J. (1994). The formation of Pliocene sapropels and carbonate cycles: dilution, diagenesis and productivity. *Paleoceanography 9*, 601-617.

Van Santvoort, P.J.M., De Lange, G.J., Thomson, J., Cussen, H., Wilson, T.R.S., Krom, M.D., Ströhle, K. (1996). Active post-depositional oxidation of the most recent sapropel (S1) in sediments of the eastern Mediterranean Sea. *Geochim. Cosmochim. Acta 60(21)*, 4007-4024.

Van Santvoort, P.J.M., De Lange, G.J., Thomson, J., Colley, S., Meysman, F.J.R., Slomp, C.P. (2002). Oxidation and Origin of Organic Matter in Surficial Eastern Mediterranean Hemipelagic Sediments. *Aqua. Geochem. 8(3)*, 153-175.

Varol, O., Houghton, S.D. (1996). A review and classification of fossil didemnid ascidian spicules. *J. Micropalaeontol. 15*, 135-149.

Verardo, D.J., McIntyre, A. (1994). Production and destruction: control of biogenous sedimentation in the tropical Atlantic 0-300,000 years B.P. *Paleoceanography 9*, 63-86.

Vogt, C., Lauterjung, J., Fischer, R.X. (2002). Investigation of the clay fraction (<2 μm) of the clay minerals society reference clay. *Clays and Clay Minerals 50(3)*, 388-400.

Von Breymann, M.T., Emeis, K.-C., Suess, E. (1992). Water depth and diagenetic constraints on the use of barium as a paleoproductivity indicator. In: Summerhayes, C.P., Prell, W.L., Emeis, K.-C. (Eds.), *Upwelling Systems: Evolution since the Early Miocene*. The Geological Society, London, 273-284.

Von Dobeneck, T. (1996). A systematic analysis of natural magnetic mineral assemblages based on modelling hysteresis loops with coercivity-related hyperbolic basis functions. *Geophys. J. Int. 124*, 675-694.

Vorlicek, T.P., Helz, G.R. (2002). Catalysis by mineral surfaces: Implications for Mo geochemistry in anoxic environments. *Geochim. Cosmochim. Acta 66*, 3679-3692.

Wagner, T., Klemd, R. (1995). Core Descriptions and Smears Slide Analysis. In: Schulz, H., Bleil, U., Henrich, R., Segl, M. (Eds.), *Geo Bremen SOUTH ATLANTIC 1994, Cruise No. 29*, 17 Juni – 5 September 1994. METEOR-Berichte, Universität Hamburg, 233-248.

Wagner, T. (1999). Petrology of organic matter in modern and late Quaternary deposits of the Equatorial Atlantic: climatic and oceanographic links. *Int. J. of Coal Geology 39*, 155-184.

Wallace, H.E., Thomson, J., Wilson, T.R.S., Weaver, P.P.E., Higgs, N.C., Hydes, D.J. (1988). Active diagenetic formation of metal-rich layers in N. E. Atlantic sediments. *Geochim. Cosmochim. Acta 52*, 1557-1569.

Wedepohl, K.H. (1991). The composition of the upper earth's crust in the natural raw materials. In: Merian, E. (Ed.), Metals and their compounds in the environment. VCH Verlagsgesellschaft, Weinheim.

Wedepohl, K.H. (1995). The composition of the continental crust – Ingerson Lecture -. *Geochim. Cosmochim. Acta 59(7)*, 1217-1232.

Weldeab, S., Emeis, K.-C., Hemleben, C., Schmiedl, G., Schulz, H. (2003). Spatial productivity during formation of sapropels S5 and S6 in the Mediterranean Sea: Evidence from the Ba contents. *Palaeogeogr. Palaeoclimatol. Palaeoecol. 191*, 169-190.

Wenzhöfer, F., Glud, R.N., 2002. Benthic carbon mineralization in the Atlantic: a synthesis based on in situ data from the last decade. *Deep-Sea Res. I 49*, 1255-1279.

Wilkinson, B.H., Given, R.K. (1986). Secular variation in abiotic marine carbonates – Constraints on Phanerozoic atmospheric carbon dioxide contents and oceanic Mg/Ca ratios. *J. Geol. 94*, 321-333.

Wilson, T.R.S., Thomson, J., Colley, S., Hydes, D.J., Higgs, N.C., Sørensen, J. (1985). Early organic diagenesis: The significance of progressive subsurface oxidation fronts in pelagic sediments. *Geochim. Cosmochim. Acta 49*, 811-822.

Wilson, T.R.S., Thomson, J., Hydes, D.J., Colley, S., Culkin, F., Sørensen, J. (1986). Oxidation fronts in pelagic sediments: diagenetic formation of metal-rich layers. *Science 232*, 972-075.

Wilson, T.S.R., Thomson, J. (1998). Calcite dissolution accompanying early diagenesis in turbiditic deep ocean sediments. *Geochim. Cosmochim. Acta 62*, 2087-2096.

Zhang, L., Chan, L.-H., Gieskes, J.M. (1998). Lithium isotope geochemistry of pore waters from Ocean Drilling Program Sites 918 and 919, Irminger Basin. *Geochim. Cosmochim. Acta 62*, 2437-2450.

Samenvatting

Dit proefschrift beschrijft recente en paleo-diagenetische processen in bepaalde mariene C_{org}-rijke sedimenten, met name in de sapropel S1 sedimenten van de oostelijke Middellandse Zee.

Vroeg diagenetische processen, die voornamelijk gestuurd zijn door de aanvoer van organisch materiaal en de afbraak ervan, bepalen gedeeltelijk de geochemische samenstelling van mariene sedimenten. Veranderingen in de productiviteit van organisch materiaal hebben een significante invloed op deze diagenetische processen en daardoor op de samenstelling van het sediment. Productiviteitsveranderingen kunnen veroorzaakt worden door variaties van het klimaat op aarde. Deze veranderingen vinden plaats over een breed bereik van tijdschalen en hangen samen met periodieke (b.v. Milankovitch cycli) of onregelmatige variaties (b.v. veroorzaakt door tektonische veranderingen).

Recente diagenetische processen kunnen met behulp van poriewater profielen worden onderzocht, terwijl de paleo-diagenetische veranderingen, door vergelijking met deze recente processen, kunnen worden gereconstrueerd. Diagenese is niet alleen verantwoordelijk voor de verwijdering van C_{org}, maar ook voor de herverdeling van sporenmetalen in de vorm van secundaire neerslag in mariene sedimenten. Hierdoor kan het bestuderen van diagenetische processen een geschikte benadering zijn voor het reconstrueren van paeloceanografische processen.

Vroege diagenese/remineralisatie van organisch materiaal

De diagenetische remineralisatie van organisch materiaal wordt gekatalyseerd door verschillende typen van micro-organismen, welke, in afhankelijkheid van afnemende energietoevoer, eerst zuurstof gebruiken gevolgd door nitraat en/of mangaanoxiden, ijzeroxiden en sulfaat als secundaire oxidatiemiddelen (e.g. Froelich et al., 1979; Berner, 1980).

Berner (1981) introduceerde de volgende verticale diagenetische zone opeenvolging: (i) het oxische milieu, waar poriewaters meetbare concentraties van opgelost zuurstof bevatten; (ii) het anoxische milieu, waar poriewaters geen meetbare concentraties opgelost zuurstof bevatten en diagenese via secundaire oxidatiemiddelen doorgaat. Het anoxische milieu kan opgedeeld worden in (a) het niet sulfidische suboxische milieu, waar poriewaters geen meetbare concentraties opgeloste sulfides bevatten; de gebruikte oxidatiemiddelen zijn nitraat, mangaanoxiden en ijzeroxiden; (b) het sulfidische milieu, waar H_2S en HS^- door bacteriële reductie van opgelost sulfaat geproduceerd worden; (c) het niet sulfidische methaan reducerende milieu, waar poriewaters meetbare concentraties opgelost methaan bevatten.

Het verbruik van secundaire oxidatiemiddelen veroorzaakt een verandering in redox condities. Deze is meestal gekarakteriseerd door een kleurwisseling in het sediment van roodbruin (oxisch) naar grijsgroen (anoxisch). Suboxische oplossing van mangaan- en ijzeroxiden en het neerslaan op de oxische/suboxische grens waar de opgeloste ionen zuurstof tegenkomen, veroorzaakt deze opvallende kleurwisseling.

Ondanks het feit dat behoorlijke hoeveelheden van het organische materiaal geremineraliseerd worden, kan het oorspronkelijke signaal toch worden gereconstrueerd met behulp van indicatoren

zoals biogeen barium (bariet). In tegenstelling tot de directe productiviteit indicatoren zoals C_{org}, calciumcarbonaat en opaal, is bariet stevig gekoppeld aan export productiviteit en onder oxische condities resistenter.

De Middellandse Zee en sapropel vorming

De Middellandse Zee is een halfafgesloten bekken. Tegenwoordig komt het Atlantische oppervlaktewater via de ondiepe Straat van Gibraltar de westelijke Middellandse Zee binnen. Het stroomt via de Straat van Sicilië de oostelijke Middellandse Zee in, waar het water getransformeerd wordt naar Levantine intermediair water. De vorming van diep water gebeurt in de noordelijke delen van de Middellandse Zee zoals de Golf van Lions en de Adriatische (b.v. Schlitzer et al., 1991) en Aegaeische Zee (b.v. Roether et al., 1996). Door de anti-estuariene circulatie is de Middellandse Zee oligotroof, wat in het bijzonder tot uiting komt in het oostelijke bekken.

De hele Holocene sedimentkolom in de oostelijke Middellandse Zee is door lage productiviteit gekarakteriseerd en bestaat uit normale lichtbruine C_{org}-arme sedimenten (0.1-0.2 wt.%; e.g.; Van Santvoort et al., 1996, 2002), die afgewisseld worden met C_{org}-rijke sapropelen. Sapropelen zijn discrete, olijfgroene tot zwarte lagen met een dikte van enkele centimeters tot decimeters, die 2 tot 30 gew.% C_{org} bevatten (Kidd et al., 1978). Hun vorming is het gevolg van de frequente verandering van de algemene circulatie situatie in de oostelijke Middellandse Zee.

Het exacte mechanisme dat tot de vorming van sapropelen heeft geleid is nog steeds onderwerp van discussie. In het algemeen worden twee verschillende scenario's of een combinatie van de twee voorgesteld om sapropel vorming te verklaren: (1) anoxische conservering: volgens deze hypothese blijft de primaire productie onveranderd, maar anoxische bodemwaters resulteren in een betere conservering van het organische materiaal (b.v. Olausson et al., 1961); (2) verhoogde productiviteit: volgens deze hypothese wordt een verhoogde primaire productie in de fotische zone als oorzaak voor een verhoogde C_{org}-accumulatie en conservering aangenomen (b.v. Calvert, 1983).

Synopsis

Het oorspronkelijke geochemische signaal in C_{org}-rijke of voorheen C_{org}-rijke sedimenten is gewoonlijk sterk veranderd door een opeenvolging van diagenetische processen. Het resultaat van deze processen is afhankelijk van de hoeveelheid van metaboliseerbaar organisch koolstof en van de condities die de redox potentiaal bepalen. Zoals boven vermeld kan biogeen barium worden gebruikt om het oorspronkelijke interval van C_{org}-rijk sediment te reconstrueren, ook als het grotendeels verwijderd is door vroege diagenese. In hoofdstuk 2 is de betrouwbaarheid van de vaak gebruikte, indirecte (normatieve) procedure voor het bepalen van het biogene barium bestudeerd. Hiervoor is een vergelijking gemaakt van de directe (door opeenvolgende extractie) en indirecte (door normatieve berekening) bepaling van biogeen barium en de detritische Ba/Al ratio. Het onderzoek van verschillende diepzee sediment milieus heeft aangetoond dat de detritische Ba/Al ratio de cruciale factor is in de normatieve procedure. Het onderzoek van de betrouwbaarheid van biogeen Ba als een indicator voor paleoproductiviteit is een essentiële basis voor verder onderzoek van sapropelen en andere C_{org}-rijke sedimenten. Voor de studies in de volgende hoofdstukken was het vooral belangrijk de grenzen van de verhoogde C_{org} accumulatie vast te stellen en deze kunnen, via

de Ba/Al ratio, zonder verdere bewerking bepaald worden.

Diagenetische processen resulteren niet alleen in de oxidatie van organisch materiaal maar ook in de remobilisatie van minerale fasen zoals Mn- en Fe-oxiden. De associatie van de ontwikkeling van een redox horizont, als gevolg van niet stationaire diagenetische condities, tussen het laatste glaciaal en het Holoceen is met behulp van geochemische en magnetische analyses in hoge resolutie in hoofdstuk 3 gereconstrueerd. De beweging van de redox horizont heeft tot de vorming van opvallende dubbele pieken van Mn en Fe in de vaste fase geleid, maar ook tot een duidelijke anomalie in de buurt van de redox horizont, die wijst op oplossing van magnetische minerale fasen veroorzaakt door suboxische diagenese. De voortgang van het oxidatiefront kon gereconstrueerd worden uit de totale ijzerconcentratie en de relatie met ferromagnetische susceptibiliteit. Verder was het mogelijk het kleinschalige voortschrijden van de redox grens te reconstrueren door de ratio van ferromagnetische en totale susceptibiliteit te combineren met die van V/Al, wat een stapsgewijze opwaarts gerichte beweging van de redox front laat zien.

Een vergelijkbare dubbele Mn piek zoals in hoofdstuk 3 beschreven, is ook bekend van de oostelijke Middellandse Zee sapropel S1 sedimenten. In deze sedimenten zijn de dubbele pieken ontwikkeld doordat na de afzetting van het sediment zuurstof penetratie en C_{org} remineralisatie heeft plaatsgevonden. In dit geval is de Mn redox grens, en dus is de actief gevormde Mn piek de onderste, die direct op de bovenkant van het overgebleven deel van sapropel S1 zit. De bovenste, passieve piek geeft het begin van de reventilatie en derhalve het einde van de sapropel vorming aan. De Mn-concentraties in de bovenste pieken zijn veel hoger (>3 wt.%) in sedimenten van intermediaire waterdiepten (1 tot 2 km) in de oostelijke Middellandse Zee. Zoals in hoofdstuk 4 is aangegeven is de verandering in redox condities in de waterkolom verantwoordelijk voor deze Mn verrijkingen. Op intermediaire waterdiepten ontmoeten anoxisch en oxisch water elkaar. Het anoxische water bevat opgelost Mn wat door diagenetische processen in oplossing is gebracht. Samen met de zuurstof in het oxische water zorgt dit voor de neerslag van mangaanhydroxiden. Dit hydrogenetische mechanisme, wat tot grote diagenetische pieken leidt, word bevestigd door de incorporatie van molybdeen en lithium met een vaste ratio tot Mn dat in een vergelijkbare verhouding in andere Mn verrijkte oxische sedimenten is aangetroffen.

De vorm van Mn-profielen in de oostelijke Middellandse Zee kan verder door diagenetische processen veranderen, in gebieden met substantiële tephra en turbidiet afzettingen, zoals veroorzaakt door de explosieve Santorini eruptie in ~1630 B.C. Deze verstoringen kunnen worden geïdentificeerd door verhogingen in de profielen van Sr/Ca en sommige andere element/Al ratios. In hoofdstuk 5 is de additionele vorming van Mn pieken dicht bij het oppervlak beschreven. Deze worden veroorzaakt door verlies van zuurstof spanning als gevolg van het oppervlak bedekking met deze afzettingen en de daaropvolgende verandering van het karakteristieke dubbele pieken kenmerk, veroorzaakt door reductie van mangaanhydroxiden in het diepere sediment.

De Sr/Ca ratio is echter niet alleen verrijkt in de door de Santorini eruptie geïnitieerde turbidieten boven sapropel S1, maar ook in de sapropel sedimenten zelf. Deze verhoogde Sr/Ca ratio hangt samen met verhoogde concentraties van Sr-rijk aragoniet in de sapropel die bij de continentale Sirte helling (noordelijk Afrika) concentraties tot 40 gew.% bereikt. Deze hoge aragoniet concentraties kunnen niet verklaard worden door pteropoden omdat die lage Sr concentraties bevatten. Een bron dicht bij de kust, die Sr-rijke aragonite skeletten of fragmenten ervan aanvoert of secundaire diagenetische vormingsprocessen kunnen de gevonden concentraties verklaren. In

hoofdstuk 6 wordt de relatie van afnemende aragoniet gehalten met toenemende afstand tot de Afrikaanse kust en met waterdiepte benadrukt. Samen met de SEM (scanning elektronen microscoop) observaties van de S1 sedimenten van het Sirte transect en het ontbreken van variaties in porositeit, wijst dit op een kust nabije detritisch/biogene bron van Sr-rijke aragoniet naaldjes. Een diagenetische bijdrage kan echter niet worden uitgesloten.

Zusammenfassung

Diese Dissertationsschrift beschreibt rezente und paläo-diagenetische Prozesse in ausgewählten marinen Sedimenten die reich an organischem Material (im Folgenden vielfach C_{org}-reich genannt) sind. Besondere Berücksichtigung finden die Sapropel-S1-Sedimente des östlichen Mittelmeeres.

Frühdiagenetische Prozesse, die im Wesentlichen durch die Zufuhr und die Zersetzung des organischen Materials gesteuert werden, bestimmen zu einem nicht unerheblichen Anteil die geochemische Zusammensetzung von marinen Sedimenten. Die Bildung von organischem Material in der Wassersäule hat einen signifikanten Einfluss auf diese diagenetischen Prozesse im Sediment und dadurch auch auf die sedimentäre Zusammensetzung. Die Produktivität kann Schwankungen unterliegen, die durch Veränderungen des Erdklimas verursacht werden. Diese Veränderungen können auf unterschiedlichsten Zeitskalen wirken, induziert durch eine bestimmte Periodizität (z. B. Milankovitch-Zyklen) oder durch irreguläre Ereignisse (z. B. durch tektonische Aktivität).

Rezente diagenetische Prozesse können mit Hilfe von Porenwasserprofilen untersucht werden, während paläo-diagenetische Veränderungen nur durch den Vergleich von Festphasenergebissen mit rezenten Porenwasserergebnissen rekonstruiert werden können. Weil die Diagenese neben dem Abbau des C_{org} auch eine Umverteilung von Spurenelementen in Form von sekundären Ausfällungen bewirkt, kann die Untersuchung von diagenetischen Prozessen ein geeignetes Mittel zur Rekonstruktion von paläo-ozeanographischen Prozessen sein.

Frühdiagenese / Remineralisierung von organischem Material

Der diagenetische Abbau von C_{org} wird durch verschiedene Arten von Mikroorganismen katalysiert, die für die Oxidation zuerst Sauerstoff verwenden. In Abhängigkeit vom abnehmenden Energiegewinn werden danach Nitrat und/oder Manganoxide, Eisenoxide und Sulfat als sekundäre Oxidationsmittel verwendet (z.B. Froelich et al., 1979; Berner, 1980).

Berner (1981) führte die folgende vertikale diagenetische Zonenabfolge ein: (i) die oxische Zone, in der im Porenwasser messbare Sauerstoffkonzentrationen nachgewiesen werden können; (ii) die anoxische Zone, in der im Porenwasser keine messbaren Sauerstoffkonzentrationen nachgewiesen werden können und in der die Diagenese mittels sekundärer Oxidationsmittel fortgeführt wird. Die anoxische Zone kann wiederum aufgeteilt werden in (a) die nicht-sulfidische suboxische Zone, in der im Porenwasser keine messbaren Sulfidkonzentrationen nachgewiesen werden können, die verwendeten Oxidationsmittel sind Nitrat, Mangan- und Eisenoxide; (b) die sulfidische Zone, in der H_2S und HS^- durch Reduktion von gelöstem Sulfat produziert werden; (c) die nicht-sulfidische Methan reduzierende Zone, in der das Porenwasser messbare Methankonzentrationen enthält.

Durch die Verwendung sekundärer Oxidationsmittel kommt es zur Veränderung der Redoxbedingungen. Suboxische Mangan- und Eisenoxidauflösung und ihre Ausfällung an der Grenze zum oxischen Milieu, wo die gelösten Ionen auf Sauerstoff treffen, produziert eine auffällige Farbgrenze von rotbraun (oxisch) nach graugrün (anoxisch).

Obwohl erhebliche Mengen organischen Materials diagenetisch remineralisiert werden, kann die ursprüngliche Ausdehnung einer C_{org}-reichen Lage mit Hilfe von Indikatoren wie biogenem Barium

(Baryt) rekonstruiert werden. Im Gegensatz zu direkten Produktivitätsindikatoren wie C_{org}, Calciumcarbonat und Opal ist Baryt unter oxischen Bedingungen eine wesentlich stabilere Spezies und eng an die Produktivität von C_{org} in der Wassersäule gekoppelt.

Das Mittelmeer und Sapropelbildung

Das Mittelmeer ist ein beinahe abgeschlossenes Becken. Gegenwärtig gelangt das Atlantische Oberflächenwasser über die Straße von Gibraltar in das westliche Mittelmeer und strömt von dort über die Straße von Sizilien in das östliche Mittelmeer, wo es absinkt und zum Levantinische Zwischenwasser wird. Die Bildung von Tiefenwasser findet in den nördlichen Bereichen des Mittelmeeres, wie dem Golf von Lions und der Adriatischen (z.B. Schlitzer et al., 1991) und der Ägäischen See (z.B. Roether et al., 1996) statt. Durch die anti-estuarine Zirkulation (oberflächennah einströmendes und bodennah ausströmendes Meerwasser) ist das Mittelmeer ein oligotrophes (d. h. nährstoffarmes, gering produktives) Meer. Dies ist besonders ausgeprägt im östlichen Becken.

Die holozänen Sedimente des östlichen Mittelmeeres sind in Folge der geringen Produktivität durch hellbraune C_{org}-arme Sedimente (0.1-0.2 Gew.%; z. B. Van Santvoort et al., 1996) charakterisiert, die von C_{org}-reichen Sapropelen unterbrochen werden. Sapropele sind separate, olivgrüne bis schwarze Lagen von wenigen Zentimetern bis zu Dezimetern Mächtigkeit, die 2 bis 30 Gew.% C_{org} enthalten (Kidd et al., 1978). Ihre Bildung ist die Folge frequent auftretender Veränderungen der allgemeinen Wasserzirkulation im östlichen Mittelmeer.

Der Mechanismus, der zur Sapropelbildung führt, wird noch stets kontrovers diskutiert. Im allgemeinen werden zwei verschiedene Szenarien oder eine Kombination aus beiden angenommen, um die Bildung zu erklären: (1) anoxische Erhaltung: dieser Hypothese zur Folge blieb die Primärproduktivität relative unverändert, während anoxische Bedingungen im Bodenwasser eine bessere Erhaltung des organischen Materials verursachten (z.B. Olaussen et al., 1961); (2) erhöhte Produktivität: dieser Hypothese zur Folge ist eine Erhöhung der Primärproduktion in der photischen Zone die Ursache für die erhöhte C_{org}-Akkumulation und -Erhaltung (z.B. Calvert, 1983).

Synopsis

Das ursprüngliche, geochemische Signal in C_{org}-reichen oder ehemals C_{org}-reichen Sedimenten ist im Allgemeinen durch eine Abfolge von diagenetischen Prozessen stark überprägt. Das Ausmaß dieser Überprägung ist abhängig von der Menge des metabolisierbaren organischen Kohlenstoffs und des Redoxpotentials der Umgebung. Mit Hilfe von biogenem Barium kann das ursprüngliche Intervall, in dem C_{org}-reiche Sedimente abgelagert wurden, rekonstruiert werden, auch wenn das organische Material selbst größtenteils durch Diagenese abgebaut wurde. Um die Zuverlässigkeit des häufig angewandten indirekten (normativen) Verfahrens zur Bestimmung des biogenen Bariums beurteilen zu können, wurde in Kapitel 2 ein Vergleich der direkten (durch sequentielle Extraktion) mit der indirekten (durch normative Berechnung) Bestimmung von biogenem Barium und des detritischen Ba/Al-Verhältnisses durchgeführt. Die Untersuchung verschiedener Tiefseesedimentmilieus hat gezeigt, dass das detritische Ba/Al-Verhältniss der entscheidende Faktor des normativen Verfahrens ist. Die Erhebung der Zuverlässigkeit von biogenem Ba als Indikator für Paläoproduktivität bildet die essentielle Basis für weitere Studien an Sapropelen und C_{org}-reichen

Sedimenten. Für die Studien in den folgenden Kapiteln wurden die Grenzen, zwischen denen eine erhöhte C_{org}-Akkumulation stattfand, über das Ba/Al-Verhältnis (ohne weitere Bearbeitung) bestimmt.

Diagenetische Prozesse führen nicht nur zur Zersetzung des organischen Materials sondern auch zur Remobilisierung von Mineralphasen wie Mn- und Fe-Oxiden. In Kapitel 3 wurde mit Hilfe der Kombination von geochemischen und gesteinsmagnetischen Analysen in hoher Auflösung die Entwicklung eines Redoxhorizontes zwischen dem letzten Glazial und dem Holozän rekonstruiert. Die Verschiebung des Redoxhorizontes hat zu Ausbildung von auffälligen Festphasen-Doppelmaxima von Mn und Fe geführt. Zusätzlich weisen deutliche gesteinsmagnetische Anomalien in der Umgebung des Redoxhorizontes, auf eine Auflösung von magnetischen Mineralphasen hin, die durch suboxische Diagenese verursacht wurde. Das Fortschreiten der Oxidationsfront konnte mit Hilfe der Gesamteisenkonzentration und dessen Verhältnis zur ferromagnetischen Suszeptibilität rekonstruiert werden. Weiterhin war es möglich, durch eine Kombination des Verhältnisses von ferromagnetischer und totaler Suszeptibilität und dem von V/Al, das detaillierte Fortschreiten der Redoxgrenze zu rekonstruieren, wobei eine schrittweise Aufwärtsbewegung der Redoxfront festgestellt werden konnte.

Ein vergleichbares Mn-Doppelmaximum wie in Kapitel 3 beschrieben ist auch von den Sapropel-S1-Sedimenten des östlichen Mittelmeeres bekannt. In diesen Sedimenten haben sich die Doppelmaxima entwickelt, indem nach der Sedimentablagerung eine Sauerstofffront in das Sediment eindrang und zur C_{org}-Remineralisierung führte. In diesem Fall liegt die Mn-Redoxgrenze, und somit auch das aktiv gebildete untere Mn-Maximum, direkt auf dem noch erhaltenen Sapropel S1, während das obere passive Maximum den Beginn der Wiederbelüftung des Beckens mit Sauerstoff und somit das Ende der Sapropelbildung anzeigt. Es ist auffällig, dass das Ausmaß dieser oberen Mn-Maxima in den Sedimenten mittlerer Wassertiefe (1 bis 2 km) am größten (>3 Gew.%) ist. Kapitel 4 beschreibt, das der Wechsel der Redoxbedingungen in der Wassersäule für diese Mn-Anreicherungen verantwortlich ist. Das mittlere Wassertiefenintervall erhält an der Grenzschicht zwischen anoxischem und oxischem Wasser viel gelöstes Mn, das dort auf Sauerstoff trifft und als Manganhydroxid ausfällt. In größeren Wassertiefen wird das gelöste Mn diagenetisch im Sediment gebildet und gelangt diffusiv in die anoxische Wassersäule. Durch diesen Mechanismus kommt es zur Ausbildung großer hydrogenetischer Mn-Maxima, dessen Mangan im Wesentlichen diagenetischen Ursprungs ist. Dieser hydrogenetische Prozess wird durch den Einbau von Molybdän und Lithium in einem festen Verhältnis zu Mn bestätigt; vergleichbare Mo:Mn- bzw. Li:Mn-Verhältnisse sind in anderen Mn-angereicherten oxischen Sedimenten beobachtet worden.

Die Mn-Profilformen im östlichen Mittelmeer können durch substantielle Tephra- und Turbiditablagerungen z. B. die ausgelöst durch die explosive Santorini Eruption ca. 1630 B.C., zusätzlich diagenetisch verändert werden. Die genannten Ablagerungen können durch ihre erhöhten Sr/Ca- und einige andere Element/Al-Verhältnisse identifiziert werden. In Kapitel 5 ist die Bildung von zusätzlichen, oberflächennahen Mn-Maxima beschrieben. Diese wurden durch rückläufige Sauerstoffkonzentrationen als Folge der Bedeckung des Oberflächensediments und der darauf folgenden Veränderung der charakteristischen Mn-Doppelmaxima durch Mangan(hydr)oxid-Reduktion in den tieferen Sedimenten verursacht.

Das Sr/Ca-Verhältnis ist jedoch nicht nur in den Turbiditen oberhalb des Sapropel S1 erhöht, sondern auch im Sapropel selbst. Das erhöhte Sr/Ca-Verhältnis ist an eine erhöhte Konzentration von

Sr-reichem Aragonit gebunden, die am Sirte-Kontinentalhang (Nordafrika) bis zu 40 Gew.% erreicht. Die beobachteten hohen Aragonitkonzentrationen können nicht durch Pteropoden verursacht werden, da diese nur geringe Sr-Konzentrationen aufweisen. Durch eine küstennahe Quelle, die Sr-reiche Aragonitskelettfragmente anliefert oder durch sekundäre, diagenetische Bildungsprozesse lassen sich diese Anreicherungen jedoch erklären. In Kapitel 6 wird der Zusammenhang zwischen abnehmendem Aragonitgehalt und zunehmendem Abstand zur Afrikanischen Küste und zunehmender Wassertiefe behandelt. Dieser Zusammenhang deutet gemeinsam mit rasterelektronenmikroskopischen Beobachtungen der Aragonitenadeln der Sedimente des Sirte-Transekt und der Tatsache, das keine Abnahme der Porosität in den S1 Sedimenten beobachtet wurde, auf eine küstennahe, detritisch/biogene Quelle für die Sr-reichen Aragonitnadeln hin. Ein diagenetischer Beitrag kann jedoch nicht ausgeschlossen werden.

Acknowledgement

Here I would like to thank all the people that supported me scientifically and non-scientifically during my PhD-project but also that people that stimulated me to do this PhD or were in one or the other way important for my decision. Some of them I would like to name specifically.

First I would like to thank my promoter Gert de Lange for giving me the opportunity to carry out this fascinating research. I am grateful for lots of interesting discussions and scientific cruises. Looking back on the past four years I can say that I primarily enjoyed the time of our co-operation.

Further, I would like to thank my co-authors and discussion partners John Thomson, Kerstin Pfeifer, Christian Hensen, Mark Dekkers, Gert-Jan Reichart, Caroline Slomp, Sabine Kasten, Jens Funk, Jens Klump, Derryl Green and Andrea Gebhardt. I appreciate in particular, the intensive e-mail discussions and the critical revisions by John and Gert-Jan's intuition to appear at the right moment when I needed some mental support. Further I would like to thank the people involved in EUROPROX.

For the technical and analytical support I am indebted to Helen de Waard (alles wat je kunt bedenken), Eric van Vilsteren, Bertil van Os (voor je enthousiasme voor speciale problemen en explosieve ideeën in het bijzonder), Arnold van Dijk (voor alle hulp om nacht en weekend metingen mogelijk te maken), Thomas Appel, Els Ufkes, Dineke van de Meert, Geert Ittmann, Gerard Klaver, Marian Reith, Thomas Nägler, Christoph Vogt, Mario Thöner, Natascha, and Herman van Roermund. The scientific cruise and student field-trips I participated in were always a great pleasure for me. Thus I would like to thank the other participants as there are Patrick (ik heb je altijd als een rustpunt met overzicht tussen al dat chaos hervaren), Anke (für dich gilt eigentlich das gleiche), Rinske, Sanella, Emelina, Shauna, Andrea, Jurgen, Fred, Simon (niet alleen voor het enigszins speciale veldwerk maar ook voor jou interesse in mijn werk), Gijs, Sjoerd, Vincent, Grishja, the Italian and Greek partners, and of course the technicians of the NIOZ and the crew of the Pelagia.

Before I come to the pure social part I would like to express my very very special thanks to Beate Bader for scientific and social support, your hospitality knows no limits. Thanks.

Coming to the social part, I would like to start acknowledging Diana (deine gute Laune und Zuversicht ist wirklich ansteckend, tausend Dank nochmals für die nette Beherberung), followed by the colleagues that shared the room, coffee, thee and cookies with me: Mariette, Nils, Laurent, Sandra, Vincent, Sokratis. Andreas, Sandra and Martin are also thanked for the nice and long DOKO nights, Gesa, Julia, Jaquceline, Yvonne and Pierre are thanked for physical distraction by joint climbing. Further I would like to thank all the other colleagues that made the Department a nice working place: Christelle, Parisa, Celine, Pieter, Pien, Philippe, Steeve, Jeff, Andy, David, Katja, Tom, Rick, Goulven, Claudette, Thilo, Nikolaj, Imogen, Christof, and the people from the AIO platform.

Meinen Eltern möchte ich dafür danken, dass sie meine Entscheidung akzeptiert und respektiert haben. Des Weiteren freue ich mich über all die Ablenkung von meiner Arbeit durch meine Familie und durch Freunde.

As usual the most important people are always named at the end, thus without many words I would like to express my warmest thanks to Chrisch.

Curriculum vitae

Anja Reitz was born on the 05th of January 1969 in Bremen, Germany. After completing secondary school in 1985 in Loxstedt she followed an apprenticeship in medical assistance and worked as a medical assistance until 1995. In the meantime she successfully completed the "Kolleg Erwachsenenschule Bremen" in Bremen and received her A-level in 1994. From 1995 to 2001 she studied Geology/Paleontology at the University of Bremen, Germany and Durham, UK. In 1999 she worked for 3 months as an assistant researcher at the Marine Information Resource Corporation and the Beltsville Agricultural Research Centre in Maryland, USA. In 2001 she achieved her Diploma in Geology and Paleontology with main focus on Geochemistry and Hydrogeology at the University of Bremen. In 2001 she was appointed as PhD-student at the Utrecht University, Faculty of Geosciences, Department of Earth Sciences – Geochemistry. The PhD-research is part of the project "Sapropel-related Paleoceanographic Studies in Sediments of the eastern Mediterranean (SAPS)" founded by NWO/ALW.